KU Leuven

Biomedical Sciences Group

Faculty of Medicine

Department of Oncology

KU LEUVEN

DOCTORAL SCHOOL
BIOMEDICAL SCIENCES

THE ROLE OF SERINE BIOSYNTHESIS IN BREAST CANCER-DERIVED LUNG METASTASIS

Gianmarco RINALDI

Jury:

Supervisor: Prof. Sarah-Maria Fendt

Chair examining committee: Prof. Kathleen Freson

Chair public defense: Prof. Baki Topal

Jury members: Prof. Marcia C. Haigis
Dr. Gabriel Leprivier
Prof. Geert Carmeliet
Prof. Frans Schuit

Dissertation presented in partial fulfilment of the requirements for the degree of Doctor in Biomedical Sciences

Contents

Summary 4

Chapter 1. Introduction 6

Breast cancer metastasis 6

Metastasis is the leading cause of death for patients with cancer 8

The metastatic cascade 9

Motility and invasion 9

Intravasation and survival in the circulation 11

Metastatic colonization 12

Cellular metabolism supports breast cancer metastasis 14

Metabolic adaptations in the primary tumor 17

Metabolic adaptations during the metastatic process 18

Nutrient availability is a determinant of cancer progression 21

mTORC1 activation during the metastatic cascade 23

OBJECTIVES 27

Chapter 2. Materials and Methods 29

Cell lines 29

Mouse models 29

Mammary fat pad model 30

Lung injection model 31

MMTV-PyMT tumor generation 32

Knockdown and overexpression strategies 32

Starvation and reactivation 33

Protein extraction and western blot analysis 33

Protein synthesis (SUnSET) 34

^{13}C tracer analysis 35

Surgery and $^{13}C_6$-glucose infusion 36

Tissue collection and preparation for protein and metabolite extraction 36

Hematoxylin and eosin staining 37

Lung interstitial fluid extraction 37

Metabolites measurements 38

Gas chromatography-mass spectrometry 39

Liquid chromatography-mass spectrometry 40
Compartment specific-metabolic measurements 41
Monitoring of tumor growth via optical imaging 42
Analysis of mTOR pathway activity in human metastases and matched primary breast cancers 43
Comparison of mTOR activity with MCT2 gene expression levels 44
Quantification and statistical analysis 44
Chapter 3. Results 45
Pyruvate supports mTORC1 signaling 45
Serine biosynthesis is required for pyruvate driven mTORC1 signaling 51
α-ketoglutarate produced by the serine biosynthesis pathway supports mTORC1 signaling 62
Serine biosynthesis is required for rapamycin sensitivity in breast cancer-derived lung tumors but not primary breast tumors 70
Chapter 4. Conclusion and discussion 74
ACKNOWLEDGMENTS, PERSONAL CONTRIUBUTION AND CONFLICT OF INTEREST STATEMENTS 80
Authors List: 80
Author Contributions 81
Conflict of interest 81
Scientific Acknowledgments 81
REFERENCES 83
ADDENDUM 90

Summary

Breast cancer is the most frequent type of tumor among women worldwide, accounting for 24.2% of all the tumor cases. Due to these tremendous incidences, breast cancer is also the type of tumor causing the highest number of deaths, indeed around 600.000 women die every year because of this disease. By taking a closer look at the prognosis of patients diagnosed with breast cancer, it appears evident that the progression of the disease towards a metastatic stage reduces the survival rates. Indeed, metastasis formation is the leading cause of death for patients with cancer, including breast cancer. The inefficacy of the current therapies highlights how the metastatic cascade, due to its complexity, is still the least understood process of cancer biology.

Thus, we are in urgent need of novel therapeutic strategies and this thesis aims at expanding our understanding of the fundamental biological processes underlying the metastatic process of breast cancer cells to provide insights for the design of new therapies. In particular, we focused in this thesis on the cross-talk between cellular metabolism and signal transduction during metastatic outgrowth.

Metabolic rewiring is now recognized as a hallmark of cancer. Specifically, metabolic pathways are highjacked by tumor cells to sustain their biomass production and energetic needs during uncontrolled proliferation. Metastatic cancer cells have been shown to rewire their metabolism during multiple steps of the metastatic cascade such as invasion and survival in the circulation. Yet, how metabolic rewiring sustains the last phase of the metastatic process, the metastatic outgrowth of disseminated cancer cells, is still poorly understood.

The nutrient composition of the extracellular environment is one of the main determinants of cellular metabolism. Recent work from our group has shown, in the context of a breast cancer murine model, that the lung nutritional microenvironment, which is a recurrent metastatic site for breast cancer cells, is defined by an increased pyruvate availability compared to the mammary tissue. Functionally, the extracellular

presence of pyruvate contributes to a permissive niche for metastatic breast cancer cells that rewire their metabolism to sustain extracellular matrix remodeling. However, the role of a pyruvate rich microenvironment on the metabolism of outgrowing metastases remains elusive.

Activation of growth signaling is critical during the last step of metastasis formation. One of the key cell signaling pathways sustaining cellular growth and proliferation is represented by mammalian target of rapamycin (mTOR), which is a serine/threonine-specific protein kinase that exists in two complexes, namely mTORC1 and mTORC2. mTORC1 represents a central hub that coordinates metabolic signals and cellular functions to ultimately sustain cell growth and proliferation. Given its crucial role, mTORC1 aberrant activation has been found in multiple cancer contributing to uncontrolled proliferation. Yet, it remains largely unknow whether and how mTORC1 signaling is activated in cancer cells that have successfully disseminated to a distant organ.

The overarching objective of this thesis was to investigate how nutrient availability impacts cellular metabolism and growth signaling in primary breast cancer cells and their corresponding lung metastasis during the metastatic outgrowth.

Mechanistically, we found that pyruvate, a nutrient available in the lung environment, supports the activation of mTORC1 signaling by fueling serine biosynthesis-derived α-ketoglutarate production during metastasis formation. Overexpression of the serine biosynthesis enzyme phosphoglycerate dehydrogenase (PHGDH) stimulated sensitivity to rapamycin in breast cancer-derived lung tumors. Accordingly, while silencing of PHGDH in breast cancer cells abolished sensitivity to rapamycin in lung tumors, it did not change sensitivity towards mTORC1 inhibition in primary breast tumors.

In summary, we show that breast cancer cells growing in the lung metastatic niche have different metabolic requirements to activate mTORC1 signaling than the same breast cancer cells growing in the primary tumor site.

Chapter 1. Introduction

Breast cancer metastasis

Breast cancer is the malignancy with the highest incidence rate in women worldwide accounting for 24.2% of all the tumor cases[1]. In 2018, cancer has caused the death of 4.2 million women, 15% of which (around 600.000) was due to breast cancer. Thus in females, breast cancer not only shows the highest incidence rate, but also the highest mortality rate worldwide[1]. However, the patient's prognosis is strictly connected with the stage of the disease at diagnosis. Indeed, patients presenting to the clinic with early-stage non-metastatic breast cancer will be curable in the 70-80% of the cases[2]. Despite this positive outcome when it is early detected, advanced breast cancer that has spread to distant organs forming secondary tumors is mostly incurable[2].

The clinical strategies available for the treatment of breast cancer are surgical removal, radiotherapy and systemic therapy. Due to the high heterogeneity of this disease, breast cancer has been classified in different molecular subtypes that are also used to predict the best therapeutic approach: estrogen receptor positive (Luminal A and Luminal B), epidermal growth factor receptor 2 (HER2) enriched, triple-negative (TNBC) that lacks expression of estrogen receptor (ER), progesterone receptor and HER2[3]. Surgical removal of the primary tumor is generally followed by a systemic treatment that can vary depending on the molecular subtype[2]. While ER positive are treated with endocrine hormone therapy and HER2 positive are treated with anti-HER2 therapy, TNBC cannot be treated with targeted therapy and thus only receive chemotherapy.

Advanced breast cancer that reaches the metastatic stage is spreading throughout the body colonizing more frequently distant organs such as lung, liver, bone and brain[2]. The classification of breast cancer also predicts the advancement of the disease and the organ tropisms of eventual metastasis. Luminal A and Luminal B

ER positive breast cancer have usually a fairly good prognosis, when they present relapses are usually after several years and the most recurrent metastatic sites are bones and lymph nodes[2]. HER2 positive tumors also show a good prognosis also thank to the effective anti-HER2 therapy and eventual metastasis are generally found in the brain. TNBCs are the subtypes with the worse prognosis with early recurrence and usually tend to colonize lung, liver and brain[2].

Different therapeutic options are available at the moment for the treatment of advanced breast cancer that have created secondary lesions in distant organs. Surgical removal of the metastasis itself or of the primary tumor is at the moment considered to be controversial and might only be effective in specific clinical cases[4–7]. Radiation therapy is used to treat the metastatic lesions and alleviate their symptoms. Additionally, the use of radiation on the primary tumor has been shown to generate a systemic activation of the immune system the can increase the overall survival[8]. A number of systemic therapies are approved for treatment of advanced breast tumors and the choice of the strategy depends on the molecular and histological characteristics of the tumor. ER-positive are treated with hormone therapy, often using tamoxifen (inhibitor of the ER), until eventual occurrence of resistance[9]. Drugs targeting CDK4/6 or mechanistic target of rapamycin (mTOR) have been shown to delay endocrine resistance and improve progression-free survival of patients[10]. HER2-positive patients are treated with the HER2-blocker trastuzumab in combination with chemotherapy[11]. However, for TNBC there are not targeted therapy or recommended specific treatments so they are treated usually with platinum-based chemotherapeutic agents[12].

To date, we reached a considerable advance in our biological understanding of the phenomena underlying the occurrence of breast cancer and this has been translated in successful therapeutic approaches that have enormously increased patients' survival and the quality of their lives. However, when the disease reaches an advanced stage, we are lacking effective therapeutic strategies and the disease is considered to be incurable. Thus, a better understanding of the molecular mechanisms underlying the metastatic processes

of breast cancer is of critical importance for the design of novel therapies and the advancement of the research field.

Metastasis is the leading cause of death for patients with cancer

The ability of cancer cells to invade and colonize distant organs, forming secondary tumors called "metastasis", is considered a hallmark of cancer [13,14]. The advancements in diagnosis and treatment have led to a significant improvement of prognosis for patients presenting a tumor restricted to a primary site. However, the dissemination of tumor cells throughout the body is, in the majority of the cases, leading to multiple organ failures and is mostly incurable[15]. For this reason, metastasis formation is the leading cause of cancer-associated mortality, accounting for more than 90% of the deaths[16]. The lack of effective therapeutic strategies highlights how metastasis formation is the least understood process in cancer biology. However, many studies in the last years have contributed to shed light on the molecular mechanisms underlying the metastatic process. This knowledge has recently led to the definition of 4 hallmarks of metastasis: motility and invasion, modulation of the microenvironment, plasticity and colonization[17]. The acquisition of these characteristics is essential to sustain the dissemination of cancer cells throughout the body. The metastatic process, also known as metastatic cascade, is a stepwise process during which cancer cells invade the surrounding environment, intravasate into the circulation where they need to survive as circulating tumor cells, extravasate in a distant organ, interact with the new microenvironment to establish the colonies and ultimately reactivate their proliferation to form the clinically detectable metastatic lesions[15,18–20]. The complexity of this process is what makes our understanding still far from being comprehensive. However, underling this complexity, there are critical steps during metastasis formation that, if deeply understood, can open novel opportunities for the design of innovative therapeutic strategies.

The metastatic cascade

Motility and invasion

The first step that allows cancer cells to leave the primary tumor and start the metastatic process is the acquisition of motility and the ability of invading the surrounding tissue. These properties are often acquired by cancer cells by hijacking the normal cellular processes that during embryonic development are allowing an epithelial-mesenchymal transition (EMT)[21]. The switch from an epithelial to a mesenchymal state activates a series of cellular processes that are sustaining loss of cell-cell junctions, motility, invasiveness and extracellular matrix remodeling[22]. At the molecular level, these programs are activated by transcription factors that act as master regulators of the EMT processes such as Twist, Zeb1, Snail and Slug. The activation of this expressional reprograming is usually attributable to external factors such as interaction with the stroma and growth factors like transforming growth factor-β(TGF- β). The most recognized molecular switches during an EMT are represented by downregulation of the cytokeratins and E-cadherin, otherwise highly expressed in epithelial cells, and upregulation of mesenchymal markers such as N-cadherin, vimentin and fibronectin[23]. Interestingly, the induction of EMT has been found to enrich the population of cancer stem cells in different types of tumor and consequently increase their tumor-initiating potential, motility and invasion[24–26]. Thus, the idea that activation of an EMT program in cancer cells is critically conferring them properties sustaining motility and invasion, is widely accepted. However, the heterogeneity of expression of EMT markers during the different steps of metastasis formation and among different tissue types, has made it difficult to identify critical mechanisms that are essential in every context[15]. One of the reasons for this heterogeneity is that the activation of an EMT program in cancer cells is not an irreversible switch, but is more often a reversible state where cells have both epithelial and mesenchymal characteristics. Indeed, the opposite program that reverts from a mesenchymal to an epithelial transition

(MET) is often occurring in cancer cells that have metastasized to a secondary organ and have to acquire again those epithelial properties that support cell-cell interactions and uncontrolled proliferation[15,21,23].

Despite the indubitable importance of initiation of EMT in sustaining motility and dissemination of cancer cells as single cells, the most recurrent type of migration into the surrounding tissue from the primary tumors is in a collective of cells[27]. For example, invasion in clusters of cells has been identified in different types of tumors, including breast and colorectal cancer[28–30]. Noteworthy, high expression of the epithelial marker E-cadherin has been found in these invading groups of cells[28–30]. The retain of epithelial properties, such as cell-cell junction, in cancer cells that are collectively migrating, has risen the debate on whether the EMT is really a critical step during metastasis formation[15]. Yet, the recent re-evaluation of the EMT process in cancer as a reversible interchange of states between a fully epithelial or mesenchymal state, could support the idea that a transition towards mesenchymal characteristics might be important in supporting collective invasion. Indeed, migrating clusters are heterogeneous and mainly formed by two populations with different characteristics: 'leader cells' interacting with the extracellular matrix and driving the front of the migration, 'follower cells' that have more proliferative properties and are following the leader cells during the migration supporting their growth capacity[27,31]. A study aimed at the characterization of these two cell populations, conducted in lung cancer cell lines, has shown how leader cells highly express the mesenchymal marker Vimentin even though they do not express a traditional EMT signature[32]. Thus, leader cells seem to have certain mesenchymal characteristics that would suggest they are in a state during the EMT process that might drive collective cell migration. In conclusion, additional data are necessary to really define the role of EMT in supporting cancer cell invasion and its potential involvement during collective migration. Further studies are needed in order to define the critical molecular mechanisms that allows cancer cells to invade as compact clusters.

Intravasation and survival in the circulation

After acquiring motility and invading the surrounding tissue, cancer cells will eventually encounter a blood vessel and intravasate. The entrance into the vascular system is indeed the next critical step of the metastatic cascade[15,17,20,33]. The intravasation into blood vessel is the continuation of the invasion process during which cancer cells will degrade the extracellular matrix underlying endothelial cells and will extend their filopodia into the blood vessel lumen, without affecting the integrity of the endothelial barrier[17].

Once they have entered into the vasculature, circulating tumor cells (CTCs) undergo a variety of molecular and mechanical stresses that will make their survival very difficult. Indeed, part of the reason why the metastatic process is very inefficient, is the poor survival of cancer cells in the blood[33]. Notably, the number of circulating tumor cells in the blood of patients, even if rare, is much higher compared to the actual metastatic lesions[34]. In support of this clinical observations, also in murine models it has been shown that only 0.02% of circulating melanoma cells injected in the portal vein are able to form macro metastases in the liver[35,36]. Not only do CTCs face some physical challenges due to the shear stress, but they also have to overcome the caspase-dependent cell death called anoikis, induced by loss of matrix attachment, and escape the surveillance of the immune system[15,33]. Thus, in order to resist shear stress and escape the immune system response, cancer cells associate with platelets that, by producing TGF-β and PDGF, can inhibit the activity of natural killer cells[37]. In addition, the progression towards EMT, the integrin switch and the continuous activation of pro-survival signals, such as the PI3K/Akt pathway, are fundamental strategies that allow CTC to overcome anoikis[38]. In addition, it has been recently shown that melanoma cells in the circulation can undergo ferroptosis, a cell death program induced by lipid oxidation. However, this is not the case for metastatic cells spreading through the lymphatic system that are protected from the oxidative stress by the lymph environment[39]. Moreover, CTC have been found to get an advantage from the formation of cell clusters that prevents ROS accumulation that is usually induced in detached cells[40]. Moreover, the

formation of cell clumps facilitates, due to the size, the entrapment of CTC in small capillaries favoring their extravasation in distant organs[33].

Metastatic colonization

The last steps of the metastatic cascade consist of colonization of the distant organ and outgrowth. Once cancer cells have extravasated and infiltrated into a distant organ, they will need to escape the immune surveillance of the host tissue, interact with a supportive niche and finally reactivate their growth signaling pathways to establish a macro-metastasis.

Infiltrating into a distant organ is a very unfavorable process because it exposes disseminating cancer cells to different checkpoints challenging their vulnerabilities. Indeed, metastasizing cells show preferential sites of colonization of distant organs, however every host tissue represent a hostile microenvironment for a newly arrived cancer cells, even if some might be less hostile then others[33]. The first barrier is represented by the interaction with cells of the immune system and the organ-resident cells. Multiple groups have shown that natural killer cells (NK) and cytotoxic T cells are critical antagonist of infiltrating cancer cells. Depletion of T cells and NK cells or their uncontrolled activation increases or decreases respectively the number of metastasis in murine models[41–43]. Also, the interaction with other resident cell types can be challenging for metastatic cells. For instance, astrocytes can actively induce a pro-apoptotic program that kills infiltrating cancer cells in the brain by releasing the serine protease plasminogen activator (PA)[44].

One of the most important factors that allows infiltrating cancer cells to survive in a host tissue is the establishment of a supportive metastatic niche. The ability of creating a favorable interaction with the microenvironment to maintain homeostasis is a characteristic of adult stem cells and is highjacked in different forms by cancer cells to sustain their survival. In order to maintain the equilibrium between proliferation and quiescence, stem cells promote niches that are rich in molecular signals such as the chemokine CXCL12, Wnt, TGF-β and hedgehog[45,46]. Not only cancer cells have been found to colonize stem

cell niches, but they also actively produce factors to help the establishment of a supportive niche. Breast cancer-derived bone metastasis are found often in CXCL12 rich area because they often express the receptor CXCR4[47]. Moreover, metastatic cancer cells are found to secrete TGF-β and the extracellular-matrix protein tenascin C, which are both involved in Wnt signaling activation[48,49].

The establishment of a supportive metastatic niche is such a critical step for the progression of a metastatic tumor that the most aggressive types of primary tumor have been found to sustain this process by secreting factors into the circulation to prime niches in distant organs[33]. Primary tumors can pre-condition a distant organ by sending factors such as exosomes and inflammatory cytokines that help in creating a less deadly microenvironment even before metastatic cancer cells have spread[50,51]. For instance, pancreatic cancers can secrete exosomes containing macrophage inhibitor factor (MIF) that induces resident liver cells to produce TGF-β and fibronectin promoting metastasis formation[52]. Additionally, melanoma tumors can also release exosomes promoting inflammation and blood vessel leakiness creating a more supporting microenvironment for extravasation and infiltration of cancer cells[53]. Interestingly, the different integrin composition confers organ-specificity to the exosomes, which could partially explain why specific metastatic sites seems to be more recurrent for certain types of tumors[50].

Once infiltrating cancer cells have occupied and established the supportive niche, they will need to reactivate their signaling pathways to sustain survival and proliferation. In particular, the activation of proliferation can be delayed for a long time, even years, during which cancer cells enter a phase of dormancy[54]. Even though it is not clear when and how, this dormancy state will be reverted and the activation of cell signaling is critical for proliferation and the consequent establishment of the metastasis. Also, in this phase, the interaction with the microenvironment is of fundamental importance. Indeed, cancer cells can either activate new pathways or potentiate pathways that were already activated in autocrine or paracrine manner through the interaction with stromal cells. Among the most upregulated signaling pathways sustaining survival and proliferation is NFkB, Stat1, Hedgehog, Hippo, mitogen-activated protein

kinase (MAPK), phosphor-inositide 3-kinase-protein kinase B (PI3K-AKT) and hypoxia-inducible factor (HIF)[33]. For instance, the production of calprotectin (S100A8/9) by myeloid precursors can induce breast cancer cells to activate MAPK[55]. The interaction with stromal cells is also important to activate PI3K-AKT of breast cancer cells growing in the bone marrow through the production of CXCL12[56]. In the case of prostate cancer-derived metastasis, it has been shown how autocrine production of interleukin 6 (IL-6) is activating Stat3[57]. Thus, it appears that the plasticity of metastatic cancer cells allows them to activate oncogenic signaling in many different ways. Notably, the activation of cell survival and proliferation is not only driven by genetic factors but is profoundly influenced by the interaction with the microenvironment. For this reason, the oncogenic signaling in the primary tumors can be different compared to the one found in the metastasis. Despite the fact that the interaction between immune cells or organ-resident cells and the metastatic cells in the tumor microenvironment has been extensively studied, much less is known about the role of nutrient availability in creating a more supportive niche for metastasis formation.

Cellular metabolism supports breast cancer metastasis

The term *metabolite* is generally used to define the small molecules that are interconverted throughout the metabolic network by *metabolic enzymes*. Linked series of chemical reactions, catalyzed by the metabolic enzymes, form the so-called *metabolic pathways* and the rate of interconversion of metabolites throughout a pathway is defined as *metabolic flux.* Specifically, metabolic pathways can be divided into two main categories: *catabolic*, that break down molecules to generate energy; *anabolic,* that consume energy to produce biomass. What commonly is referred to as "cellular metabolism" is this complex network of biochemical reactions that allows the interconversion of metabolites and that is ultimately crucial for sustaining most cellular processes that are vital for a cell such as energy generation, anti-oxidant defense , biomass production and crosstalk with cell signaling pathways. Thus, metabolism is at the center of a

network of interactions that ultimately determines the cellular phenotype (**Figure 1.1**)[58]. Interestingly, these metabolic interactions have evolved to maintain plasticity in order to sustain the functional needs of different normal cell types. It is now well understood that cancer cells highjack these interactions in order to sustain their survival and uncontrolled proliferation.

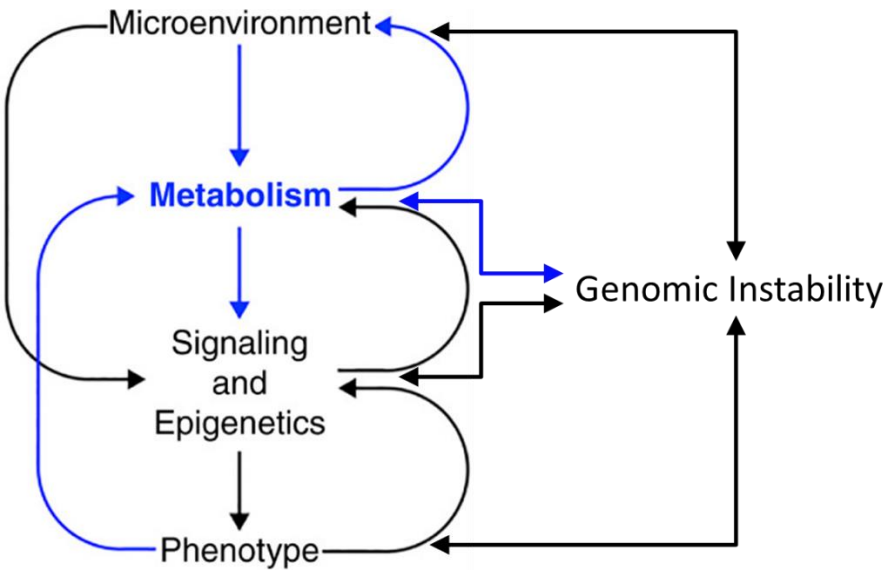

Fig 1.1 Schematic representation of the interactions governing the cell functions. In blue are highlighted the metabolic interactions. Adapted from the review Rinaldi et al. 2018,[58].

Glucose represents the major carbon source for proliferating cancer cells. Glycolysis converts glucose to pyruvate which can then be oxidized in the mitochondria during the tricarboxylic acid (TCA) cycle to efficiently produce high quantity of energy under the form of ATP through oxidative phosphorylation. However, most cancer cells are known to reduce pyruvate to lactate which is then passively released even in presence of oxygen, a phenomenon that is much less energy efficient and that is known as Warburg effect[59]. Already in 1924, Otto Warburg described this particular behavior of tumor cells and later postulated that, due to a defective mitochondrial function, aerobic glycolysis represents the metabolic origin of cancer cells[60]. Subsequently, different studies have shown that the Warburg effect is not only a characteristic of tumor cells, but more in general a feature of non-transformed highly proliferating cells *in vitro*[61].

Interestingly, it has been suggested that biomass production is a limiting factor for proliferating cancer cells and it can be fulfilled by aerobic glycolysis[61]. The increased glycolytic rate is needed to maintain sufficient levels of glycolytic intermediates that are necessary to produce amino acids, lipids and sustain the antioxidant response and nucleotides synthesis[61]. However, upregulation of glycolysis is only one of many metabolic adaptations that cancer cells acquire in order to sustain their survival and proliferation. Thus, metabolic rewiring is since 2011 considered as a hallmark of cancer[14]. During the last 20 years, the study of metabolic rewiring in cancer cells has received a lot of attention and has led to the discovery of novel therapeutic targets[62]. For example, the treatment of acute lymphoblastic leukemia (ALL) patients with L-asparaginase is currently approved (FDA, Biologic License Application (BLA): 101063). In many cases of ALL, cancer cells are dependent on extracellular asparagine because they lack the expression of the asparagine synthase enzyme. Thus, the treatment with L-asparaginase is used to deplete asparagine that is converted in aspartate and consequently starving leukemic cells[63]. Another successful example concerns the inhibition of a mutated version of the enzyme isocitrate dehydrogenase (IDH). IDH is a metabolic enzyme that has been found to be mutated in different types of tumor and generates an oncometabolite, which is a metabolite that acts as oncogenic signaling molecule[64].. The mutation induces the IDH enzyme to convert α-ketoglutarate (αKG) in the oncometabolite 2-hydroxyglutarate (2HG) inducing epigenetic changes that support cancer progression[65]. Recently, the small molecule inhibitors of mutant IDH Enasidenib and Ivosidenib have been approved for the treatment of patients with acute myeloid leukemia (AML) carrying an IDH mutation[65]. Moreover, the treatment of other types of tumor such as glioma, cholangiocarcinoma and chondrosarcoma is still under investigation[65].

While extensive studies have been carried out on the metabolic adaptations of primary tumors, only recently an increasing interest has focused on the role of metabolism during metastasis formation. The current knowledge on the metabolic rewiring of cancer cells during the metastatic process will be reviewed

in the next paragraphs, with particular focus on breast cancer which is of special interest for the topics treated in this thesis.

Metabolic adaptations in the primary tumor

Many different metabolic adaptations have been described in breast cancer involving both catabolic and anabolic pathways of glucose, glutamine, cholesterol, fatty acid synthesis and cofactors metabolism[62]. Given the focus of this thesis, particular attention will be given to the metabolic rewiring involving glucose metabolism (**Figure 1.2**).

The molecular diversity of breast tumors, already described in the previous paragraphs, is also reflected in their cellular metabolism. While ER-positive breast cancer cells are often characterized by an oxidative metabolism, TNBC are much more relying on the glycolysis to sustain their proliferative phenotype[62]: ER-positive tumors display the so-called reverse Warburg effect, which allows cancer cells to rely on oxidative metabolism thanks to the interaction with stromal cells. Cancer cell induce activation of HIF1α and NFκB in cancer-associated fibroblast (CAFs) that are thus becoming glycolytic. As a consequence, CAFs increase their release of lactate and pyruvate which become available for cancer cells to fuel their oxidative metabolism[66,67]. Conversely, triple-negative breast tumors have been found to be highly glycolytic[62]. In support of this notion, not only TNBC show increased glucose uptake in vivo, but also overexpression of glucose and lactate transporters and of the lactate dehydrogenase enzyme (LDH), which converts pyruvate to lactate and vice versa[68–71]. One of the reasons why cancer cells become glycolytic, is the activation of the branching pathways of the glycolysis that is necessary to fulfill the biomass production need of highly proliferating cells[61]. In particular, TNBC cells have been shown to activate the serine-glycine biosynthesis pathway which is branching from the glycolysis at the level of the 3-phosphoglycerate (3PG)[72,73]. Besides producing serine and glycine, the activation of this pathway produces αKG and contributes to the synthesis of glutathione, an important antioxidant, and nucleotides production. The first enzyme of *de novo* serine

biosynthesis, phosphoglycerate dehydrogenase (PHGDH), has been found to be genetically amplified and consequently overexpressed at the protein level in 70% of TNBC, supporting the hypothesis that serine synthesis activation is a common feature of these tumors[73]. Interestingly, genetic or pharmacological inhibition of PHGDH decreases *de novo* serine synthesis and proliferation of TNBC cells[72,73]. However, supplementation of additional amounts of extracellular serine is not sufficient to rescue this phenotype, suggesting that the critical role of this pathway in sustaining cancer proliferation goes beyond the sole maintenance of serine or glycine intracellular concentrations [72,73]. Notably, since inhibition of PHGDH proved to be effective in reducing tumor growth, also in other tumor types such as melanoma, different pharmacological inhibitors have been produced and are now available for pre-clinical studies[74,75].

Metabolic adaptations during the metastatic process

As discussed in earlier paragraphs, the study of metabolic adaptations in cancer cells has proven to be effective in discovering new potential therapeutic targets. Since metastasis formation is one of the least understood processes in cancer biology, the attention of the research is now focusing on finding new metabolic dependencies of metastatic tumor cells (Figure 1.2).

The involvement of metabolism in sustaining the metastatic process of breast cancer cells starts from the early phases. Indeed, different metabolic pathway have been found to be involved in the stimulation of motility and migration. For example, lactate and ketones can act as chemo-attractants stimulating cancer cell migration and metastasis formation in murine model of MDA-MB-231 cells[76]. Additionally, oxidative metabolism has been linked to activation of invasion in different types of cancer[77]. In particular in breast cancer, the increased expression of the transcription coactivator peroxisome proliferator-activated receptor gamma, coactivator 1 alpha (PGC-1α) promotes firstly mitochondrial biogenesis, oxidative

metabolism and consequently increases motility and metastatic potential[78]. As already introduced in earlier paragraphs, the activation of EMT is one of the key steps of the metastatic process. In breast cancer, different metabolites species have been connected to at least a partial activation of an EMT program. This is the case of arginine and phospholipid metabolism that when are increased they induce activation of EMT genes and in particular of its master regulator ZEB1[79,80].

Once breast cancer cells have acquired motility they will disseminate and attempt to colonize a distant organ. The success of this colonization depends on the ability of tumor cells to adapt the new microenvironment. However, this process is highly inefficient and leads to cell death of most of the disseminated cancer cells[33]. Interestingly, in order to prime the distant microenvironment and create a more permissive niche, primary breast tumors have been shown to secrete factors that can influence the nutritional composition of distant host tissues. Particularly, cancer-secreted exosomes have been shown to carry miR-122, a modulator of glucose metabolism that has been found to promote metastatic colonization by inhibiting glucose uptake of the resident cells of the host tissue, consequently increasing glucose availability for disseminating cancer cells[81].

The detachment from the extracellular matrix creates a metabolic need for more energy production[82]. Thus, colonizing breast cancer cells have been shown to adapt their cellular metabolism in multiple ways to produce more ATP[77]. The activation of the proline cycle has been shown to be critical in producing ATP in colonizing breast cancer cells[83]. One of the products of the proline cycle is FADH2, which is linked to the electron transport chain in the mitochondria, ultimately producing ATP. Interestingly, the disruption of this cycle by inhibition of the enzyme proline dehydrogenase (PRODH) leads to a decreased metastasis formation in murine models of breast cancer. Moreover, detached breast cancer cells have been found to increase the flux through pyruvate dehydrogenase (PDH) and consequently ATP levels by upregulation of Erbb2[84]. In addition, also the activity of PGC-1α has been found to be critical for breast cancer cells

metastasizing to the lung because it induces ATP production both through glycolysis and oxidative phosphorylation[85].

Once the metastasis if formed, the metabolic adaptations of secondary tumors can differ compared to the primary tumor. This is indeed the case for breast-cancer derived lung metastasis that are adapted to the nutritional microenvironment of the distant organ. The increased availability of pyruvate in the lung interstitial fluid, induces metastatic cells to activate pyruvate anaplerosis[86].In the case of breast cancer-derived metastasis growing in the lymph nodes, an increased expression of the enzyme transketolase of the pentose phosphate pathway (PPP) has been observed in comparison with the primary tumor[87]. Moreover, brain metastasis can be less dependent on glucose metabolism to proliferate and rely more on acetate as a carbon source for oxidative TCA cycle[88,89]. Interestingly, breast cancer cells metastasizing to the bones have been found to increase serine and lactate release[90,91]. As a consequence, osteoclasts become more fit and active and can create a more spacious and permissive metastatic niche[92].

In conclusion, despite the fact that there is not one single metabolic adaptation that is required during the whole metastatic process of breast cancer cells, essential differences in metabolic rewiring have been identified among the different steps of the metastatic cascade. Thus, studying the metabolic adaptations of cancer cells at the different steps of metastatization will be critical to have a deep understanding of this biological process and might allow the discovery of new therapeutic targets.

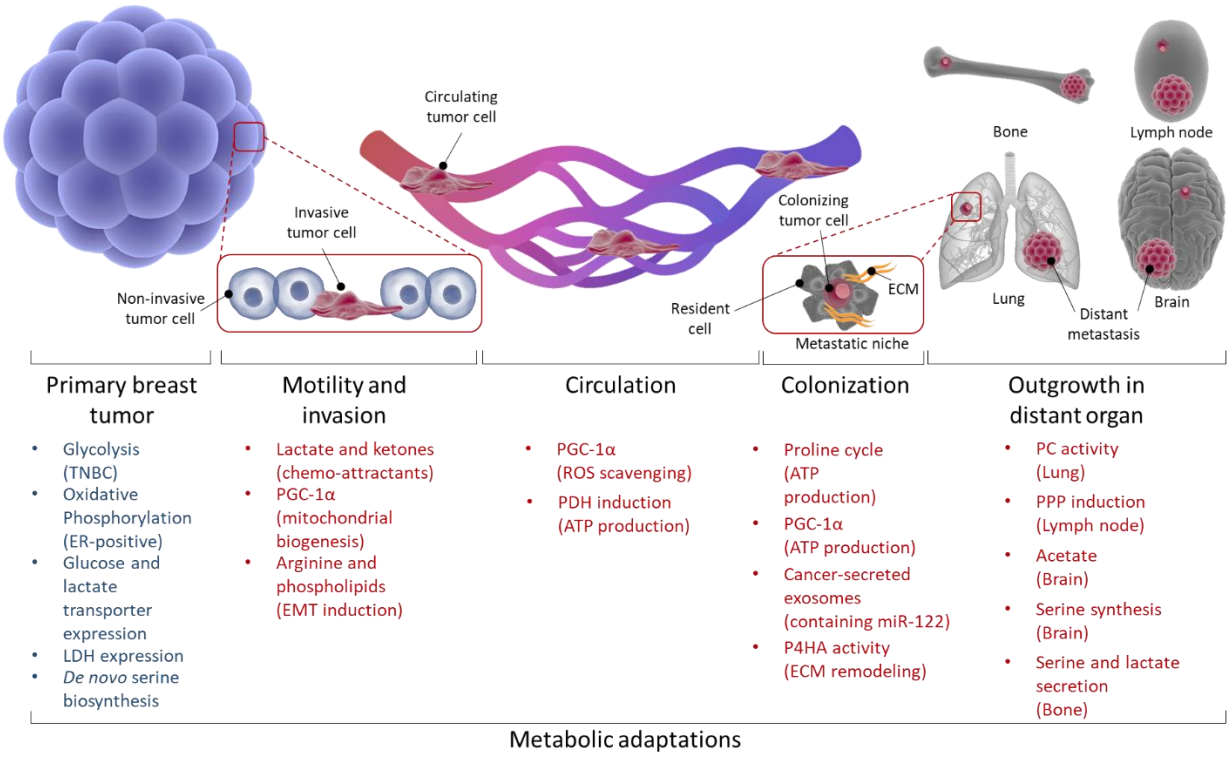

Fig 1.2 Schematic representation of the metabolic adaptations during the metastatic process that are described in this thesis. In blue are highlighted the metabolic adaptations of primary breast tumor. In red are highlighted the metabolic adaptations during the different steps of metastasis formation. List of abbreviation: TNBC, triple negative breast cancer; LDH, lactate dehydrogenase; PGC1-α, peroxisome proliferator-activated receptor gamma, coactivator 1 alpha; EMT, epithelial to mesenchymal transition; ROS, reactive oxygen species; ATP, adenosine triphosphate; PDH, pyruvate dehydrogenase; collagen prolyl-4-hydroxylase; PC, pyruvate carboxylase; PPP, pentose phosphate pathway; ECM, extracellular matrix.

Nutrient availability is a determinant of cancer progression

Cellular metabolism is highly plastic and influenced by the interactions with the extracellular environment[93]. In particular, the availability of nutrients is a determinant of intracellular metabolic rewiring and consequently of the cellular phenotype. This concept is of particular relevance for the biology of metastatic cells, because cancer cells growing in different tissues are exposed to different nutritional

microenvironments. Despite the fact that the term *nutrient* is generally referred to the substances that allow an intact organism to survive and grow, in the field of tumor microenvironment it is often utilized to refer to metabolites present in the extracellular environment that can be necessary for the survival and growth of cells within the tissues[93–97]. Thus, in this thesis with the term *nutrient* I will refer to metabolites available in the tissue microenvironment.

Recently, multiple studies have shown discrepancies between *in vitro* nutrient utilization by cancer cell compared to tumors growing *in vivo* in mouse models[93]. For instance, while lung cancer cell lines *in vitro* are highly dependent on glutamine contribution to the TCA cycle, lung tumors *in vivo* have been shown to have a minimal consumption of glutamine[96]. Additionally, breast cancer spheroids grown in a medium containing more physiological concentration of nutrients have been found to better recapitulate the metabolism of mammary tumors[95].

Based on these concepts, many recent studies have focused their attention on better understanding the role of the nutritional microenvironment in sustaining the metastatic process of breast cancer cells. In this respect it was observed that, the brain microenvironment contains very limited amounts of serine and glycine[98]. However, these two metabolites are critical to sustain proliferating cancer cells because they are involved in the synthesis of nucleotides and antioxidants production. Thus, brain metastasis are dependent on *de novo* serine and glycine synthesis to survive and proliferate[98]. Therefore, the availability of different concentrations of nutrients are depending on the host tissues and this can determine distinct metabolic dependencies in primary tumor and metastasis. This is the case of the lung microenvironment, which is characterized by an increased pyruvate availability[86]. Pyruvate metabolism plays also a critical role in sustaining the colonization phase of lung metastasis, activating the enzyme collagen prolyl-4-hydroxylase (P4HA) for collagen hydroxylation[99]. In particular, the generation of hydroxylated collagen is a fundamental step for the re-shaping of the extracellular matrix to allow cancer cell to build the metastasis. The pyruvate availability found in the nutritional microenvironment of the lung, determines an increased α-ketoglutarate

intracellular level which in turn activates the enzyme collagen prolyl-4-hydroxylase (P4HA)[99]. Noteworthy, inhibition of pyruvate uptake impairs metastasis formation of breast cancer-derived lung metastasis in mice. In addition, multiple metabolite transporters have been found to be overexpressed and functionally relevant in sustaining metastasis formation. For example, the glucose transporter GLUT3 is highly expressed in breast cancer-derived brain metastasis[100]. Moreover, overexpression of the cystine-glutamate antiporter SLC7A11 has been found in brain and lung metastasis[101,102].

Thus, it is clear that the nutritional composition of the microenvironment is a crucial determinant of intracellular metabolism and consequently plays a central role during breast cancer metastasis. In particular, this indicates that metastasis might adapt to the new environment and be dependent on different metabolic pathways compared to the primary tumor. Therefore, studying the relationship between nutrient availability and intracellular metabolism might allow the discovery of new vulnerabilities of metastatic cells. Specifically, still very little is known about the contribute of metabolic pathways in sustaining activation of cell signaling in cancer cells that have colonized a distant organ.

mTORC1 activation during the metastatic cascade

The activation of cell signaling sustaining the establishment of primary tumors has been widely studied and described[103], however much less is known about signal transduction during the metastatic process. One of the most important signaling pathways, that coordinates nutrient availability and cellular proliferation, is mammalian target of rapamycin (mTOR), which is a serine/threonine-specific protein kinase that exists in two complexes, namely mTORC1 and mTORC2[104]. The two complexes share the core subunits mTOR, which is the catalytic subunit, DEP- domain-containing mTOR-interacting protein (Deptor) and mammalian lethal with Sec13 protein 8 (mLST8). The major difference is the presence of regulatory-associated protein for mTOR (Raptor) in mTORC1 and rapamycin-insensitive companion of mTOR (Rictor) in mTORC2. Raptor and

Rictor act as scaffold subunits interacting with mTOR and other regulatory subunits that are exclusive for complex 1 or 2. On the one hand, mTORC1 contains also proline-rich AKT substrate 40kDa (PRAS40), and on the other hand, mTORC2 contains mammalian stress-activated protein kinase-interacting protein 1 (mSIN1) and Protein observed with Rictor (Protor)[94,104]. The mTOR complex 1 is of particular interest for this thesis because it has been shown to be a regulator of cell growth and proliferation and its activation has been linked to availability of growth factors and nutrients[94,104].

mTORC1 activation is often dysregulated in many types of tumors, including breast cancer[105]. The increased phosphorylation of the mTORC1 pathway components has been correlated with a worse prognosis for patients and this dysregulation seems to be more common in triple-negative breast cancers[106,107]. However, multiple studies have highlighted the involvement of mTORC1 activation also during the metastatic process. For example, epithelial cell adhesion molecule (EpCAM) promotes EMT and metastasis formation of nasopharyngeal carcinoma through activation of the mTORC1 pathway by increasing the phosphorylation of the downstream targets p70 S6K kinase and 4EBP1[108]. In non-small-cell lung cancer, miRNA-193a-3p and -5p have been identified as metastatic suppressors. Interestingly, mTORC1 is among the targets of these miRNAs and its inhibition is required to suppress invasion, EMT and metastasis formation[109]. In the same tumor type, a second study has shown that the long non-coding RNA MetaLnc9 is a driver of metastasis formation and acts through activation of the AKT/mTOR signaling pathway[110]. Also, in the context of breast cancer cells, mTORC1 activation has been connected with increased motility and metastasis formation[111]. In particular, caveolin-1 is activated in low shear stress in MDA-MB-231 cells and this induces invadopdia formation, motility and consequently metastasis via activation of the mTORC1 pathway[111].

mTORC1 is a central hub that coordinates and senses extracellular stimuli and translates them in activation of cell growth and proliferation[104]. For example, growth factors can induce mTORC1 activity via the mediation of the tuberous sclerosis complex 2 (TSC2)[112]. In particular, growth factors sensing activates the PI3K/Akt and Ras/MAPK pathways that induce mTORC1 by inhibiting TSC2, which negatively regulates

mTORC1 by blocking the activity of Rheb, a positive regulator of mTORC1[104] (**Figure 1.3**). However, also other nutrients can regulate mTORC1 including metabolites such as amino acids, glucose, α-KG and nucleotides[113]. Different amino acids, including leucine, serine and arginine, have been involved in the activation of the mTORC1 pathway[114]. In particular, amino acids are able to induce mTORC1 via the RagGTPases that allow the translocation of the complex to the lysosomal surface which is considered a hub for mTORC1 signaling[112]. The need for the physical presence of mTORC1 on the lysosomal surface, guarantees that only when the conditions for proliferation are optimal, so when both amino acids and growth factors are present, the complex can be activated[104]. In addition, low levels of glucose can induce an inhibitory binding between the glycolytic enzyme hexokinase 2 and mTORC1[115]. Moreover, multiple groups have recently shown how increasing intracellular a-ketoglutarate levels, through activation of pathways glutamine catabolism, can induce activation of mTORC1[116–119].

Thus, mTORC1 is a central coordinator of nutrient availability and cellular phenotype. Extensive studies have revealed the key role of mTORC1 hyperactivation in sustaining primary tumor progression and the early stages of metastatization, however how this pathway is activated in breast cancer metastasis remains elusive. The recent findings showing a differential nutrient availability in primary tumors and metastatic sites, suggest that the metabolic mechanism of activation of mTORC1 signaling might be tissue-specific.

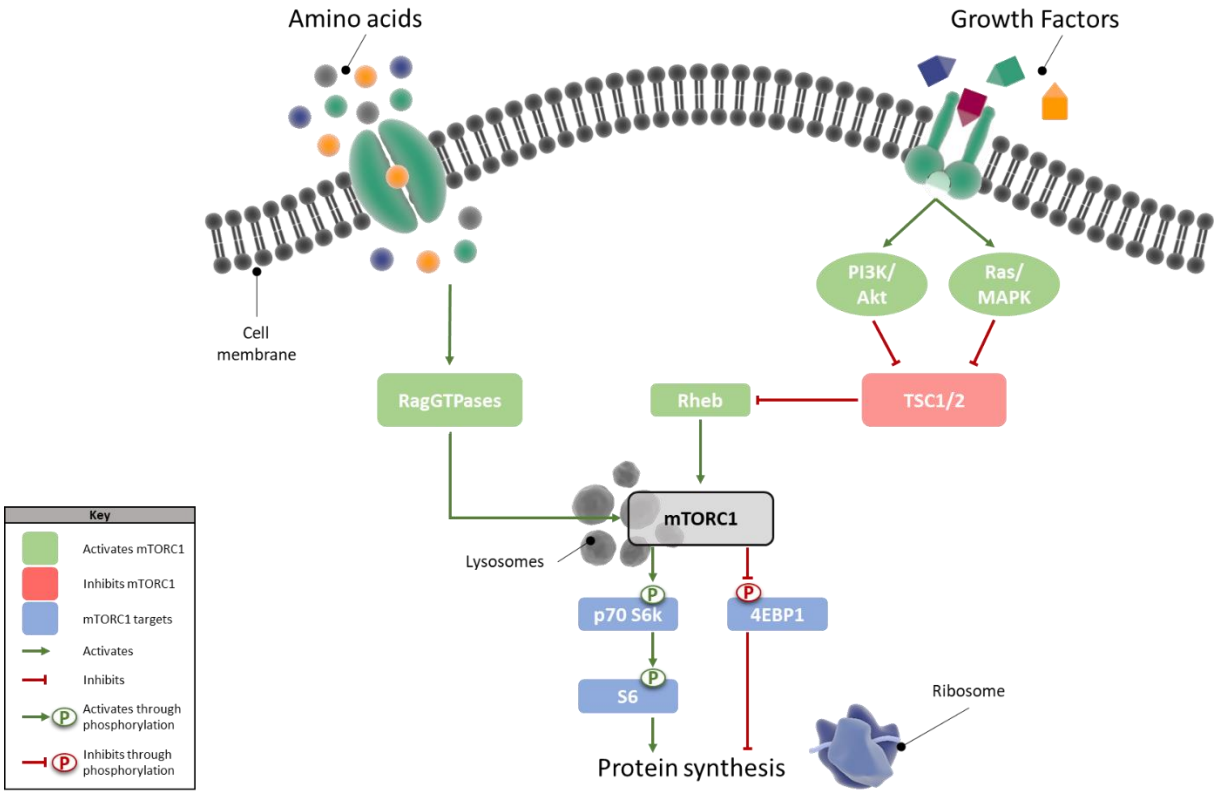

Fig 1.3 Simplified schematic representation of the mechanisms of regulation of mTORC1 that are described in this thesis. For simplicity, PI3K/Akt and Ras/MAPK signaling pathways are represented as a single entity, but in reality, they consist of a series of consecutive chemical reactions catalyzed by different enzymes. List of abbreviation: mTORC1, mammalian target of rapamycin complex 1; p70 S6K, ribosomal protein S6 kinase beta-1; S6, ribosomal protein S6; 4EBP1, eukaryotic translation initiation factor 4E-binding protein 1; Rheb, Ras homolog enriched in brain; TSC1/2, tuberous sclerosis complex.

OBJECTIVES

Despite the enormous advancement in the understanding of breast cancer biology, many aspects of metastasis formation remain elusive. In particular, little is known about the activation of cell signaling that sustains proliferation during the metastatic outgrowth. However, understanding the molecular mechanisms that are behind the proliferation of metastatic cells is of critical relevance for the discovery of new therapeutic targets.

Interestingly, the composition of the nutritional microenvironment has recently emerged as a major determinant of cellular metabolism, suggesting that primary tumors and distant metastasis might depend on distinct metabolic rewiring induced by the microenvironment. Notably, both extracellular nutrient availability and intracellular metabolic activities are involved in the activation of the mTORC1 pathway, which is a key signaling hub sustaining cell growth and proliferation of primary tumors. However, still little is known about the effects of the nutrient microenvironment both on the cellular metabolism and on the activation of the mTORC1 signaling pathway during metastatic outgrowth.

Thus, we have investigated whether the specific nutrient availability in the metastatic site can lead to metabolic adaptations and cell signaling activation that sustain metastatic proliferation in a distinct manner compared to the primary tumor. We focused our attention on comparing nutrient metabolism and metabolic regulation in primary breast tumors versus lung metastases. Specifically, we addressed the following questions:

- Is nutrient availability a determinant of metabolic rewiring and mTORC1 activation in breast cancer cells growing in the lung?
- Are primary tumors and lung metastasis relying on the same signaling pathways or metabolic dependencies to sustain their proliferation?

To answer these questions, we performed metabolomics and ^{13}C-tracer analysis to define cellular metabolism and western blot-based assays to assess mTORC1 activation both *in vitro* and *in vivo*. A comprehensive description of the experimental techniques used for this thesis can be found in chapter 2. In chapter 3, we identified the metabolic requirements for cell signaling activation of breast cancer cells growing in the lung. In particular, we found that pyruvate extracellular abundance in the lung interstitial fluid is a driver of intracellular serine biosynthesis and increases α-ketoglutarate production in lung metastasis. As a consequence of this metabolic adaptation, the increased α-ketoglutarate levels are inducing activation of the mTORC1 pathway. Finally, we demonstrate that lung metastases have different metabolic requirements for the activation of the mTORC1 pathway compared to the primary breast tumors. Chapter 4 presents an overarching summary with concluding remarks.

Chapter 2. Materials and Methods

Cell lines

Human HEK293T epithelial cells, MDA-MB-231, MCF-7 and MDA-MB-468 breast adenocarcinoma cells, murine 4T1 mammary gland cancer cells, A549 human epithelial lung carcinoma cells and HCT 116 colorectal carcinoma cells were obtained from ATCC. HEK293 T, MDA-MB-231, MCF-7, MDA-MB-468, A549 and HCT 116 cells were cultured in high glucose (4.5 g/L) Dulbecco's modified Eagle's medium (DMEM) (Life Technologies) supplemented with 10% heat-inactivated fetal bovine serum (Life Technologies), 1% penicillin (final concentration of 50 U/mL) (Life Technologies) and 1% streptomycin (final concentration of 50 μ/mL) (Life technology). 4T1 cells were cultured in Roswell Park Memorial Institute (RPMI) 1640 Medium (Life Technologies) supplemented with 10% heat-inactivated fetal bovine serum (Life Technologies), 1% penicillin (final concentration of 50 U/mL) (Life technologies) and 1% streptomycin (final concentration of 50 μg/mL) (Life Technologies). The heat-inactivation of the fetal bovine serum was performed at 55°C for 45 minutes. Hygromycin B and puromycin dihydrochloride (Life Technologies) were added to the growth medium for selection of overexpression and knockdown cell lines, respectively. Blasticidin S HCl (Life Technologies, R21001) was added to the growth medium for selection of Luciferase-expressing cells. All cell lines were confirmed to be mycoplasma-free by Mycoalert detection kit (Lonza). HEK 293T, MDA-MB-231, MCF-7 and MDA-MB-468 cells were validated by DNA fingerprinting.

Mouse models

All animal experiments were approved by the local authorities in compliance with all relevant ethical regulations. For injection models, mice were randomized before injection of cancer cells. All samples were

analyzed blinded. Sample size was determined using power calculations with B = 0.8 and P < 0.05 based on preliminary data and in compliance with the 3R system: Replacement, Reduction, Refinement.

Mammary fat pad model

Six-week-old female BALB/c (Envigo) or NMRI nu/nu (Taconic) mice were inoculated with 4T1, 4T1 CTR or 4T1 shPHGDH cells in the mammary fat pad (m.f.; 1x106 cells, in 50µL PBS using a 30G syringe). Rapamycin (Selleckchem, S1039) treatment was started 5 days after cell injection. Rapamycin (1 mg per kg) was intraperitoneally injected every 48h. Rapamycin was dissolved in a solution of 2% DMSO (Merck Sigma, D4540), 30% polyethylene glycol 300 (Merck Sigma, 90878), 5% Tween80 (Merck Sigma, P4780) and ddH20 and used promptly after mixing as indicated by the manufacturer. The drug was dissolved at a concentration of 0.0002 mg per µL. α-Cyano-4-hydroxycinnamic acid (Merck Sigma, C2020) acute treatment consisted of two injections in the last two days of the experiment to only investigate short-term effects of the molecular mechanisms triggered by pyruvate uptake inhibition on the phosphorylation of mTORC1 targets. α-Cyano-4-hydroxycinnamic acid (60 mg per kg) was intraperitoneally injected. α-Cyano-4-hydroxycinnamic acid was dissolved in a mix containing 1.5% DMSO, 60% β-cyclodextrin (Santa Cruz, SC-203461A) (from an initial 30% aqueous solution), 35% polyethylene glycol 300 and 5% ethanol and pH neutralized with NaOH. The drug was dissolved at a concentration of 0.03 mg per µL. The same mix without drug was injected as a vehicle to control animals. Treated and control mice were randomly chosen. Mice were euthanized 21 days after cell injection. The last dose of drug was given on the last day, two hours before euthanasia. To follow the effect on the primary tumor of Rapamycin treatment, tumor volumes were measured during the experiment using a caliper. Additionally, at the end of the experiment, primary tumors were dissected and weighted. Humane end points were determined as follows: tumor size of 1.8 cm3, loss of ability to ambulate, labored respiration, surgical infection or weight loss over 10% of initial body weight. Mice were monitored and upon detection of one of the previous mentioned symptoms, the animal was euthanized. BALB/c mice and NMRI

nu/nu mice were housed respectively in filter top cages and IVC cages. Housing and experimental animal procedures were approved by the Institutional Animal Care and Research Advisory Committee of KU Leuven, Belgium. The animal study complies with ethical regulations and was approved by the KU Leuven ethics committee.

Lung injection model

Six-week-old female NMRI nu/nu (Taconic) mice were inoculated with 4T1 CTR, shPHGDH (l.i.; 4x104 cells) or MDA-MB-231 CTR, overexpressing PHGDH (OE PHGDH) (l.i.; 9x105 cells) in the lung. Mice were first anesthetized using a ketamine/xylazine solution (37.5% Ketamine, 12.5% xylazine, 50% saline solution at 0.9%). Ketamine initial concentration was 100 mg per mL. Xylazin initial concentration was 20mg per mL. Subsequently, 40µL of cell suspension (50% PBS, 50% Matrigel) were injected into the right side of the mouse, under the armpit between 5th and 6th costal rib, 5mm deep using a 29G syringe (Becton Dickinson Medical, BDAM324892). Immediately after injection, the mice were turned on their right side and monitored until they woke up.

When 4T1 cells were injected, Rapamycin (1mg per kg) treatment was started the day after cell injection. Rapamycin was injected intraperitoneally every 48h until the end of the experiment. Mice were euthanized after 10 days from cells injection. When MDA-MB-231 cells were injected, Rapamycin (1mg per kg) treatment was started 9 days after cell injection. Rapamycin was injected intraperitoneally every 48h until the end of the experiment. Mice were euthanized 21 days after cell injection. Treated and control mice were randomly chosen. The last dose of Rapamycin was given on the last day, two hours before euthanasia. Humane end points were determined as follows: loss of ability to ambulate, labored respiration or weight loss over 10% of initial body weight. Mice were monitored and upon detection of one of the previous mentioned symptoms, the animal was euthanized. NMRI nu/nu mice were housed in IVC cages. Housing and experimental animal procedures were approved by the Institutional Animal Care and Research Advisory

Committee of KU Leuven, Belgium. The animal study complies with ethical regulations and was approved by the KU Leuven ethics committee.

MMTV-PyMT tumor generation

Mouse experiments were performed under the Animal Study Protocol LPG-002, approved by the National Cancer Institute (NCI) Animal Use and Care Committee. BL10 (MMTV-PyMT/FVB x C57BL/10J), BL6 (MMTV-PyMT/FVB x C57BL/6J), CAST (MMTV-PyMT/FVB x CAST/EiJ) or MOLF (MMTV-PyMT/FVB x MOLF/EiJ) mice were generated as previously reported (Lifsted et al., 1998). Mice were euthanized by cervical dislocation following anesthesia by Avertin at humane end point as determined by the institute veterinarian. Tumor tissue was excised and immediately flash-frozen in liquid nitrogen, then placed at -80°C for long term storage.

Knockdown and overexpression strategies

The plasmids pLKO expressing the shRNA sequences for PHGDH #1 and #2 were obtained from BCCM (Belgian co-ordinated collections of micro-organisms). PHGDH knock down #3 in 4T1 cells was generated using the plasmid pLKO-shRNA2 vector expressing the shRNA against PHGDH obtained from the Peter Carmeliet's lab (VIB/KU Leuven) (Vandekeere et al., 2018, PHGDH KD1). The same plasmid expressing a non-targeting shRNA sequence was used as control. Lentiviral particles were produced in HEK293T cells. Transduction of 4T1 cells was performed overnight and the medium was replaced the next day. Cells were selected with puromycin at a concentration of 2 μg/mL. The overexpression of PHGDH in MDA-MB-231 and MCF-7 cells was generated using the plasmid pLHCX expressing the PHGDH cDNA obtained from the lab of Prof. Matthew Vander Heiden (MIT). The empty plasmid pLHCX was used as a control. Retroviral particles were produced in HEK293T cells. Transduction of MDA-MB-231 and MCF-7 cells was performed overnight

with freshly prepared virus and the medium was replaced the next day. Cells were selected with hygromycin in a concentration of 400 µg/mL. Knock down or overexpression of PHGDH was validated by western blot analysis.

Starvation and reactivation

Cells were seeded in a 10 cm dish to be 70-80% confluent at the end of the experiment. The day after seeding, cells were starved from serum over night for 16h. Subsequently, cells were washed with Dulbecco's phosphate-buffered saline (dPBS) and starved 1 additional hour in Hanks' Balanced Salt Solution (HBSS) (Thermo scientific, 14025050). Next, cells were reactivated with medium containing dialyzed FBS in presence or absence of2mM Sodium Pyruvate (Merck Sigma, P8574), in presence or absence of 1mM Dimethyl α-ketoglutarate (Merck Sigma, 349631) and collected after the indicated time points. Time 0' conditions were collected immediately after the starvation with HBSS.

Protein extraction and western blot analysis

Cells were collected in dPBS and lysed in RIPA lysis and extraction buffer (Thermo Scientific, 89901) supplemented with protease (Merck Sigma, 5892970001) and phosphatase inhibitors (Merck Sigma, 4906845001). Frozen tissue samples were placed in 1.5 mL tubes with sufficient amount of RIPA buffer and grinded with a tissue lyser to help the lysis of the tissue.

Extracted proteins were quantified using a Pierce BCA Protein Assay Kit (Thermo Scientific, 23225). Subsequently, 15-40 µg of proteins were loaded on a precast gel NuPAGE Novex 4-12% Bis-Tris (Thermo Scientific, NP0336BOX) or a freshly casted 16% Acrylamide/Bis-acrylamide 29:1 (Biorad, 1610156) gel for 4EBP1 separation. Proteins were then transferred on a nitrocellulose membrane using an iBlot dry blotting

system with iBlot transfer stacks (Thermo Scientific, IB301031). Membranes were incubated for 1h at room temperature in a blocking solution of 5% milk TRIS Buffer Saline 0.05% Tween (TBS-T). Subsequently, membranes were incubated over night at 4°C with primary antibodies against either p70 S6K kinase (Cell Signaling Technology, 9202S), Phospho-p70 S6K Kinase (Thr389) (Cell Signaling Technology, 9205), S6 Ribosomal Protein (5G10) (Cell Signaling Technology, 2217S), Phospho-S6 Ribosomal Protein (Ser240/244) (D68F8) (Cell Signaling Technology, 5364S), β-Actin (Merck Sigma, A5441), PHGDH (Merck Sigma, HPA021241), PSAT1 (Bio-techne, H00029968-A01), PSPH (Merck Sigma, HPA020376), 4EBP1 (Cell Signaling Technology, 9452S), Phospho-4EBP1 (Ser65)(Cell Signaling Technology, 9451S), Vinculin (Cell Signaling Technology, 4650S). All primary antibodies were used in a 1:1000 dilution in 5% bovine serum albumin in TBS-T. The following day, membranes were incubated with HRP-linked secondary antibodies anti rabbit (Cell Signaling Technologies, 7074S) or mouse (Cell Signaling Technologies, 7076S) used 1:2000 in 5% milk in TBS-T. Bound antibodies were visualized using SuperSignal West Femto Maximum Sensitivity Substrate (Thermo Scientific, 34095) or SuperSignal West Pico PLUS Chemiluminescent Substrate (Thermo Scientific, 34580). Images were acquired using an ImageQuant LAS 4000.

To detect both the total and phosphorylated form of p70 S6K kinase, S6 Ribosomal protein and 4EBP1, samples were loaded twice on two different gels. β-Actin or Vinculin were used as loading control. In the figures showing the phosphorylation status of the mTOR target, one representative β-Actin blot is shown. The β-Actin shown is always coming from the very same gel were the phosphorylated proteins are blotted. Images were quantified using the software Image Studio Lite.

Protein synthesis (SUnSET)

Puromycin incorporation into newly synthesized protein was used to quantify protein synthesis as previously described[120]. Cells were seeded in a 6cm dish to be 70-80% confluent at the end of the

experiment. The day after seeding, cells were starved from serum over night for 16h in medium in presence or absence of 2mM Sodium Pyruvate, in presence or absence of Dimethyl α-ketoglutarate. Subsequently, cells were washed with Dulbecco's phosphate-buffered saline (dPBS) and starved 1 additional hour in Hanks' Balanced Salt Solution (HBSS) in presence or absence of 2mM Sodium Pyruvate, in presence or absence of 1mM Dimethyl α-ketoglutarate. Next, cells were reactivated with medium containing dialyzed FBS in presence or absence of 2mM Sodium Pyruvate, in presence or absence of 1mM Dimethyl α-ketoglutarate and 100nM cycloheximide or 0.001% DMSO for a total of 30 minutes. During the last 10 minutes of reactivation, puromycin was added to the medium at a concentration of 10µg per mL. After cell collection and protein extraction, puromycin incorporation was evaluated by western blot analysis using an anti-puromycin antibody (Merck, MABE343).

^{13}C tracer analysis

The utilization of stable heavy isotopes, such as ^{13}C in used in this thesis, allows to assess nutrient utilization and relative metabolic pathways activity[121]. A specific tracer can be added to the *in vitro* culture conditions to be metabolized by the cells. Thus, the fate of the heavy isotopes can be followed through the metabolic network generating labeling enrichments until no further changes can be detected. This condition is called isotopic steady state and it is dependent on the tracer utilized, on the pathway of interest and on the cell type[121]. In the case of a tracing with fully labeled (all the carbons are heavy isotopes) $^{13}C_6$-glucose, a steady state of the glycolytic intermediates is generally reached in a few minutes while it might take even some days for this to happen when looking at fatty acid metabolism. The tracer determines the mass distribution vector (MDV) of the metabolite of interest. The MDV represents the fractions of a metabolite that differ only in their heavy isotope composition (isotopologues). The incorporation of ^{13}C atoms generates a mass increase that allows the identification of the different isotopologues of a metabolite by gas or liquid

chromatography followed by mass spectrometry. Thus, a given metabolite can be either completely unlabeled (m+0) or labeled until m+*n* (m+1; m+2;…m+*n*; with n being the maximum number of carbons that can be labeled from the tracer). The fractional distribution of the isotopologues provides information about the relative activity of a pathway[121]. For example, relative activation of *de novo* serine biosynthesis can be measured from fully labeled glucose. The serine biosynthesis pathway produces *de novo* serine using glucose as a carbon source. Thus, activation of serine biosynthesis generates an enrichment of the m+3 serine isotopologue that can be used as readout for the activity of the pathway. These concepts can be applied to assess pathway activity at tissue or organ level in *in vivo* mouse models through $^{13}C_6$-glucose infusion.[122]

Surgery and $^{13}C_6$-glucose infusion

The mammary fat pad model in BALB/c mice was used for the $^{13}C_6$-glucose infusion experiment. Mice were implanted with a jugular vein catheter and, after one week of recovery time, infused with $^{13}C_6$-glucose as previously described[123]. Briefly, after mice anesthetization with isoflurane, a catheter was inserted in the jugular vein and connected to an antenna protruding from the dorsal part of the mice. Mice were left recovering single housed for 1 week after surgery. Next, mice were infused for 6h with a solution of 500 mg per mL of $^{13}C_6$-glucose, at a rate of 30 mg per kg per min. At the end of the infusion protocol, mice were sacrificed and all tissues of interest were collected and stored.

Tissue collection and preparation for protein and metabolite extraction

At the end of every in vivo experiment, mice were sacrificed by injecting approximately 50 µL of a 60 mg per mL Dolethal (pentobarbital sodium) solution (Vetoquinol). Blood was quickly collected via cardiac puncture, stored in heparin-coated tubes and centrifuged to separate the plasma. Primary tumors, lung

metastases, lung tumors and lung healthy tissue were dissected and washed in ice-cold saline, placed into pre-labelled bags and frozen using a liquid-nitrogen-cooled Biosqueezer (Biospec Products). The bags were then placed in liquid nitrogen until all collections were finished and finally stored at -80°C until further processing.

For tissue preparation for metabolite extraction, the tissue was weighed (10–15 mg) and pulverized (Cryomill, Retsch) under liquid-nitrogen conditions. The pulverized tissue was next used for metabolite extraction as described below.

Hematoxylin and eosin staining

Hematoxylin and eosin staining were used to measure the area of cancerous lesions in the lung of the different mouse models. During dissection, the lungs were gently infused via the trachea with 10% neutral buffered formalin. Next, samples were embedded in paraffin and sliced in 5 µm thick sections that were stained with hematoxylin and eosin. Metastatic area was quantified by ZEN Blue software (Zeiss).

Lung interstitial fluid extraction

The lung interstitial fluid extraction method has been adapted and modified from Nagahashi M, et al. J Mammary Gland Biol Neoplasia, 2016 and from Wiig H, et al, Am J Physiol Heart Circ Physiol, 2003. For collection of human samples, the study was approved by the local ethics committee (Medical Ethics Committee UZ/KU Leuven) under the protocol S57123. Human 'normal' lung tissue was collected from patients who underwent lung surgery for emphysematous lung volume reduction or tumorectomy. In the latter case, lung tissue from the resection specimen was taken as far away as possible from the tumor front. Following surgical resection, lung samples were taken and transported to our research facility. For the collection of lung samples from mice, five 9-weeks old healthy Balb/c female mice have been euthanized

with 50µL of 60mg/ml of Dolethal (pentobarbital sodium), lungs were harvested by surgical resection, washed with a blood bank saline solution and dried from liquid excess by carefully tapping in a gauze. Subsequently, the organs were placed in a filtered centrifuge tube created by using a column-centrifuge tube in which the pre-existent filter has been substituted with a nylon mesh filter with 20 µm opening pores (Spectrum Labs, Product code: 145811). For the human samples, the tissue was cut in pieces of around 100 mg that were placed in distinct filtered centrifuge tubes. The interstitial fluids (around 2-5 µL for mouse samples, around 3-10 µL) was collected in the column-centrifuge tubes by centrifugation at 400g, 4 °C for 10 minutes. The lung interstitial fluid was stored in dry ice immediately after extraction.

Gender	Age (y)	Reason of surgery
M	68	volume reduction surgery in emphysema
M	69	volume reduction surgery in emphysema
M	58	peritumoral normal lung tissue from tumorectomy
F	64	volume reduction surgery in emphysema
F	56	peritumoral normal lung tissue from tumorectomy
F	34	peritumoral normal lung tissue from tumorectomy
M	66	peritumoral normal lung tissue from tumorectomy

Table 1, Metadata related to Figure 1d and Figure2d.

Metabolites measurements

All experiments where Sodium Pyruvate was supplemented in the culture medium, as well as labeling experiments, were performed in media with 10% dialyzed serum for the indicated time points. Metabolites for the subsequent mass spectrometry analysis were prepared by quenching the cells in liquid nitrogen followed by a cold two-phase methanol-water-chloroform extraction. Phase separation was achieved by centrifugation at 4 °C. The methanol-water phase containing polar metabolites was separated and dried using a vacuum concentrator. Dried metabolite samples were stored at −80 °C.

The extraction of metabolites from the tissues of the MMTV-PyMT mouse model was conducted as following. Metabolites were extracted from tumors using a modification of the Bligh and Dyer method (Bligh and Dyer, 1959) . Flash-frozen tumor chunks were immersed in a mixture of HPLC-grade methanol and water (5:3 ratio) kept at −20°C and homogenized on a Precellys Evolution tissue homogenizer (15 s × 1 cycle, 10,000 rpm). HPLC-grade chloroform was added (methanol:water:chloroform ratio to 5:3:5), the mixture vortexed for 10 min at 4°C, and centrifuged at maximum speed (16,000 × g) for 10 min at 4°C to achieve phase separation. The methanol-water phase containing polar metabolites was separated and dried under a stream of nitrogen gas. The dried metabolite samples were stored at −80°C until analysis. The protein interphase was also dried down and dissolved in 1 mL 0.2 mM potassium hydroxide, and the protein concentration was then quantified using the Pierce BCA Protein Assay Kit (Thermo Fisher). To normalize sample concentrations, the dried metabolite extracts were resuspended in HPLC-grade water at volumes corresponding to their protein quantification values.

Gas chromatography-mass spectrometry

Amino acids and organic acids of the central carbon metabolism were measured with gas chromatography-mass spectrometry. Polar metabolites were derivatized for 90 min at 37 °C with 20 µl (13 µl in the case of the interstitial fluids) of 20 mg per ml methoxyamine (Merck Sigma, 226904) in pyridine (Merck Sigma, 270970). Subsequently, 15 µL of N-(tert-butyldimethylsilyl)-N-methyl-trifluoroacetamide, with 1 % tert-butyldimethylchlorosilane were added to 7.5 µL of each derivative and incubated for 60 min at 60 °C (Merck Sigma, 375934)[124]. Isotopologue distributions and metabolite concentrations were measured with a 7890 A GC system (Agilent Technologies) combined with a 5975C Inert MS system (Agilent Technologies). 1 µl of sample was injected into a DB35MS column in split mode (ratio 1 to 3) using an inlet temperature of 270 °C. The carrier gas was helium with a flow rate of 1 ml per min. Upon injection, the GC oven was set at 100 °C

for 1 min and then increased to 105 °C at 2.5°C/min and with a gradient of 2.5 °C/min finally to 320°C at 22°C/min. The measurement of metabolites has been performed under electron impact ionization at 70 eV using a selected-ion monitoring (SIM) mode. Isotopologue distributions were extracted from the raw ion chromatograms using a custom Matlab M-file, which applies consistent integration bounds and baseline correction to each ion[125]. In addition, we corrected for naturally occurring isotopes using the method of Fernandez and colleagues [126]. All labeling fractions were transformed to a natural abundance-corrected mass distribution vector (MDV)[121].

Liquid chromatography-mass spectrometry

Nucleotides, amino acids and α-ketoglutarate from the dynamic metabolomic experiment were measured on liquid chromatography-mass spectrometry system. The separation of metabolites was performed by liquid chromatography coupled to tandem mass spectrometry (LC-MS/MS). Metabolite separation was performed at 28 °C with an Ultra High-Performance Liquid Chromatography (UHPLC) from Thermo Scientific on a HILIC Fusion (P) column (150 x 2.1 mm, 5 µm). Polar metabolites were separated at a flow rate of 0.2 ml/min for 43 min as follows: 0–2 min: 8 % B; 2–7 min: 8%–30% B, 7–20 min: 30%–47% B; 20–26 min: 90% B; 26–30 min: 90% B, 30–34 min: 90–8% B and 34–43 min: 8% B (solvent A: acetonitrile; solvent B: ammonium acetate 10 mM pH=9.3). The UHPLC autosampler was set at 4°C and 12 µL of sample were injected. A Thermo TSQ Quantiva triple quadrupole with an electrospray source was used for the analysis. The detection of metabolites was performed in Multiple reaction Monitoring mode (MRM) mode in negative mode. The ion transfer tube was set at 350 °C and the vaporizer temperature at 400°C. Data were collected and integrated using Xcalibur software (Thermo Scientific).

The measurements of α-ketoglutarate and serine in the MMTV-PyMT mouse model was conducted as following. Liquid chromatography tandem mass spectrometry (LC-MS/MS) analysis was performed with ion-

pairing reverse phase chromatography using an Ascentis Express column (C18, 5 cm × 2.1 mm, 2.7 µm, Sigma-Aldrich) for separation and a Waters Xevo TQ-S triple quadrupole mass spectrometer operated in negative mode as mass analyzer. The LC parameters were as follows: autosampler temperature, 5°C; injection volume, 5 µl; column temperature, 50°C and flow rate, 400 µl/min. The LC solvents were solvent A: 10 mM tributylamine and 15 mM acetic acid in 97:3 water:methanol (pH 4.95) and solvent B: methanol. Elution from the column was performed over 12 min with the following gradient: t = 0, 0% solvent B, flow rate 0.4 ml/min; t = 1, 0% solvent B, flow rate 0.4 ml/min; t = 2, 20% solvent B, flow rate 0.3 ml/min; t = 3, 20% solvent B, flow rate 0.25 ml/min; t = 5, 55% solvent B, flow rate 0.15 ml/min; t = 8, 95% solvent B, flow rate 0.15 ml/min; t = 9.5, 95% solvent B, flow rate 0.15 ml/min; t = 10, 0% solvent B, flow rate 0.4 ml/min; t = 12, 0% solvent B, flow rate 0.4 ml/min. Mass spectra were acquired using negative-mode electrospray ionization operating in multiple reaction monitoring (MRM) mode. The capillary voltage was 3,000 V, and cone voltage was 50 V. Nitrogen was used as cone gas and desolvation gas, with flow rates of 150 and 600 l/h, respectively. The source temperature was 150°C, and desolvation temperature was 500°C. Argon was used as collision gas at a manifold pressure of 4.3 × 10−3 mbar. Precursor and product ion m/z, collision energies and source cone potentials were optimized using Waters QuanOptimize software. The MRM transition for alpha-ketoglutarate is as follows: parent m/z = 145, daughter m/z = 100.77, cone voltage = 22 V, collision energy = 5 V. Two replicate injections/runs of each sample was performed. Peaks were quantified using MAVEN[127].

Compartment specific-metabolic measurements

Selective permeabilization of the cytosolic membrane using digitonin was used to separate the cytosolic metabolic content from the mitochondrial metabolic content as previously described[128,129]. Briefly, cells were seeded in a 6-well plate to be 70-80% confluent after 48h. After 24h from the seeding, the medium

was replaced with one containing dialyzed FBS + or – 2mM Sodium Pyruvate. After 24h, the supernatant was removed and cells were washed with 2 ml of dPBS. Permeabilization of the cytosolic membrane was achieved by incubation with 500 µl digitonin solution (40 µg/ml in mitochondrial assay buffer for 4T1, 25 µg/ml in mitochondrial assay buffer for MDA-MB-231) for 2 min. Afterwards, supernatants containing the cytosolic components were collected and stored at -80°C, while the 6-well plates containing the intact mitochondrial component were washed once with two volumes of saline, quenched in liquid nitrogen and stored at -80°C until metabolite were extracted as already described. The cytosolic supernatants were dried overnight at 4°C in a speedvac concentrator and next metabolite were extracted as already described.

Monitoring of tumor growth via optical imaging

In order to monitor tumor growth in the lung injection model, we generated MDA-MB-231 CTR and OE PHGDH expressing the firefly luciferase using the lentiviral particles pCH-EF1a-eGFP-T2A-Luc2-Ires-BsdR obtained from the Leuven Viral Vector Core. Transduction of 4T1 cells was performed overnight and the medium was replaced the next day. To minimize the possibility of multiple transductions of the same cells, we used a viral dilution that ensured only 20% of transduction efficacy. Transduction efficacy was evaluated by checking the percentage of GFP positive cells under a fluorescence microscope. Next, cells were selected with Blasticidin (Thermo Scientific, R21001) at a concentration of 5 µg per mL. Before each imaging session, the mice were injected intraperitoneally with 126 mg/kg D-luciferin (Promega, Madison, WI, USA) dissolved in PBS (15 mg/ml). Next, 5 animals per time, belonging to the same group, were positioned in the IVIS Spectrum (Perkin Elmer, Waltham, MA) and images were acquired after 10 min under 2% isoflurane inhalation. Images were acquired at day 4, 7, 9, 11, 14, 16, 18, 21 after cell injection. Bioluminescence images were analyzed using the LivingImage (Perkin Elmer, Waltham, MA) processing software. The same regions of interest (ROIs) were drawn around the lungs of every mouse, and measurements were generated as the total flux (photon per second) from the selected ROIs.

Analysis of mTOR pathway activity in human metastases and matched primary breast cancers

For comparison of mTOR pathway activity in human metastases versus matched primary breast cancers, publicly available phosphoproteomics RPPA data from The Cancer Genome Atlas (TCGA; RPPA profiles) were accessed and downloaded from the UCSC Xena browser (http://xena.ucsc.edu)[130,131], which contains five matched pairs. For each sample, an mTOR pathway signature could be scored based on their RPPA profiles, as defined previously[130]. This signature was defined as the sum of phosphoprotein levels of mTOR, 4EBP1 (S65, T37/T46, and T70 RPPA features), P70S6K, and S6 (S235/236 and S240/244 features)[130]. For each matched pair, we calculated the fold change of the sum score of the metastatic over the primary tumor sample. The TCGA sample identifier for the data presented are the following: #1 TCGA-BH-A1ES, #2 TCGA-BH-A1FE, #3 TCGA-E2-A15A, #4 TCGA-BH-A18V, #5 TCGA-E2-A15K.

Patient ID in Figure 1c	SampleID	Sample type	AJCC Stage	Gender	Age at initial pathologic diagnosis	Year of initial pathologic diagnosis	Days to date of death	PAM50Call RNAseq	ER Status	HER2 Status	PR Status
#1	TCGA-BH-A1ES-01	Primary Tumor	Stage IIB	F	35	1999	3462	LumA	Positive	Negative	Positive
	TCGA-BH-A1ES-06	Metastatic		F	35	1999	3462	LumA			
#2	TCGA-BH-A1FE-01	Primary Tumor	Stage IIB	F	31	1998	2273	LumA	Positive	Negative	Positive
	TCGA-BH-A1FE-06	Metastatic		F	31	1998	2273	Normal			
#3	TCGA-E2-A15A-01	Primary Tumor	Stage IIIC	F	45	2009		LumB	Positive	Negative	Positive
	TCGA-E2-A15A-06	Metastatic		F	45	2009		LumB			
#4	TCGA-BH-A18V-01	Primary Tumor	Stage IIB	F	48	2001	1555	Basal	Negative	Negative	Negative
	TCGA-BH-A18V-06	Metastatic		F	48	2001	1555	Basal			
#5	TCGA-E2-A15K-01	Primary Tumor	Stage IIA	F	58	2010		LumB	Positive	Negative	Positive
	TCGA-E2-A15K-06	Metastatic		F	58	2010		LumB			

Table 2, Metadata related to Figure 1c.

Comparison of mTOR activity with MCT2 gene expression levels

The activity of the mTOR pathway in n=859 primary breast cancer samples from The Cancer Genome Atlas (TCGA) was assessed as previously described (Zhang Y 2018 Cancer Cell) by generating activity sum scores of the following parameters from proteomic RPPA (reverse phase protein assay) data, which are publicly available via the UCSC Xena browser (https://xena.ucsc.edu/): MTOR_pS2448, X4EBP1_pS65, X4EBP1_pT37T46, X4EBP1_pT70, P70S6K_pT389, S6_pS235S236, and S6_pS240S244. Matching MCT2 gene expression data for the same primary tumors was retrieved from the NIH Genomic Data Commons (GDC) data portal (https://portal.gdc.cancer.gov/). The mTOR activity sum scores were stratified in quartiles and compared with the MCT2 expression levels using a two-sided Mann-Whitney test.

Quantification and statistical analysis

Statistical data analysis was performed using GraphPad Prism version 7.0 (GraphPad Software) on $n \geq 3$ biological replicates. Details on statistical tests and post-tests are presented in the figure legends. Sample size for all experiments was chosen empirically. Independent experiments were pooled and analyzed together whenever possible as detailed in figure legends. Quantification of the western blots was performed using the software Image Studio Lite. For the human MDA-MB-231 mouse model both H&E and BLI were correlated (90% prediction bands) to ensure we only evaluate breast cancer-derived tumors established and growing in the lung. The rationale is that mice that show consistent results between both measurements had established and growing breast cancer-derived lung tumors. While mice where the BLI and the H&E data did not match either did not have established and growing tumors or had tumors outside the lung. The latter mice where BLI and H&E data did not match were excluded from the analysis.

Data are presented as mean ± s.d., or as mean ± s.e.m., as indicated in the figure legends.

Chapter 3. Results

Once cancer cells reach a distant organ they need to activate growth signaling in order to form a fully grown metastasis[33]. While activation of signal transduction has been extensively described in primary tumors[103], still little is known about the mechanisms supporting cell growth and proliferation during metastatic outgrowth.

The mTORC1 pathway is a key signaling hub that has a critical role in regulating cell growth and proliferation and is often dysregulated in breast cancer[105]. Multiple studies have shown that mTORC1 activation sustains early events during the metastatic process in different types of tumor[108–111], however it is still largely unknown whether and how mTORC1 is supporting the latest phases of metastasis formation.

Growth factors, nutrients and different metabolites have been found to be main regulators of mTORC1 activation[94]. Recent literature has highlighted a different nutrient and metabolite availability in the microenvironment of primary tumors and distant organs[77,92], raising the question whether the distinct nutrient composition can be a determinant of mTORC1 signaling during metastatic outgrowth in the distant site.

In this thesis, we have defined how the different metabolite availability in the lung microenvironment determines specific metabolic adaptations and activation of mTORC1 in lung metastasis compared to breast primary tumors.

Pyruvate supports mTORC1 signaling

Growth signaling is relevant for primary tumor proliferation and outgrowth of metastases. We therefore asked whether primary breast cancers and their corresponding lung metastases both rely on the same growth signaling pathway, namely mTORC1 signaling, for proliferation and outgrowth. Specifically, we used

4T1 mouse breast cancer cells to initiate primary cancers in the mammary fat pad, which resulted in spontaneous lung metastasis formation in mice. Subsequently, we resected matched pairs of primary 4T1 breast tumors and lung metastases and evaluated mTORC1 signaling based on the phosphorylation of S6 and eukaryotic translation initiation factor 4E (eIF4E)-binding protein 1 (4EBP1). We observed that both, the proliferating primary breast tumors and the outgrowing metastases, showed substantial S6 and 4EBP1 phosphorylation compared to adjacent healthy lung tissue (Figure 1a). Thus, we concluded that 4T1 primary breast tumors and their corresponding metastases use mTORC1 dependent growth signaling.

Despite the fact that primary breast tumors and corresponding lung metastases both showed activated mTORC1 growth signaling, we found that the metastases exhibited a higher ratio of phosphorylated to total S6 and 4EBP1 compared to primary tumors (Figure 1b). Accordingly, we found that four out of five matched metastases samples from human breast cancer patients exhibited an elevated mTOR activity signature compared to the corresponding primary breast cancer samples based on phospho-proteomics data available through TCGA (Figure 1c, Table 2). This indicates an increased activity of mTORC1 signaling specifically in the outgrowing metastases.

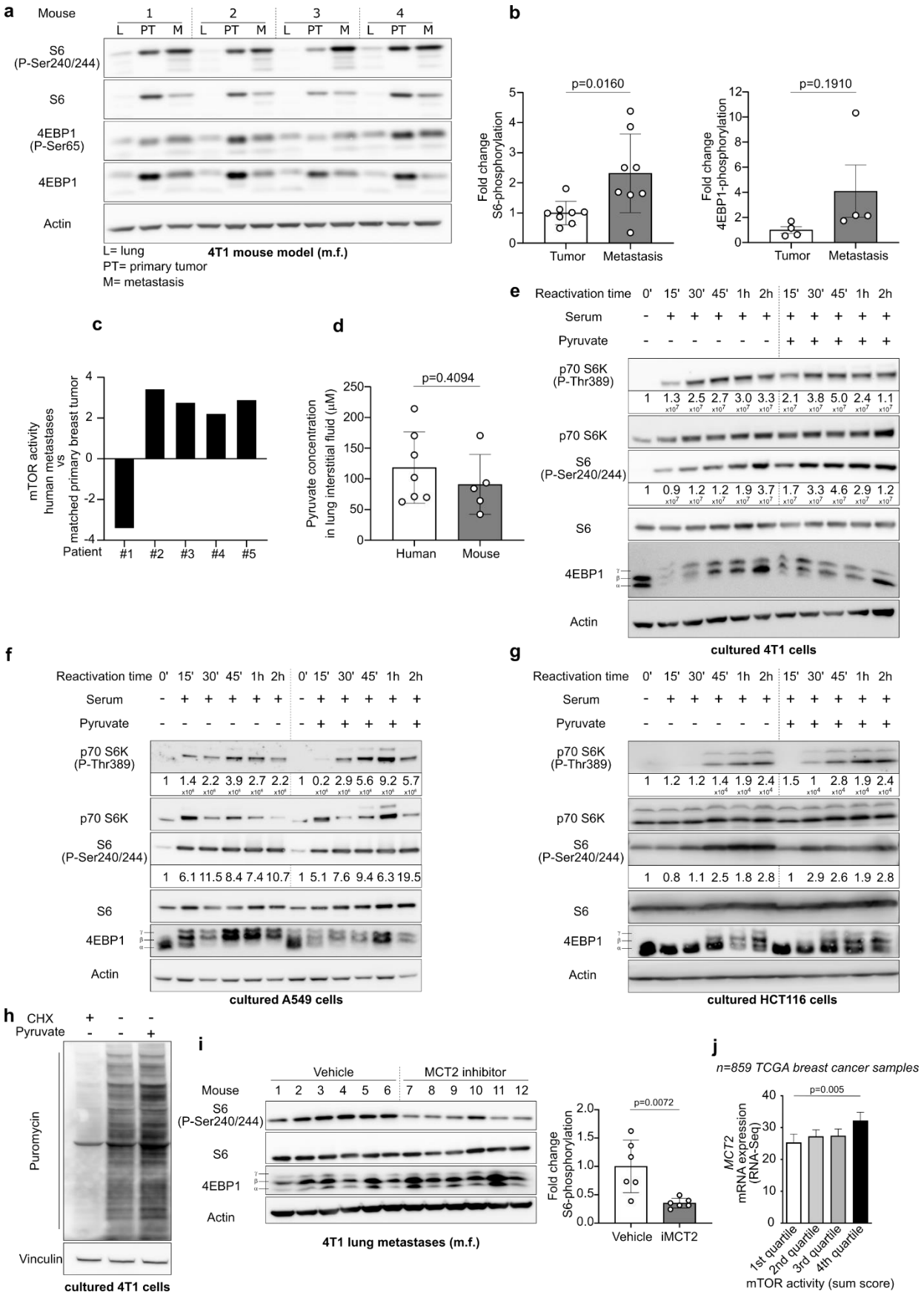
a
Mouse
1
2
3
4
L PT M L PT M L PT M L PT M
S6 (P-Ser240/244)
S6
4EBP1 (P-Ser65)
4EBP1
Actin
L= lung
PT= primary tumor
M= metastasis
4T1 mouse model (m.f.)
b
p=0.0160
Fold change S6-phosphorylation
Tumor
Metastasis
p=0.1910
Fold change 4EBP1-phosphorylation
Tumor
Metastasis
c
mTOR activity human metastases vs matched primary breast tumor
Patient #1 #2 #3 #4 #5
d
p=0.4094
Pyruvate concentration in lung interstitial fluid (µM)
Human
Mouse
e
Reactivation time 0' 15' 30' 45' 1h 2h 15' 30' 45' 1h 2h
Serum - + + + + + + + + + +
Pyruvate - - - - - - + + + + +
p70 S6K (P-Thr389)
1 1.3 2.5 2.7 3.0 3.3 2.1 3.8 5.0 2.4 1.1
p70 S6K
S6 (P-Ser240/244)
1 0.9 1.2 1.2 1.9 3.7 1.7 3.3 4.6 2.9 1.2
S6
4EBP1
Actin
cultured 4T1 cells
f
Reactivation time 0' 15' 30' 45' 1h 2h 0' 15' 30' 45' 1h 2h
Serum - + + + + + - + + + + +
Pyruvate - - - - - - - + + + + +
p70 S6K (P-Thr389)
1 1.4 2.2 3.9 2.7 2.2 1 0.2 2.9 5.6 9.2 5.7
p70 S6K
S6 (P-Ser240/244)
1 6.1 11.5 8.4 7.4 10.7 1 5.1 7.6 9.4 6.3 19.5
S6
4EBP1
Actin
cultured A549 cells
g
Reactivation time 0' 15' 30' 45' 1h 2h 15' 30' 45' 1h 2h
Serum - + + + + + + + + + +
Pyruvate - - - - - - + + + + +
p70 S6K (P-Thr389)
1 1.2 1.2 1.4 1.9 2.4 1.5 1 2.8 1.9 2.4
p70 S6K
S6 (P-Ser240/244)
1 0.8 1.1 2.5 1.8 2.8 1 2.9 2.6 1.9 2.8
S6
4EBP1
Actin
cultured HCT116 cells
h
CHX + - -
Pyruvate - - +
Puromycin
Vinculin
cultured 4T1 cells
i
Vehicle
MCT2 inhibitor
Mouse 1 2 3 4 5 6 7 8 9 10 11 12
S6 (P-Ser240/244)
S6
4EBP1
Actin
4T1 lung metastases (m.f.)
p=0.0072
Fold change S6-phosphorylation
Vehicle
iMCT2
j
n=859 TCGA breast cancer samples
p=0.005
MCT2 mRNA expression (RNA-Seq)
1st quartile
2nd quartile
3rd quartile
4th quartile
mTOR activity (sum score)

Fig 1. Pyruvate supports mTORC1 signaling.

a, Phosphorylation of the mTORC1 targets S6 and 4EBP1 in the lung (L), primary tumor (PT) and metastasis (M) of BALB/c mice injected with 4T1 cells in the mammary fat pad (m.f.). *n=4*

b, Protein quantification of S6 (P-Ser240/244) and 4EBP1 (P-Ser65) shown in panel a. Data are presented as fold change compared to the primary tumor levels. Since comparing different tissues, data are normalized both on Actin and the respective band for total protein. Tissues from 4 additional mice were run on a second western blot (data not shown) and the quantification of S6 (P-Ser240/244) was included in the graph shown in panel b. Two-tailed unpaired Student's t-test. S6 *n=8, 4EBP1 n=4.*

c, mTORC1 activity based on a publicly available phospho-proteomics dataset in human metastases compared to matched primary tumor from 5 different patients.

d, Concentration of pyruvate in the interstitial fluid of lung samples collected from human patients and BALB/c mice. Two-tailed unpaired Student's t-test. Human *n=7, Mouse n=5.*

e-g, Phosphorylation of the mTORC1 targets p70 S6K, S6 and 4EBP1 upon 16h of serum starvation, 1h starvation in HBSS and subsequent reactivation (from 15 minutes to 2h) in serum containing culture medium with or without 2mM sodium pyruvate in 4T1, A549 or HCT116 cells. Protein quantification of phosho-p70 S6K and phospho-S6 is shown below the immunoblot. Data are normalized on Actin and are shown as fold change compared to the time 0. One representative image is shown, *n=3.*

h, Total protein synthesis in presence or absence of 2mM pyruvate and puromycin (10µg per mL) in 4T1 cells based on the incorporation of puromycin into newly synthesized proteins. 4T1 cells were starved from serum for 16h, starved in HBSS for 1h and subsequently reactivated (30 minutes) in serum containing culture medium with or without 2mM sodium pyruvate. The protein synthesis inhibitor cycloheximide (CHX, 100nM) was used as a negative control. One representative image is shown, *n=3.*

i, Phosphorylation of the mTORC1 targets S6 and 4EBP1 in 4T1 lung metastases upon acute inhibition of pyruvate uptake using the MCT2 inhibitor α-cyano-4-hydroxycinnamic acid (60 mg per kg; i.p.). m.f. refers to mammary fat pad injection. 4EBP1 phosphorylation increases from α to γ (δ) band. Quantification of phospho-S6 is shown in the graph. Data are normalized on Actin and are shown as fold change compared to the group of mice treated with the vehicle. Two-tailed unpaired Student's t-test. *n=6*

j, Correlation between the *MCT2* gene expression with the mTOR activity as measured by a sum-score of the phospho-targets by RPPA, protein level. Samples were divided in quartiles, with the 1st quartile comprising all samples with lowest and the 4th quartile with the highest mTOR activity. Two sided Mann-Whitney test. *n=859*

Error bars represent s.d. (panels b,d and i) and s.e.m (panel j) from mean of biologically independent samples.

mTORC1 signaling is highly influenced by nutrient availability[94,132]. We have previously shown that the nutrient pyruvate is available in the lung environment (i.e. lung interstitial fluid) of mice [86] and that pyruvate enables cancer cells to shape the extracellular environment of the metastatic niche [99]. To relate this prior finding to humans, we measured absolute pyruvate concentration in the intestinal fluid of non-cancerous lung tissue of human individuals. Strikingly, we observed a similar pyruvate concentration in human and mouse lung interstitial (**Figure 1d**). These data show that pyruvate availability is not only a particularity of

the mouse lung environment but is reflected in the human lung environment. Thus, pyruvate availability in the lung metastatic niche may support mTORC1 growth signaling. A prerequisite for this hypothesis is that pyruvate abundance is increased in metastases compared to primary tumors. In line with our previous work[86], we confirmed a 2.5-fold increase in pyruvate abundance in lung metastases compared to primary 4T1 breast tumors (**Figure 2a**). Based on this *in vivo* measurement, we next defined which concentration of pyruvate supplemented to media *in vitro* would result into a similar increase in intracellular pyruvate abundance as observed in metastases versus primary breast tumors (**Figure 2**). Consequently, we cultured 4T1 breast cancer cells *in vitro* and assessed the phosphorylation dynamics of mTORC1 targets after starvation and reactivation with serum in the presence or absence of 2mM pyruvate and evaluated phosphorylation of mTORC1 targets based on phospho-antibodies (p70 S6K and S6) and band shift (4EBP1; phosphorylation increases from α to γ(δ) band). Strikingly, we observed a more pronounced phosphorylation of S6 kinase 1 (p70 S6K) and S6 ribosomal protein (S6) in the presence of pyruvate until 45-60 minutes after reactivation (**Figure 1e**). We then asked the question whether these changes, despite being small, are also found in different cell lines. First, we tested the same experiment in the lung cancer cell line A549. In contrast with what we found for the 4T1 cell line, pyruvate slightly reduced the phosphorylation status of p70 S6K and S6 at early time point (first 30 minutes) but increased it at later time points (between 45 minutes and 2 hours) (**Figure 1f**). Second, we assessed the dynamic of activation of mTORC1 in the colon cancer cell line HCT116. Similarly, to what we observed in the 4T1 cells, the phosphorylation status of p70 S6K, S6 and in addition also of 4EBP1, is increased during the early time points (until 45 minutes) of reactivation in presence of pyruvate (**Figure 1g**). Despite the changes induced by pyruvate on the phosphorylation status of the mTORC1 targets were too small and not enough consistent across the cell lines tested, they provided an indication that pyruvate might be part of the many signals activating mTORC1. To further investigate this possibility, we have decided to measure the total protein translation, which is a function of mTORC1 growth signaling, after starvation and reactivation, using

puromycin in 4T1 cells [133]. In brief, puromycin, which is incorporated into the nascent polypeptide chain and prevents elongation, is detected by western blotting. Based on this technique it is expected that increased protein translation is reflected in increased puromycin detection. In accordance with the increased phosphorylation dynamics of mTORC1 targets, we found that total protein translation was increased in the presence of pyruvate compared to control condition in 4T1 breast cancer cells (**Figure 1h**). Thus, we concluded that pyruvate boosts the activation dynamics of mTORC1 signaling in cultured 4T1, A549 and HCT116 cancer cells.

Next, we asked whether pyruvate is needed for the activation of mTORC1 signaling in outgrowing breast cancer-derived lung metastases. To address this question, we initiated 4T1 breast cancer-derived lung metastases as described above and treated the mice acutely with two doses of α-cyano-4-hydroxycinnamic acid (60 mg per kg per day, 24 and 2h before sacrificing the mice; i.p.), which is an inhibitor of monocarboxylate transporter 2 (MCT2) that we have previously shown to inhibit pyruvate uptake in lung metastases [99]. Subsequently, we resected metastases from MCT2 inhibitor or vehicle treated mice and assessed mTORC1 signaling based on the phosphorylation of S6 and 4EBP1. We observed a decreased S6 phosphorylation and increased fraction of lower-phosphorylated (α and β band) 4EBP1 in metastases tissue upon MCT2 inhibition (**Figure 1i**). Accordingly, we found a positive correlation between *MCT2* gene expression and mTOR activity in breast cancer samples from patients (**Figure 1j**). Based on these data we concluded that pyruvate supports mTORC1 signaling in breast cancer-derived lung metastases.

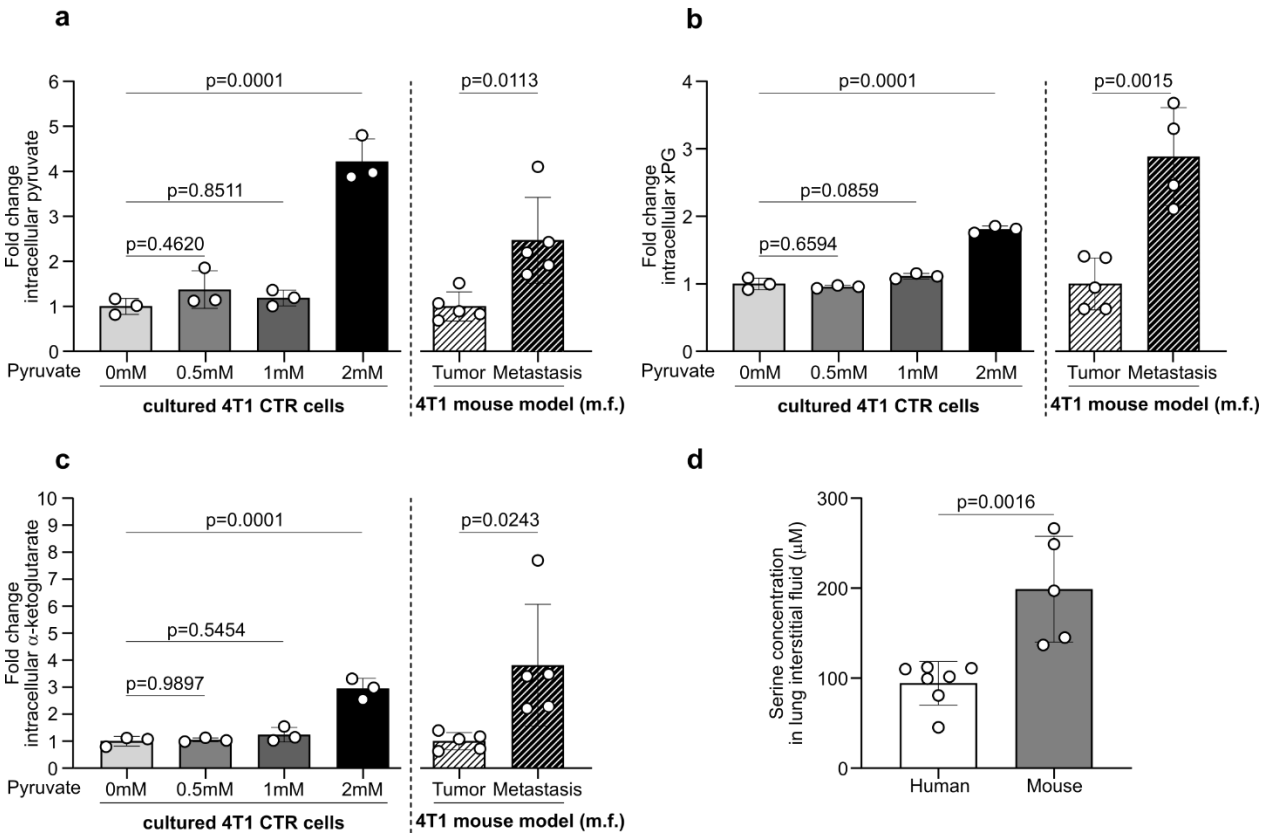

Fig 2. Pyruvate supplementation *in vitro* recapitulates some of the metabolic features of lung metastases compared to the primary tumors.

a-c, Intracellular pyruvate, xPG and α-ketoglutarate abundance in 4T1 CTR cells incubated for 24h hour in medium containing increasing concentration of sodium pyruvate or in primary tumor and metastasis of BALB/c mice injected with 4T1 cells in the mammary fat pad (m.f.) . Data are presented as fold-change compared to the 0mM (in the case of cultured 4T1 CTR cells) or the tumor (in the case of 4T1 mouse model). One-way ANOVA with Dunnet's multiple comparison test (comparison between the 0mM conditions and all the others), *n=3* for the cultured 4T1 CTR cells. Two-tailed unpaired Student's t-test, *n=5* for the 4T1 mouse model.

d, Concentration of serine in the interstitial fluid of lung samples collected from human patients and BALB/c mice. Two-tailed unpaired Student's t-test. Human n=7, Mouse n=5.

All error bars represent s.d. from mean of biologically independent samples or mice.

Serine biosynthesis is required for pyruvate driven mTORC1 signaling

Next, we investigated the mechanism by which pyruvate supports mTORC1 growth signaling. We hypothesized that metabolites which changed most in abundance upon pyruvate supplementation could mechanistically link pyruvate to mTORC1 signaling. Thus, we cultured 4T1 breast cancer cells, in the

presence of increasing amounts of pyruvate and performed a metabolomics analysis. We found that upon pyruvate supplementation several metabolites changed in abundance, yet serine, alanine, x-phosphoglycerate (sum of 2- and 3-phosphoglycerate) and α-ketoglutarate abundance showed the most pronounced increase (**Figure 3a-d**), while dihydroxyacetone phosphate (DHAP), which was recently discovered to signal glucose availability to mTOR [134], was not altered in abundance (**Figure 4a**). Interestingly, serine and α-ketoglutarate can be directly linked via the serine biosynthesis pathway which produces serine and equimolar amounts of α-ketoglutarate because the enzyme phosphoserine aminotransferase 1 (PSAT1) converts 3-phosphohydroxypyruvate and glutamate to 3-phospho-L-serine and α-ketoglutarate (**Figure 3e**). Thus, we hypothesized that pyruvate stimulates serine biosynthesis. Therefore, we measured *de novo* serine biosynthesis using ^{13}C tracer analysis in 4T1, MDA-MB-468, A549 and HCT116 cells [121]. We observed that pyruvate supplementation increased the fraction of serine produced from glucose (**Figure 3f-i**), which is indicative of an elevated *de novo* serine biosynthesis in the presence of pyruvate. Moreover, MDA-MB-468, A549 and HCT116 cells showed – similar to 4T1 cells – an elevated serine and α-ketoglutarate abundances upon pyruvate supplementation (**Figure 3j-l**). Based on these data we concluded that pyruvate stimulates the serine biosynthesis pathway.

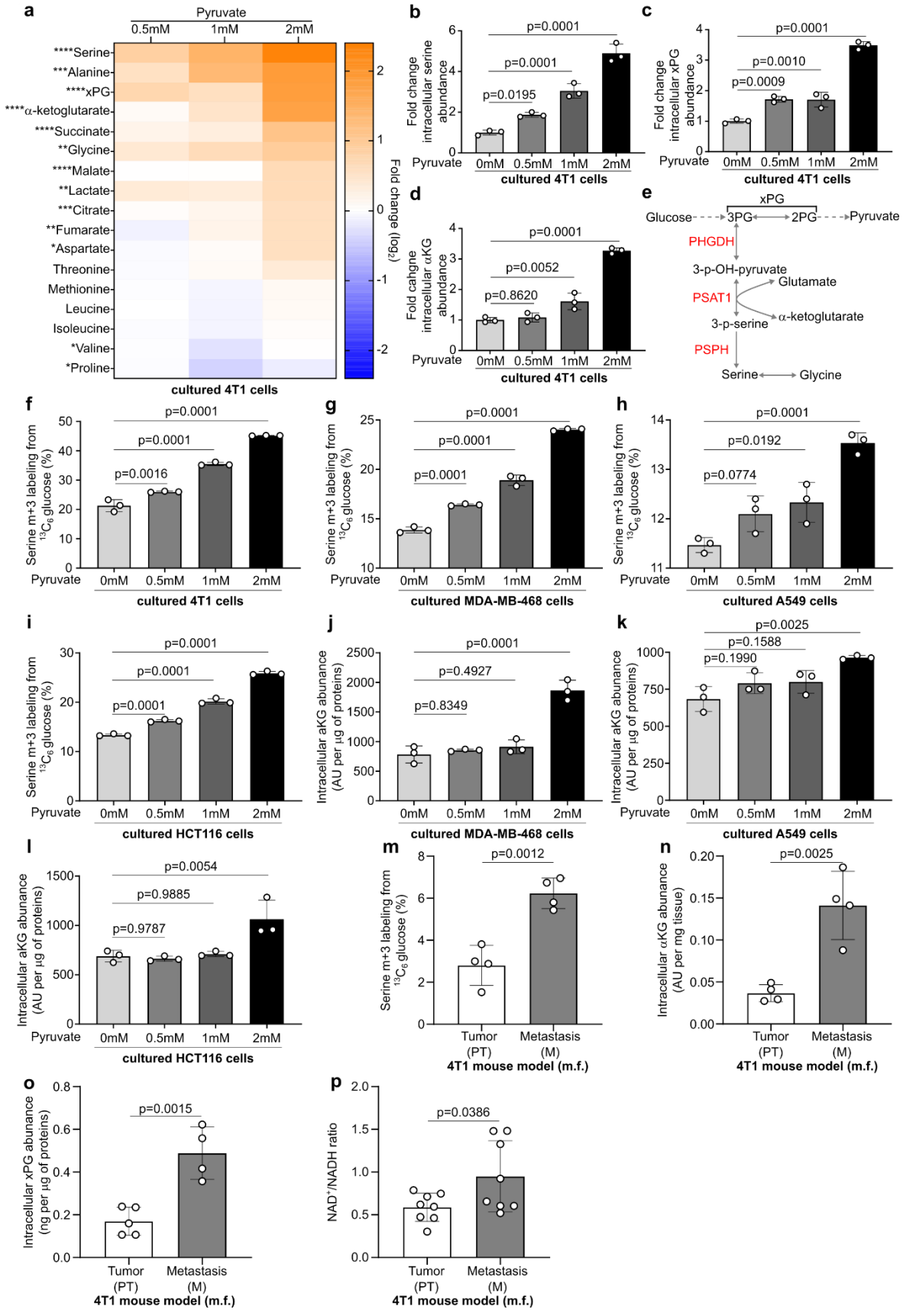
a
Pyruvate
0.5mM
1mM
2mM
****Serine
***Alanine
****xPG
****α-ketoglutarate
****Succinate
**Glycine
****Malate
**Lactate
***Citrate
**Fumarate
*Aspartate
Threonine
Methionine
Leucine
Isoleucine
*Valine
*Proline
Fold change (log2)
cultured 4T1 cells
b
Fold change intracellular serine abundance
p=0.0001
p=0.0001
p=0.0195
Pyruvate
0mM 0.5mM 1mM 2mM
cultured 4T1 cells
c
Fold change intracellular xPG abundance
p=0.0001
p=0.0010
p=0.0009
Pyruvate
0mM 0.5mM 1mM 2mM
cultured 4T1 cells
d
Fold cahgne intracellular αKG abundance
p=0.0001
p=0.0052
p=0.8620
Pyruvate
0mM 0.5mM 1mM 2mM
cultured 4T1 cells
e
xPG
Glucose
3PG
2PG
Pyruvate
PHGDH
3-p-OH-pyruvate
Glutamate
PSAT1
α-ketoglutarate
3-p-serine
PSPH
Serine
Glycine
f
Serine m+3 labeling from $^{13}C_6$ glucose (%)
p=0.0001
p=0.0001
p=0.0016
Pyruvate
0mM 0.5mM 1mM 2mM
cultured 4T1 cells
g
Serine m+3 labeling from $^{13}C_6$ glucose (%)
p=0.0001
p=0.0001
p=0.0001
Pyruvate
0mM 0.5mM 1mM 2mM
cultured MDA-MB-468 cells
h
Serine m+3 labeling from $^{13}C_6$ glucose (%)
p=0.0001
p=0.0192
p=0.0774
Pyruvate
0mM 0.5mM 1mM 2mM
cultured A549 cells
i
Serine m+3 labeling from $^{13}C_6$ glucose (%)
p=0.0001
p=0.0001
p=0.0001
Pyruvate
0mM 0.5mM 1mM 2mM
cultured HCT116 cells
j
Intracellular aKG abunance (AU per µg of proteins)
p=0.0001
p=0.4927
p=0.8349
0mM 0.5mM 1mM 2mM
cultured MDA-MB-468 cells
k
Intracellular aKG abunance (AU per µg of proteins)
p=0.0025
p=0.1588
p=0.1990
Pyruvate
0mM 0.5mM 1mM 2mM
cultured A549 cells
l
Intracellular aKG abunance (AU per µg of proteins)
p=0.0054
p=0.9885
p=0.9787
Pyruvate
0mM 0.5mM 1mM 2mM
cultured HCT116 cells
m
Serine m+3 labeling from $^{13}C_6$ glucose (%)
p=0.0012
Tumor (PT)
Metastasis (M)
4T1 mouse model (m.f.)
n
Intracellular αKG abunance (AU per mg tissue)
p=0.0025
Tumor (PT)
Metastasis (M)
4T1 mouse model (m.f.)
o
Intracellular xPG abunance (ng per µg of proteins)
p=0.0015
Tumor (PT)
Metastasis (M)
4T1 mouse model (m.f.)
p
NAD+/NADH ratio
p=0.0386
Tumor (PT)
Metastasis (M)
4T1 mouse model (m.f.)

Fig 3. Environmental pyruvate activates *de novo* serine biosynthesis

a, Heat map representing metabolite abundance changes upon supplementation of different concentrations of sodium pyruvate to the culture medium of 4T1 cells after 24h of incubation. Data represent the fold changes compared to the no pyruvate condition. One-way ANOVA. *n=3.* Asterisks represent statistical significance as follow: *= p ≤ 0.05 **= p ≤ 0.01 ***= p ≤ 0.001 ****=p ≤ 0.0001

b-d, Fold changes of serine, α-ketoglutarate and xPG (3PG and 2PG) extracted from the heat map in panel a. One-way ANOVA with Dunnet's multiple comparison test (comparison between the 0mM conditions and all the others). *n=3*

e, Schematic representation of the *de novo* serine biosynthesis pathway branching from glycolysis at the level of 3PG. In black: metabolites. In red: enzymes of serine biosynthesis.

f-i, Activation of *de novo* serine biosynthesis assessed through measurement of serine m+3 labeling enrichment after incubation of 4T1, MDA-MB-468, A549 or HCT116 cells for 24h in culture medium containing $^{13}C_6$ glucose and increasing concentrations of sodium pyruvate. One-way ANOVA with Dunnet's multiple comparison test (comparison between the 0mM conditions and all the others). *n=3*

j-l, Intracellular levels of α-ketoglutarate in MDA-MB-468, A549 and HCT116 cells incubated for 24h in culture medium containing increasing concentrations of sodium pyruvate. One-way ANOVA with Dunnet's multiple comparison test (comparison between the 0mM conditions and all the others). *n=3*

m-p, Activation of *de novo* serine biosynthesis,α-ketoglutarate and x-phosphoglycerate (xPG) abundance, NAD^+/NADH ratio in 4T1 primary breast tumors (PT) and lung metastases (M). *De novo* serine synthesis was assessed through measurement of serine m+3 labeling enrichment after a 6h infusion of $^{13}C_6$ glucose to tumor harboring BALB/c mice. m.f. refers to mammary fat pad injection. Two-tailed unpaired Student's t-test. *Serine synthesis and αKG levels n=4, xPG PT n=5, xPG M n=4, NAD^+/NADH n=8*

All error bars represent s.d. from mean of biologically independent samples or mice.

Serine biosynthesis is metabolically regulated by 3-phosphoglycerate [135] and constrained by the NAD^+ to NADH ratio[136]. Accordingly, we found that pyruvate supplementation increased x-phosphoglycerate abundance and the NAD^+ to NADH ratio in 4T1 and MDA-MB-231 cells (**Figure 3c, Figure 4b-d**). To investigate the relevance of this finding we used the electron acceptor α-ketobutyrate (AKB)[136], and lactate (which decreases the NAD^+ to NADH ratio) and measured pyruvate, x-phosphoglycerate, and α-ketoglutarate as well as ^{13}C glucose contribution to serine in 4T1 cells. We found that AKB elevated pyruvate, x-phosphoglycerate and α-ketoglutarate abundance as well as ^{13}C glucose contribution to serine (**Figure 4e-h**), while lactate supplementation increased pyruvate and x-phosphoglycerate abundance but did only to a very minor extent elevate α-ketoglutarate abundance and ^{13}C glucose contribution to serine (**Figure 4i-l**). These data suggest that both 3-phosphoglycerate and a favorable NAD^+ to NADH ratio are needed to activate serine biosynthesis. In line, we found that 4T1 breast cancer-derived lung metastases, which are in a pyruvate-enriched environment, exhibited a higher fraction of serine biosynthesis from glucose, elevated

α-ketoglutarate as well as x-phosphoglycerate abundances and an increased NAD^+ to NADH ratio compared to the corresponding primary breast tumors (**Figure 3m-p**). Thus, these data are consistent with the notion that pyruvate activates serine biosynthesis by elevating 3-phosphoglycerate abundance and the NAD^+ to NADH ratio.

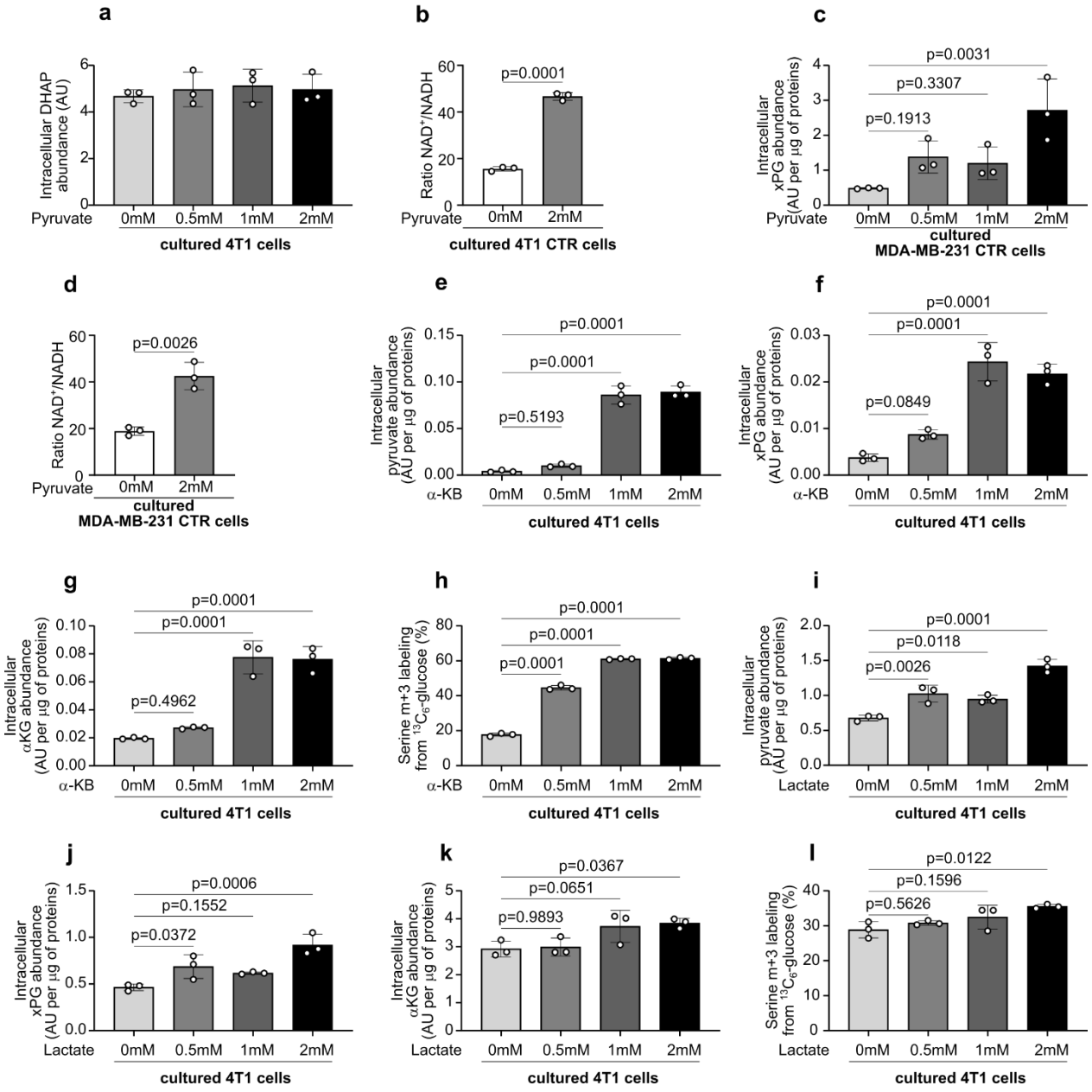

Fig 4. Increased xPG levels and NAD+/NADH ratio support serine biosynthesis activation in presence of extracellular pyruvate.

a-l, Intracellular DHAP, xPG, pyruvate, α-ketoglutarate abundance, NAD+/NADH ratio in 4T1 CTR cells incubated for 24h hour in medium containing increasing concentration of sodium pyruvate, α-ketobutarate or sodium lactate. To assess d*e novo* serine biosynthesis, 4T1 cells were grown in culture medium containing $^{13}C_6$ glucose and increasing concentrations of sodium pyruvate, α-ketobutarate (AKB) or sodium lactate. One-way ANOVA with Dunnet's multiple comparison test (comparison between the 0mM conditions and all the others). Two-tailed unpaired Student's t-test in panel b and d. *n=3*
All error bars represent s.d. from mean of biologically independent samples.

Next, we hypothesized that the serine biosynthesis pathway is required for pyruvate to boost mTORC1 signaling. To address this hypothesis, we silenced phosphoglycerate dehydrogenase (PHGDH) (**Figure 5a-b**), which is an essential enzyme of the serine biosynthesis pathway, in 4T1 breast cancer cells. As expected, silencing *PHGDH* decreased the fraction of serine produced from glucose and the intracellular α-ketoglutarate abundance (**Figure 5c-h**). Next, we measured the phosphorylation dynamics of mTORC1 targets after starvation and reactivation with serum and pyruvate. In accordance with our hypothesis, we observed that *PHGDH* silencing impaired the phosphorylation dynamics of p70 S6K, S6 and 4EBP1 (decreased γ band) phosphorylation particular in the presence of pyruvate (**Figure 6a, Figure 5i-j**). However, also in this case, the changes that we have observed between the 4T1 shPHGDH cell line and CTR were not very strong or completely consistent in terms of dynamics across the different shPHGDH (#1, #2, and #3). Thus, we have interpreted these results as an indication that PHGDH might be involved in the regulation of mTORC1 activation in presence of extracellular pyruvate, but we decided to further investigate this possibility. In line, we found that inhibition of PHGDH with the pharmacological inhibitor PH-755[98] mildly decreased the pyruvate-induced phosphorylation dynamics in MDA-MB-468 breast cancer cells after 30 minutes of reactivation (**Figure 6b**). Also in this case, the changes are mild, so to further understand whether PHGDH activity modulates the cellular functions regulated by mTORC1, we measured the total protein synthesis in presence or absence of PHGDH expression. Protein synthesis was reduced upon *PHGDH* silencing in the presence of pyruvate in 4T1 breast cancer cells (**Figure 6c**). Notably, there was only a minor effect of *PHGDH* silencing on protein synthesis in the absence of pyruvate which is expected due to low

activity of the serine biosynthesis pathway in the absence of pyruvate stimulation. Subsequently, we injected 4T1 control and *PHGDH*-silenced breast cancer cells into the lung of mice and assessed mTORC1 growth signaling in the arising tumors. Strikingly, we found that p70 S6K phosphorylation was decreased and 4EBP1 showed a trend towards a shift to lower phosphorylation (increased β band) in PHGDH-silenced breast cancer-derived lung tumors compared to control tumors (Figure 6d). Thus, we concluded that activity of the serine biosynthesis pathway mediates the boost in mTORC1 signaling upon pyruvate supplementation *in vitro* and in breast cancer-derived lung tumors.

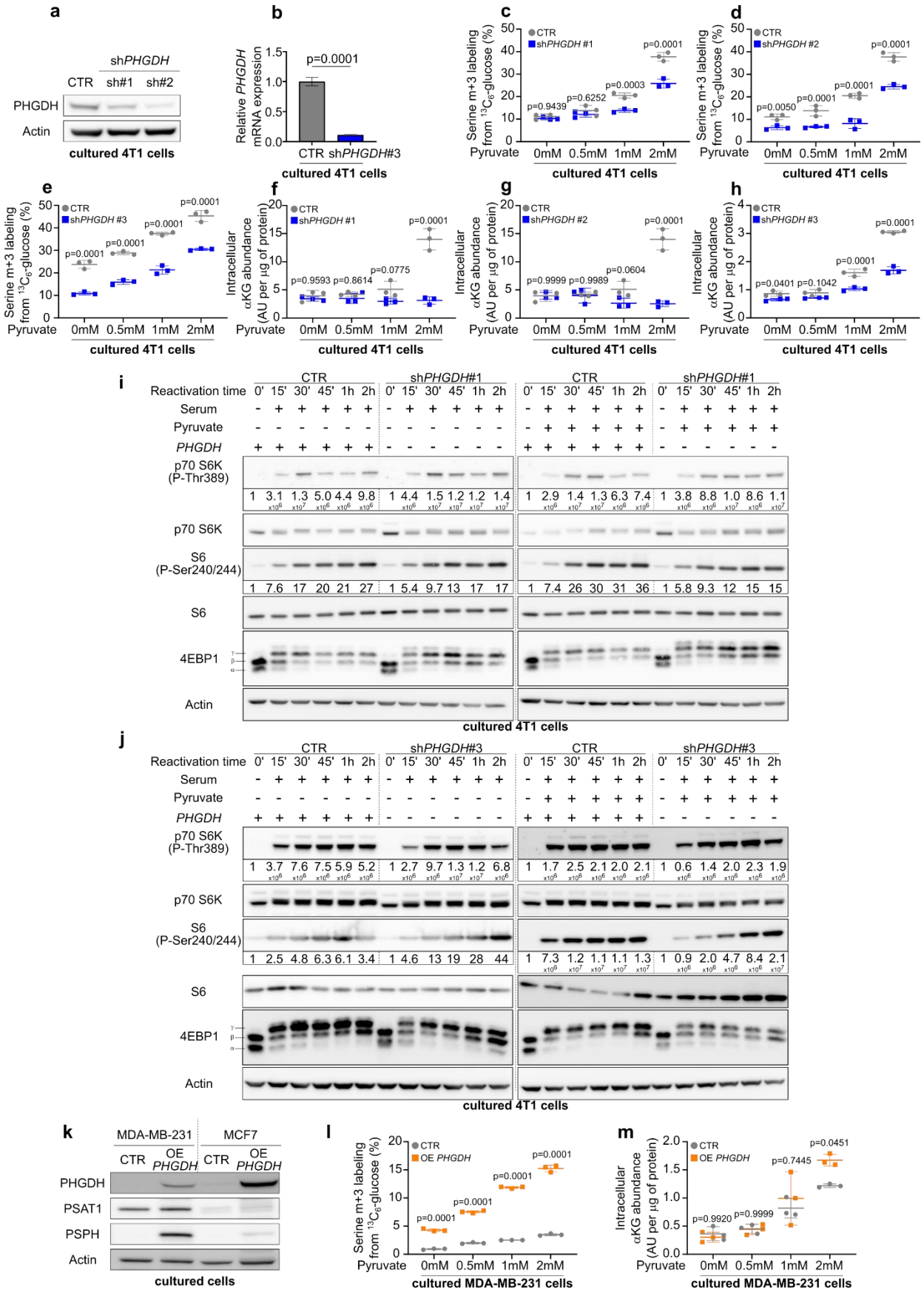
a
shPHGDH
CTR sh#1 sh#2
PHGDH
Actin
cultured 4T1 cells
b
Relative PHGDH mRNA expression
p=0.0001
CTR shPHGDH#3
cultured 4T1 cells
c
Serine m+3 labeling from 13C6-glucose (%)
CTR
shPHGDH #1
p=0.9439
p=0.6252
p=0.0003
p=0.0001
Pyruvate 0mM 0.5mM 1mM 2mM
cultured 4T1 cells
d
CTR
shPHGDH #2
p=0.0050
p=0.0001
p=0.0001
p=0.0001
cultured 4T1 cells
e
CTR
shPHGDH #3
p=0.0001
p=0.0001
p=0.0001
p=0.0001
cultured 4T1 cells
f
Intracellular αKG abundance (AU per µg of protein)
CTR
shPHGDH #1
p=0.9593
p=0.8614
p=0.0775
p=0.0001
cultured 4T1 cells
g
CTR
shPHGDH #2
p=0.9999
p=0.9989
p=0.0604
p=0.0001
cultured 4T1 cells
h
CTR
shPHGDH #3
p=0.0401
p=0.1042
p=0.0001
p=0.0001
cultured 4T1 cells
i
Reactivation time 0' 15' 30' 45' 1h 2h
CTR
shPHGDH#1
Serum
Pyruvate
PHGDH
p70 S6K (P-Thr389)
p70 S6K
S6 (P-Ser240/244)
S6
4EBP1
Actin
cultured 4T1 cells
j
Reactivation time 0' 15' 30' 45' 1h 2h
CTR
shPHGDH#3
Serum
Pyruvate
PHGDH
p70 S6K (P-Thr389)
p70 S6K
S6 (P-Ser240/244)
S6
4EBP1
Actin
cultured 4T1 cells
k
MDA-MB-231
MCF7
CTR
OE PHGDH
PHGDH
PSAT1
PSPH
Actin
cultured cells
l
Serine m+3 labeling from 13C6-glucose (%)
CTR
OE PHGDH
p=0.0001
p=0.0001
p=0.0001
p=0.0001
Pyruvate 0mM 0.5mM 1mM 2mM
cultured MDA-MB-231 cells
m
Intracellular αKG abundance (AU per µg of protein)
CTR
OE PHGDH
p=0.9920
p=0.9999
p=0.7445
p=0.0451
cultured MDA-MB-231 cells

Fig 5. PHGDH expression modulates pyruvate-induced serine biosynthesis activation

a, PHGDH protein levels upon knockdown in 4T1 cells expressing the shPHGDH sequences #1 and #2. **b,** PHGDH gene expression upon knockdown in 4T1 cells expressing the shPHGDH sequence #3. Two-tailed unpaired Student's t-test. *n=3.* **c-e,** Activation of *de novo* serine biosynthesis assessed through measurement of serine m+3 labeling enrichment after incubation of 4T1 control (CTR) or PHGDH-silenced (shPHGDH sequences #1,#2 and #3) cells for 24h in culture medium containing $^{13}C_6$ glucose and increasing concentrations of sodium pyruvate. 4T1 cells control (CTR) or knockdown for PHGDH (shPHGDH). Two-way ANOVA with Sidak's multiple comparison test *n=3*.

f-h, Intracellular α-ketoglutarate abundance in 4T1 control (CTR) or PHGDH-silenced (shPHGDH sequences #1,#2 and #3) cells after 24h incubation in culture medium containing increasing concentrations of sodium pyruvate. Two-way ANOVA with Sidak's multiple comparison test. *n=3*

i-j, Phosphorylation of the mTORC1 targets p70 S6K, S6 and 4EBP1 upon 16h of serum starvation, 1h starvation in HBSS and subsequent reactivation (from 15 minutes to 2h) in serum containing culture medium with or without 2mM sodium pyruvate in 4T1 control (CTR) or PHGDH knockdown (shPHGDH#1 or #3) cells. Protein quantification of phosho-p70 S6K and phospho-S6 is shown below the immunoblot. Data are normalized on Actin and are shown as fold change compared to the time 0. One representative image is shown, *n=3.*

k, Protein expression of serine biosynthesis enzymes upon overexpression (OE) of PHGDH in MDA-MB-231 and MCF7 cells.

l, Activation of *de novo* serine biosynthesis assessed through measurement of serine m+3 labeling enrichment after incubation of MDA-MB-231 control (CTR) and PHGDH-overexpressing (OE) cells for 24h in culture medium containing $^{13}C_6$ glucose and increasing concentrations of sodium pyruvate. MDA-MB-231 cells control (CTR) or overexpressing PHGDH (OE PHGDH). Two-way ANOVA with Sidak's multiple comparison test. *n=3*

m, Intracellular α-ketoglutarate abundance in MDA-MB-231 control (CTR) or PHGDH-overexpressing (OE PHGDH) cells after 24h incubation in culture medium containing increasing concentrations of sodium pyruvate. Two-way ANOVA with Sidak's multiple comparison test. *n=3*

Error bars represent s.d. from mean of biologically independent samples except in panel b where the error bars represent s.d. of technical replicates.

Next, we addressed the question whether increasing serine biosynthesis activity is sufficient to drive mTORC1 signaling activation. To do so, we used the human MDA-MB-231 breast cancer cell line, which expresses very low levels of PHGDH, but significant levels of all serine biosynthesis enzymes upon PHGDH overexpression (**Figure 5k**). Thus, while control cells have almost no activity of *de novo* serine biosynthesis from glucose, overexpression of *PHGDH* resulted in increased serine biosynthesis from glucose, which was further elevated through pyruvate supplementation (**Figure 5l**). Accordingly, α-ketoglutarate abundance increased in MDA-MB-231 breast cancer cells overexpressing *PHGDH* upon supplementation of 2mM of pyruvate (**Figure 5m**). Subsequently, we determined dynamic phosphorylation of mTORC1 targets in MDA-

MB-231 control and *PHGDH* overexpression cells in the presence and absence of pyruvate. In line with our previous results, we found that pyruvate boosted the phosphorylation dynamics of the mTORC1 targets p70 S6K, S6 and 4EBP1 (decreased α band) particular in *PHGDH* overexpressing cells (Figure 6e). This effect was counteracted by treating *PHGDH* overexpressing MDA-MB-231 cells with the PHGDH inhibitor PH-755 (Figure 6f), which demonstrates that the effects on mTORC1 target phosphorylation were mediated through PHGDH. Consequently, protein synthesis was elevated in MDA-MB-231 cells overexpressing *PHGDH* in the presence of pyruvate (Figure 6g). Notably, pyruvate supplementation also elevated mTORC1 activity in control MDA-MB-231 cells, which indicates that in cells that are deficient for *de novo* serine biosynthesis pyruvate stimulates alternative metabolic pathways that impinge on mTORC1 activation. Next, we injected MDA-MB-231 control and *PHGDH* overexpressing breast cancer cells into the lungs of nude mice and determined mTORC1 signaling in the arising tumors. We observed a correlation trend of *PHGDH* overexpression with elevated phosphorylation of p70 S6K and 4EBP1 (increased γ and δ band) compared to control lung tumors (Figure 6h). Thus, we concluded that activation of the serine biosynthesis pathway is sufficient to drive mTORC1 signaling *in vitro* and in breast cancer-derived lung tumors.

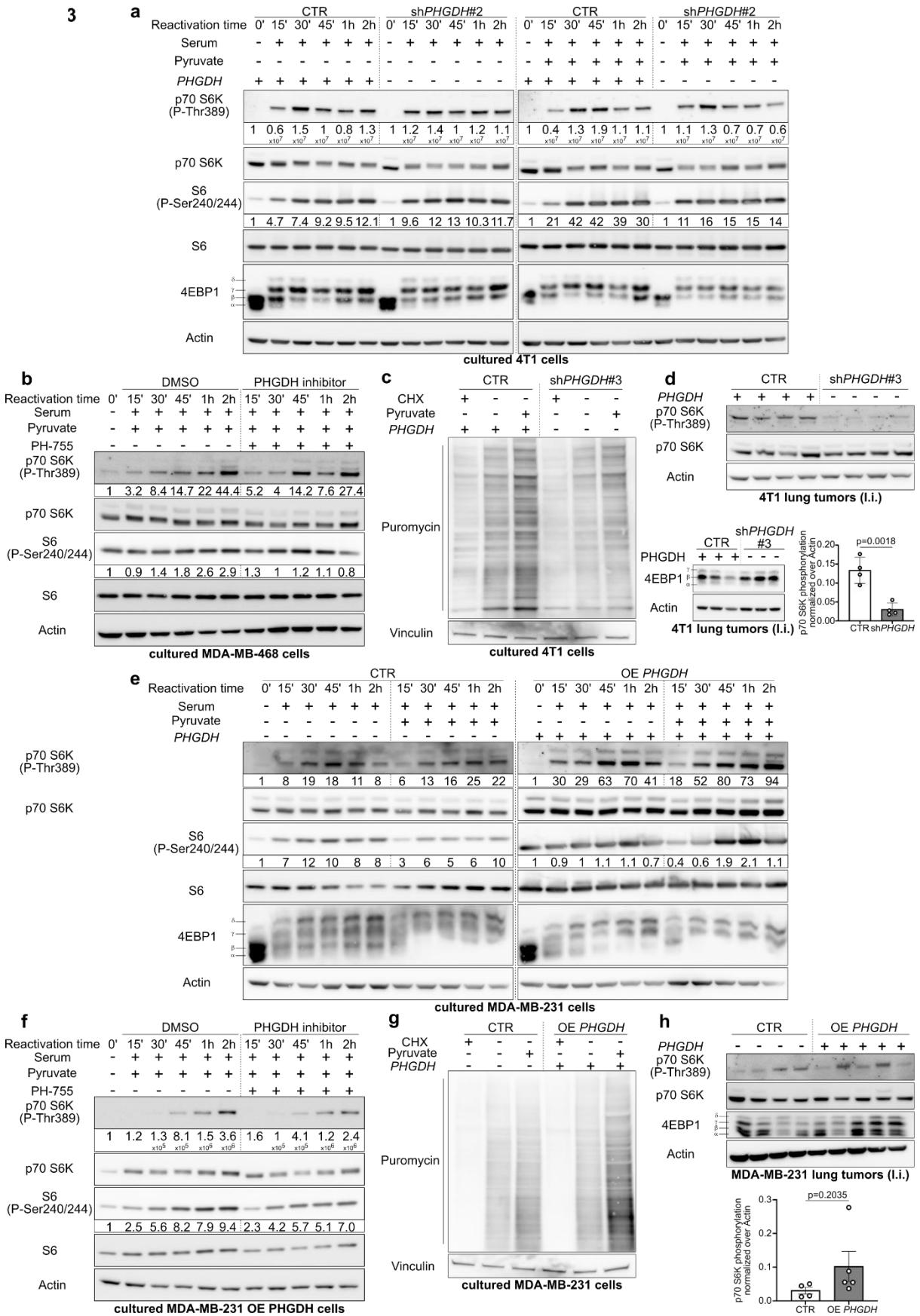
3
a
CTR
shPHGDH#2
Reactivation time
Serum
Pyruvate
PHGDH
p70 S6K (P-Thr389)
p70 S6K
S6 (P-Ser240/244)
S6
4EBP1
Actin
cultured 4T1 cells
b
DMSO
PHGDH inhibitor
PH-755
cultured MDA-MB-468 cells
c
CHX
Puromycin
Vinculin
cultured 4T1 cells
d
4T1 lung tumors (l.i.)
p=0.0018
p70 S6K phosphorylation normalized over Actin
e
OE PHGDH
cultured MDA-MB-231 cells
f
cultured MDA-MB-231 OE PHGDH cells
g
cultured MDA-MB-231 cells
h
MDA-MB-231 lung tumors (l.i.)
p=0.2035

Fig 6. PHGDH is required for pyruvate supported mTORC1 signaling

a, Phosphorylation of the mTORC1 targets p70 S6K, S6 and 4EBP1 upon 16h of serum starvation, 1h starvation in HBSS and subsequent reactivation (from 15 minutes to 2h) in serum containing culture medium with or without 2mM sodium pyruvate in 4T1 control (CTR) or *PHGDH* knockdown (sh*PHGDH*#2) cells. Protein quantification of phosho-p70 S6K and phospho-S6 is shown below the immunoblot. Data are normalized on Actin and are shown as fold change compared to the time 0. One representative image is shown, *n=3.*

b, Phosphorylation of the mTORC1 targets p70 S6K, and S6 upon 16h of serum starvation, 1h starvation in HBSS and subsequent reactivation (from 15 minutes to 2h) in serum containing culture medium with 2mM sodium pyruvate and with or without 1µM of PHGDH inhibitor PH-755 in MDA-MB-468 cells. Protein quantification of phosho-p70 S6K and phospho-S6 is shown below the immunoblot. Data are normalized on Actin and are shown as fold change compared to the time 0. One representative image is shown, *n=3.*

c, Total protein synthesis in presence or absence of 2mM pyruvate in 4T1 control (CTR) or *PHGDH*-silenced (sh*PHGDH*) cells based on the incorporation of puromycin (10µg per mL) into newly synthesized proteins. 4T1 cells were starved from serum for 16h, starved in HBSS for 1h and subsequently reactivated (30 minutes) in serum containing culture medium with or without 2mM sodium pyruvate. The protein synthesis inhibitor cycloheximide (CHX; 100nM) was used as negative control. One representative image is shown, *n=3.*

d, Phosphorylation of the mTORC1 targets p70 S6K and 4EBP1 in 4T1 control (CTR) or *PHGDH* silenced (sh*PHGDH*) lung metastases. l.i. refers to lung injection into NMRI nu/nu mice. Quantification of phospho-p70 S6K is shown in the graph. Data are normalized on Actin. Two-tailed unpaired Student's t-test. *n=4*

e, Phosphorylation of mTORC1 targets as described for panel a for MDA-MB-231 control (CTR) or *PHGDH*-overexpressing (OE *PHGDH*) cells. Protein quantification of phosho-p70 S6K and phospho-S6 is shown below the immunoblot. Data are normalized on Actin and are shown as fold change compared to the time 0. One representative image is shown, *n=3.*

f, Phosphorylation of mTORC1 targets as described for panel b for MDA-MB-231 *PHGDH*-overexpressing (OE *PHGDH*) cells. Protein quantification of phosho-p70 S6K and phospho-S6 is shown below the immunoblot. Data are normalized on Actin and are shown as fold change compared to the time 0. One representative image is shown, *n=3.*

g, Total protein synthesis as described for panel c for MDA-MB-231 control (CTR) or *PHGDH*-overexpressing (OE *PHGDH*) cells. One representative image is shown, *n=3.*

h, Phosphorylation of the mTORC1 targets p70 S6K and 4EBP1 in MDA-MB-231 control (CTR) or *PHGDH*-overexpressing (OE *PHGDH*) lung metastases. l.i. refers to lung injection into NMRI nu/nu mice. Quantification of phospho-p70 S6K is shown in the graph. Data are normalized on Actin. Two-tailed unpaired Student's t-test. *n=4* for CTR group, *n=5* for OE PHGDH group.

Error bars represent s.d. from mean of biologically independent mice.

α-ketoglutarate produced by the serine biosynthesis pathway supports mTORC1 signaling

Next, we asked which aspect of serine biosynthesis is required for the activation of mTORC1 growth signaling. The first possibility we addressed was that PHGDH itself without the requirement of a serine biosynthesis flux supports mTORC1 activation. To address this possibility, we overexpressed *PHGDH* in

human MCF7 breast cancer cells which lack expression of the other serine biosynthesis enzymes (**Figure 5k**). We confirmed that in these cells despite *PHGDH* overexpression no flux from glucose to serine occurred and that α-ketoglutarate abundance was unaltered by pyruvate supplementation (**Figure 7a,b**). Using these cells, we would expect more pronounced phosphorylation dynamics of p70 S6K, S6 and 4EBP1 compared to control if sole PHGDH expression without flux through the pathway is sufficient to activate mTORC1 signaling. In contrast to this hypothesis, we observed that *PHGDH*-overexpressing and control MCF7 cells had similar dynamics in mTORC1 target phosphorylation (**Figure 7c**). This result is in line with the earlier discussed finding that catalytic PHGDH inhibition with the compound PH-755 decreased mTORC1 activity (**Figure 6b,f**) and suggests that flux through the serine biosynthesis pathway is required to drive mTORC1 growth signaling.

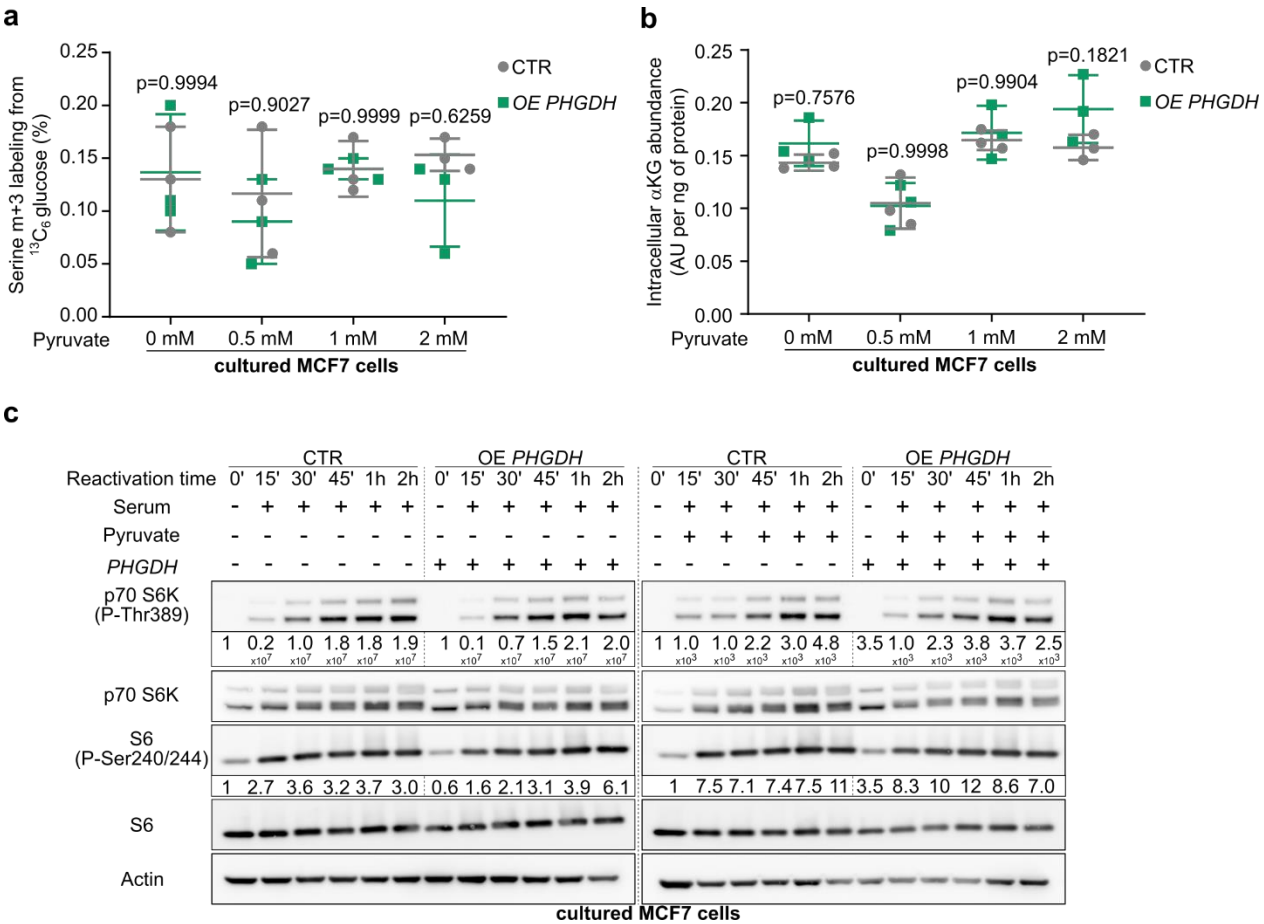

Fig 7. Sole overexpression of PHGDH without serine biosynthesis activity is not sufficient to support pyruvate-induced mTORC1 signaling

a, Activation of *de novo* serine biosynthesis assessed through measurement of serine m+3 labeling enrichment after incubation of MCF7 control (CTR) or PHGDH-overexpressing (OE PHGDH) cells for 24h in culture medium containing $^{13}C_6$ glucose and increasing concentrations of sodium pyruvate. Two-way ANOVA with Sidak's multiple comparison test *n=3*.

b, Intracellular α-ketoglutarate abundance in MCF7 control (CTR) or PHGDH-overexpressing (OE PHGDH) cells after 24h incubation in culture medium containing increasing concentrations of sodium pyruvate. Two-way ANOVA with Sidak's multiple comparison test. *n=3*

c, Phosphorylation of the mTORC1 targets p70 S6K, S6 and 4EBP1 after in MCF7 control (CTR) or PHGDH-overexpressing (OE PHGDH) cells upon 16h of serum starvation, 1h starvation in HBSS and subsequent reactivation (from 15 minutes to 2h) in culture medium containing or not 2mM Sodium Pyruvate. Protein quantification of phosho-p70 S6K and phospho-S6 is shown below the immunoblot. Data are normalized on Actin and are shown as fold change compared to the time 0. One representative image is shown, *n=3.*

Error bars represent s.d. from mean of biologically independent samples.

Subsequently, we asked which metabolite products of the serine biosynthesis pathway changed in a PHGDH dependent manner using mass spectrometry. We observed that predominantly α-ketoglutarate, serine and glycine decreased in abundance upon *PHGDH* silencing in 4T1 cells in the presence of pyruvate, while α-ketoglutarate showed the most pronounced increase in MDA-MB-231 cells upon *PHGDH* overexpression in the presence of pyruvate (**Figure 9a,b**). Notably, nucleotides, which are downstream metabolites of serine biosynthesis, did not consistently change in abundance upon *PHGDH* silencing or overexpression in the presence of pyruvate (**Figure 8**). Based on literature, both serine and α-ketoglutarate could support mTORC1 signaling[117–119,137]. However, serine was abundantly available in our culture conditions (286 µM in RPMI, 400 µM in DMEM) and in the lung environment (199±58.6 µM mouse, 94±24.1 µM human, **Figure 2d**), which suggests that this metabolite is not limiting in availability. Moreover, α-ketoglutarate, but not serine was consistently increased in abundance in 4T1 and MMTV-PyMT-derived lung metastases compared to the corresponding primary breast cancers (**Figure 9c-f**). Thus, we focused on α-ketoglutarate.

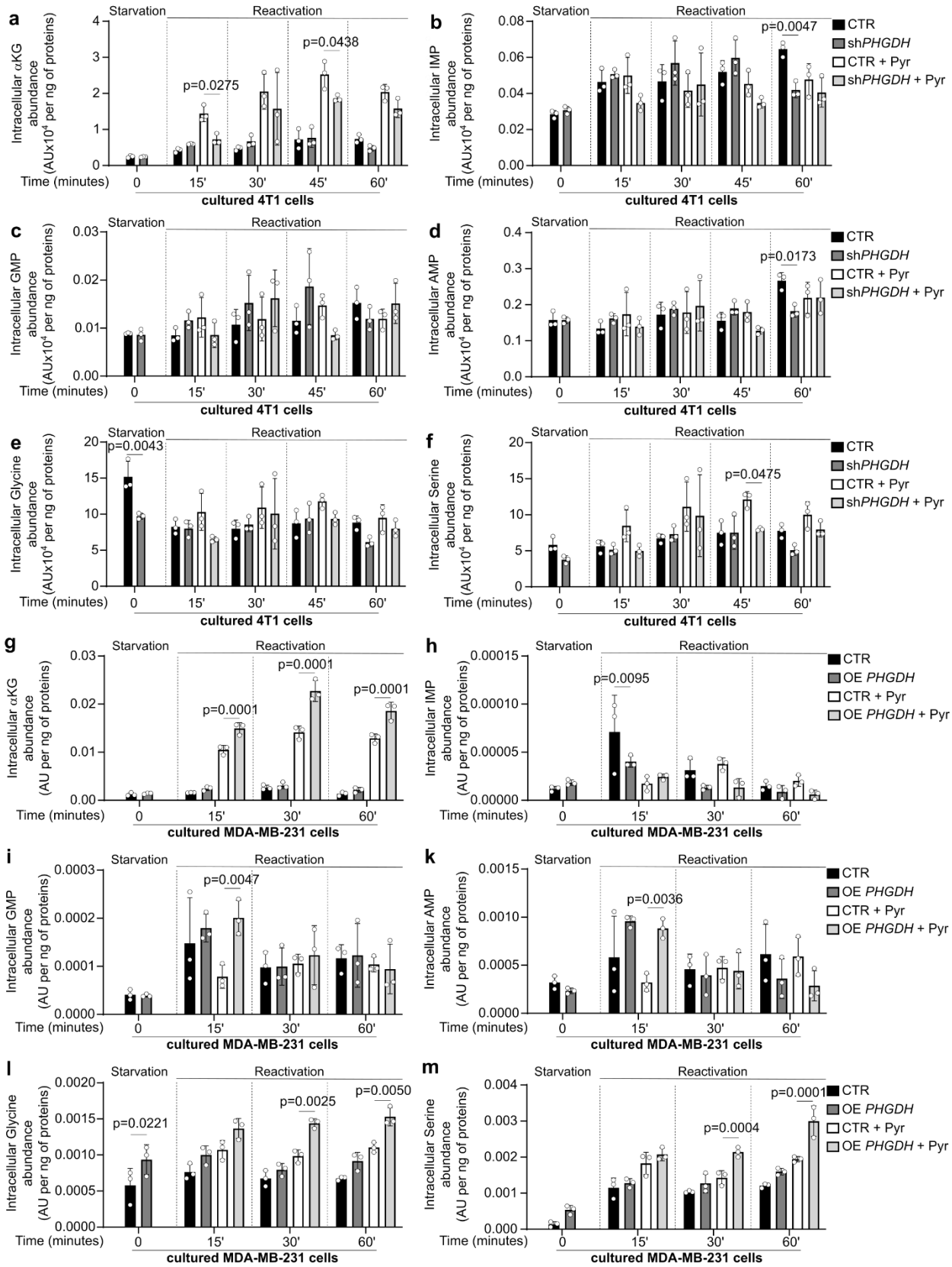
a
Intracellular αKG abundance (AUx10^4 per ng of proteins)
Starvation
Reactivation
p=0.0275
p=0.0438
Time (minutes)
0
15'
30'
45'
60'
cultured 4T1 cells
b
Intracellular IMP abundance (AUx10^4 per ng of proteins)
p=0.0047
CTR
shPHGDH
CTR + Pyr
shPHGDH + Pyr
c
Intracellular GMP abundance (AUx10^4 per ng of proteins)
d
Intracellular AMP abundance (AUx10^4 per ng of proteins)
p=0.0173
e
Intracellular Glycine abundance (AUx10^4 per ng of proteins)
p=0.0043
f
Intracellular Serine abundance (AUx10^4 per ng of proteins)
p=0.0475
g
Intracellular αKG abundance (AU per ng of proteins)
p=0.0001
p=0.0001
p=0.0001
cultured MDA-MB-231 cells
h
Intracellular IMP abundance (AU per ng of proteins)
p=0.0095
OE PHGDH
OE PHGDH + Pyr
i
Intracellular GMP abundance (AU per ng of proteins)
p=0.0047
k
Intracellular AMP abundance (AU per ng of proteins)
p=0.0036
l
Intracellular Glycine abundance (AU per ng of proteins)
p=0.0221
p=0.0025
p=0.0050
m
Intracellular Serine abundance (AU per ng of proteins)
p=0.0004
p=0.0001

Fig 8. Modulation of PHGDH expression does not consistently alter nucleotide abundances in presence of pyruvate

a-m, Metabolites abundance changes in 4T1 control (CTR) or PHGDH-silenced (shPHGDH) cells as well as MDA-MB-231 control (CTR) or PHGDH overexpressing (OE PHGDH) cells upon 16h of serum starvation, 1h starvation in HBSS and subsequent reactivation (15, 30, 45 and 60 minutes) in culture medium containing or not 2mM Sodium Pyruvate. *n=3*

Two-way ANOVA with Tukey's multiple comparison test. For clarity, only p values lower than 0.05 comparing CTR vs shPHGDH, CTR vs OE PHGDH, CTR + Pyr vs shPHGDH + Pyr or CTR +Pyr vs OE PHGDH + Pyr are shown on the graphs.

Error bars represent s.d. from mean of biologically independent samples.

To activate mTORC1 signaling, cytosolic but not mitochondrial abundance of α-ketoglutarate is relevant. Therefore, we measured cytosolic versus mitochondrial α-ketoglutarate abundance in 4T1 control and *PHGDH* silenced cells as well as in MDA-MB-231 control and *PHGDH* overexpressing cells upon pyruvate supplementation using a digitonin-based cell permeabilization method[128]. In line with the possibility that α-ketoglutarate produced by the serine biosynthesis pathway influences mTORC1 signaling, we found an increased α-ketoglutarate abundance particularly in the cytosolic fraction of 4T1 cells and MDA-MB-231 cells overexpressing *PHGDH* compared to 4T1 cells silenced for *PHGDH* and MDA-MB-231 control cells upon pyruvate supplementation (Figure 9g,h). Thus, this shows that cytosolic α-ketoglutarate abundance is consistently altered upon silencing or overexpression of *PHGDH*, which indicates that this metabolite could be involved in the serine biosynthesis-driven regulation of mTORC1 signaling.

Next, we reasoned that α-ketoglutarate supplementation rescues the activation of mTORC1 signaling upon *PHGDH* silencing in 4T1 cells. Indeed, we observed that α-ketoglutarate supplementation elevated the phosphorylation dynamics of p70 S6K, S6 and 4EBP1 (decreased α and β band) in PHGDH silenced 4T1 cells after starvation and reactivation with serum and pyruvate (Figure 9i). Accordingly, α-ketoglutarate supplementation increased protein translation in 4T1 cells with *PHDGH* silencing (Figure 9j). These data show that α-ketoglutarate can rescue mTORC1 signaling upon *PHGDH* silencing.

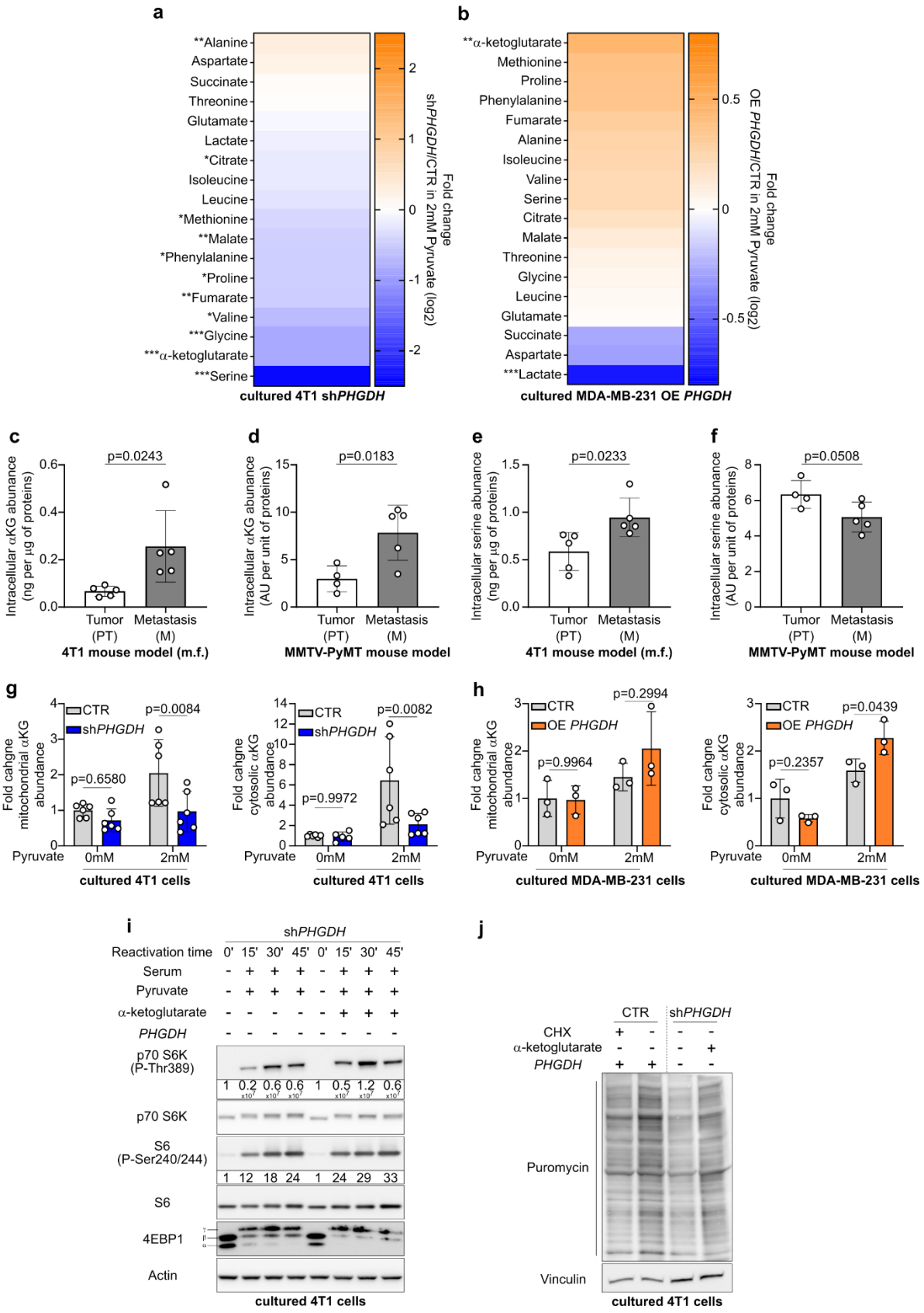
a
**Alanine
Aspartate
Succinate
Threonine
Glutamate
Lactate
*Citrate
Isoleucine
Leucine
*Methionine
**Malate
*Phenylalanine
*Proline
**Fumarate
*Valine
***Glycine
***α-ketoglutarate
***Serine
shPHGDH/CTR in 2mM Pyruvate (log2)
Fold change
cultured 4T1 shPHGDH
b
**α-ketoglutarate
Methionine
Proline
Phenylalanine
Fumarate
Alanine
Isoleucine
Valine
Serine
Citrate
Malate
Threonine
Glycine
Leucine
Glutamate
Succinate
Aspartate
***Lactate
OE PHGDH/CTR in 2mM Pyruvate (log2)
Fold change
cultured MDA-MB-231 OE PHGDH
c
Intracellular αKG abunance (ng per µg of proteins)
p=0.0243
Tumor (PT)
Metastasis (M)
4T1 mouse model (m.f.)
d
Intracellular αKG abunance (AU per unit of proteins)
p=0.0183
Tumor (PT)
Metastasis (M)
MMTV-PyMT mouse model
e
Intracellular serine abunance (ng per µg of proteins)
p=0.0233
Tumor (PT)
Metastasis (M)
4T1 mouse model (m.f.)
f
Intracellular serine abunance (AU per unit of proteins)
p=0.0508
Tumor (PT)
Metastasis (M)
MMTV-PyMT mouse model
g
CTR
shPHGDH
Fold cahgne mitochondrial αKG abundance
p=0.0084
p=0.6580
Pyruvate
0mM
2mM
cultured 4T1 cells
Fold cahgne cytosolic αKG abundance
p=0.0082
p=0.9972
cultured 4T1 cells
h
CTR
OE PHGDH
Fold cahgne mitochondrial αKG abundance
p=0.2994
p=0.9964
cultured MDA-MB-231 cells
Fold cahgne cytosolic αKG abundance
p=0.0439
p=0.2357
cultured MDA-MB-231 cells
i
shPHGDH
Reactivation time 0' 15' 30' 45' 0' 15' 30' 45'
Serum - + + + - + + +
Pyruvate - + + + - + + +
α-ketoglutarate - - - - - + + +
PHGDH - - - - - - - -
p70 S6K (P-Thr389)
1 0.2 0.6 0.6 1 0.5 1.2 0.6
p70 S6K
S6 (P-Ser240/244)
1 12 18 24 1 24 29 33
S6
4EBP1
Actin
cultured 4T1 cells
j
CTR
shPHGDH
CHX + - - -
α-ketoglutarate - - - +
PHGDH + + - -
Puromycin
Vinculin
cultured 4T1 cells

Fig 9. Pyruvate supports mTORC1 signaling through serine biosynthesis-derived α-ketoglutarate

a, b, Heat map representing metabolite abundance changes in 4T1 cells silenced for *PHGDH* (sh*PHGDH*) or MDA-MB-231 cells overexpressing *PHGDH* (OE *PHGDH*) compared to the respective control cells in culture media containing 2mM of sodium pyruvate. Two-tailed unpaired Student's t-test. *n=3.* Asterisks are representing statistical significance as follow: *= p ≤ 0.05 **= p ≤ 0.01 ***= p ≤ 0.001 ****=p ≤ 0.0001.

c-f, Intracellular α-ketoglutarate and serine abundance in 4T1 or PyMT primary breast tumors (PT) and lung metastases (M). m.f. refers to mammary fat pad injection. Two-tailed unpaired Student's t-test. *n=5 for the 4T1 model, n=4 for the PT group of the PyMT model, n=5 for the M group of the MMTV-PyMT model*

g-h, Mitochondrial and cytosolic α-ketoglutarate abundance in 4T1 control (CTR) or *PHGDH*-silenced (sh*PHGDH*) as well as MDA-MB-231 control (CTR) or *PHGDH* overexpressing (OE *PHGDH*) cells after 24h of incubation with culture medium with or without 2mM sodium pyruvate. 40 µg per mL (4T1 cells) or 25 µg per mL (MDA-MB-231) digitonin treatment of 2 minutes was used to permeabilize the cells and separate the cytosolic fraction from the mitochondrial fraction. Two-way ANOVA with Sidak's multiple comparison test (comparison between CTR and sh*PHGDH* or OE *PHGDH*). 4T1 *n=6 ,* MDA-MB-231 *n=3*.

i, Phosphorylation of mTORC1 targets p70 S6K, S6 and 4EBP1 in presence or absence of 1mM α-ketoglutarate in 4T1 *PHGDH* silenced (sh*PHGDH*) cells. 4T1 cells were starved for 16h of serum, starved in HBSS for 1h and subsequently reactivated (from 15 minutes to 45 minutes) in serum and 2mM sodium pyruvate containing culture medium with and without 1mM α-ketoglutarate. Protein quantification of phosho-p70 S6K and phospho-S6 is shown below the immunoblot. Data are normalized on Actin and are shown as fold change compared to the time 0. One representative image is shown, *n=3.*

j, Total protein synthesis in presence or absence of 1mM α-ketoglutarate and puromycin in 4T1 control (CTR) or PHGDH silenced (shPHGDH) cells based on the incorporation of puromycin into newly synthesized proteins. 4T1 cells were starved from serum for 16h, starved in HBSS for 1h and subsequently reactivated (30 minutes) in serum containing culture medium with or without 1mM α-ketoglutarate. The protein synthesis inhibitor cycloheximide (CHX; 100nM) was used as negative control. One representative image is shown, *n=3.*

Error bars represent s.d. from mean of biologically independent samples.

Subsequently, we asked whether replacing pyruvate supplementation with another nutrient that drives serine biosynthesis but does not increase net α-ketoglutarate production in the cytosol can induce mTORC1 signaling. To this end, we supplemented alanine, which is converted in the expense of α-ketoglutarate to pyruvate to 4T1 cells (**Figure 10a**). We confirmed that alanine increased pyruvate abundance, x-phosphoglycerate abundance and *de novo* serine biosynthesis from glucose, but not α-ketoglutarate abundance (**Figure 10b-e**). Subsequently, we determined mTORC1 signaling upon starvation and reactivation with serum and alanine. In line with our hypothesis that α-ketoglutarate is required for mTORC1 activation, we found no substantial increase in the phosphorylation dynamics of p70 S6K, S6 and 4EBP1 upon alanine supplementation in 4T1 cells (**Figure 10f**).

Thus, we concluded that α-ketoglutarate produced by the serine biosynthesis pathway can mechanistically link pyruvate to mTORC1 signaling activation.

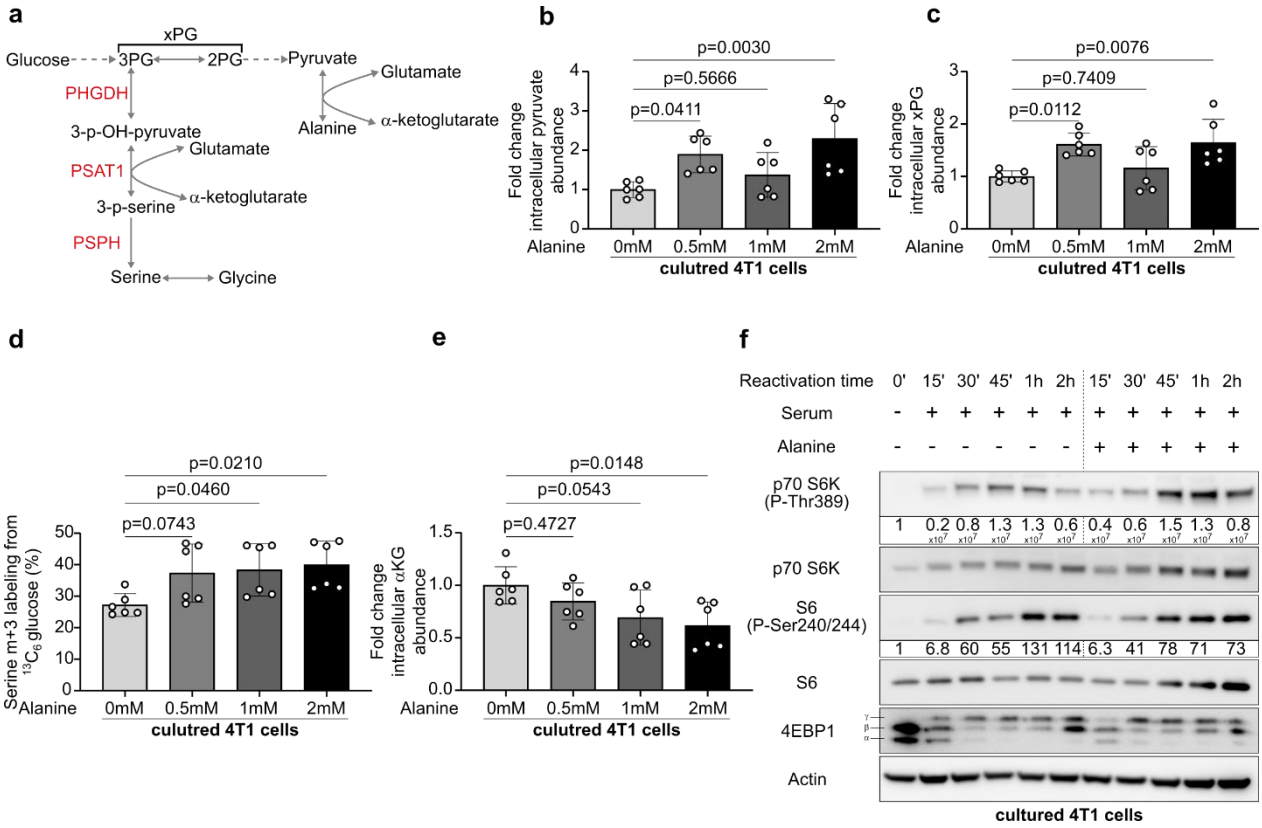

Fig 10. Increasing serine biosynthesis without increasing α-ketoglutarate abundance is not sufficient to support mTORC1 signaling

a, Scheme representative of the *de novo* serine biosynthesis pathway branching from glycolysis at the level of 3PG and alanine conversion to pyruvate, a reaction that consumes α-ketoglutarate. In black: metabolites. In red: enzymes of serine biosynthesis.

b-e, Intracellular pyruvate, xPG, and α-ketoglutarate abundance in 4T1 CTR cells incubated for 24h hour in medium containing increasing concentration of alanine. Activation of *de novo* serine biosynthesis assessed through measurement of serine m+3 labeling enrichment after incubation of 4T1 cells for 24h in culture medium containing $^{13}C_6$ glucose supplemented with increasing amounts of alanine. One-way ANOVA with Dunnet's multiple comparison test. *n=3*.

f, Phosphorylation of the mTORC1 targets p70 S6K, S6 and 4EBP1 in 4T1 cells upon 16h of serum starvation, 1h starvation in HBSS and subsequent reactivation (from 15 minutes to 2h) in culture medium with or without 2mM Alanine. Protein quantification of phosho-p70 S6K and phospho-S6 is shown below the immunoblot. Data are normalized on Actin and are shown as fold change compared to the time 0. One representative image is shown, *n=3.*

Error bars represent s.d. from mean of biologically independent samples.

Serine biosynthesis is required for rapamycin sensitivity in breast cancer-derived lung tumors but not primary breast tumors

Next, we asked whether serine biosynthesis is required for the sensitivity of breast cancer-derived lung metastases to mTORC1 inhibition. To address this question, we injected MDA-MB-231 control and *PHGDH* overexpressing cells into the lung of nude mice and treated them with rapamycin (1 mg per kg every 2nd day i.p., starting 9 days after cancer cell injection). Subsequently, we assessed outgrowth of the breast cancer-derived tumors based on combined H&E staining and bioluminescence. We observed that only *PHGDH*-overexpressing MDA-MB-231 lung tumors, but not control tumors, were sensitive to rapamycin treatment (**Figure 11a**). Subsequently, we performed the same experiment with 4T1 control and *PHGDH* silenced breast cancer cells injected into the lung of nude mice. In line with the overexpression results, we observed that only 4T1-derived lung tumors with PHGDH expression were sensitive to rapamycin (**Figure 11b**). Therefore, we concluded that serine biosynthesis activity is required for rapamycin sensitivity in breast cancer-derived lung tumors. Interestingly, the overexpression or downregulation of PHGDH in the two models, in absence of rapamycin, did not significantly change the tumor growth in the lungs, but it shows a trend. A possible explanation is that in the 4T1 model (**Figure 11b**), a complete knockout of PHGDH, instead of a downregulation, would be necessary to reveal a statistically significant difference in tumor growth. In the MDA-MB-231 model (**Figure 11a**), the overexpression of PHGDH seems to induce a slight increase of tumor growth that is only enough to highlight an increased response to the rapamycin treatment and not a significant growth advantage in absence of rapamycin. This result indicate that activation of serine biosynthesis is not a driver of cancer growth, but it makes tumor cells to functionally rely on mTORC1 activation and therefore more sensitive to the rapamycin treatment.

Finally, we hypothesized that only in pyruvate-enriched environments such as the lung, serine biosynthesis is required for rapamycin sensitivity. Consequently, we expect that primary breast tumors do not depend on pyruvate uptake and serine biosynthesis to activate mTORC1 signaling. To address this hypothesis, we

analyzed phosphorylation of S6 and 4EBP1 in primary breast tumors upon acute inhibition of pyruvate uptake with α-cyano-4-hydroxycinnamic acid (60 mg per kg per day, injections at 24 and 2h before sacrificing the mice; i.p.) and found that, differently to lung metastases (**Figure 1i**), acute MCT2 inhibition did not change phosphorylation of S6 and 4EBP1 (**Figure 11c**). Next, we injected either *PHGDH*-silenced or control 4T1 cells into the mammary fat pad of nude mice and measured mTORC1 target phosphorylation and rapamycin sensitivity. In line with the idea that the requirement of serine biosynthesis for mTORC1 activity is environment dependent, we found that primary breast tumors growing in the mammary fat pad did not exhibit an altered phosphorylation of S6 and 4EBP1 upon *PHGDH* silencing (**Figure 11d**). Moreover, we treated primary breast tumors upon PHGDH silencing with rapamycin (1 mg per kg ever 2nd day i.p., starting 5 days after cancer cell injection). Subsequently we assessed primary breast tumor growth by volume as well as size. We found that 4T1 primary breast cancers were sensitive to rapamycin, but that this sensitivity did not depend on PHGDH status and thus activity of serine biosynthesis (**Figure 11e,f**). Therefore, we concluded that only breast cancer cells in the lung environment, but not the mammary fat pad, rely on serine biosynthesis to activate mTORC1 growth signaling.

Taken together, we discovered that breast cancer-derived lung metastases, but not primary breast tumors, require pyruvate-driven serine biosynthesis for activating mTORC1 growth signaling.

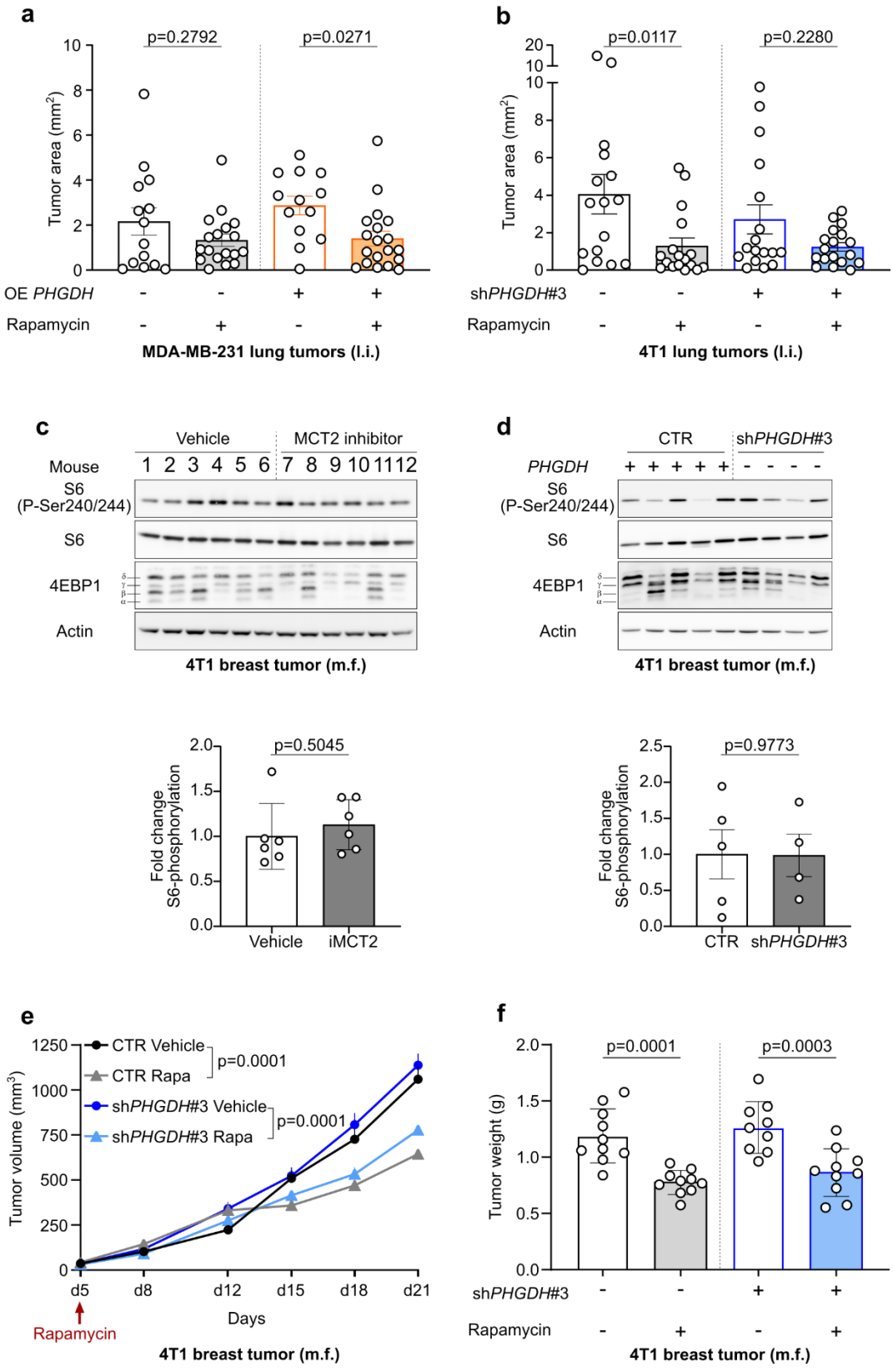
a
p=0.2792
p=0.0271
Tumor area (mm²)
OE PHGDH
Rapamycin
MDA-MB-231 lung tumors (l.i.)
b
p=0.0117
p=0.2280
Tumor area (mm²)
shPHGDH#3
Rapamycin
4T1 lung tumors (l.i.)
c
Vehicle
MCT2 inhibitor
Mouse
S6 (P-Ser240/244)
S6
4EBP1
Actin
4T1 breast tumor (m.f.)
d
CTR
shPHGDH#3
PHGDH
S6 (P-Ser240/244)
S6
4EBP1
Actin
4T1 breast tumor (m.f.)
p=0.5045
Fold change S6-phosphorylation
Vehicle
iMCT2
p=0.9773
Fold change S6-phosphorylation
CTR
shPHGDH#3
e
CTR Vehicle
CTR Rapa
shPHGDH#3 Vehicle
shPHGDH#3 Rapa
p=0.0001
p=0.0001
Tumor volume (mm³)
Days
Rapamycin
4T1 breast tumor (m.f.)
f
p=0.0001
p=0.0003
Tumor weight (g)
shPHGDH#3
Rapamycin
4T1 breast tumor (m.f.)

Fig 11. Serine biosynthesis supports mTORC1 signaling in breast cancer-derived lung tumors, but not in primary breast tumors

a, MDA-MB-231 lung tumor area in NMRI nu/nu mice treated with Rapamycin (1mg per kg, every two days, i.p., starting 9 days after tumor initiation) based on hematoxylin and eosin staining. OE *PHGDH* refers to *PHGDH* overexpression, l.i. refers to lung injection. Two-way ANOVA with Sidak's multiple comparison test.MDA-MB-231 CTR Vehicle *n=14.* MDA-MB-231 CTR Rapamycin *n=18.* MDA-MB-231 OE PHGDH Vehicle *n=13.* MDA-MB-231 OE PHGDH Rapamycin *n=19.*

b, 4T1 lung tumor area in NMRI nu/nu mice treated with Rapamycin (1mg per kg, every two days, i.p. starting the day after tumor initiation) based on hematoxylin and eosin staining. sh*PHGDH* refers to *PHGDH* silencing, l.i. refers to lung injection. Two-way ANOVA with Sidak's multiple comparison test. 4T1 CTR Vehicle *n=16.* 4T1 CTR Rapamycin *n=17.* 4T1 shPHGDH Vehicle *n=17.* 4T1 shPHGDH Rapamycin *n=18.*

c, Phosphorylation of the mTORC1 targets S6 and 4EBP1 in 4T1 primary tumors upon acute inhibition of pyruvate uptake using the MCT2 inhibitor α-cyano-4-hydroxycinnamic acid (60 mg per kg; i.p.). m.f. refers to mammary fat pad injection. Quantification of phospho-S6 is shown in the graph. Data are normalized on Actin and are shown as fold change compared to the group of mice treated with the vehicle. Two-tailed unpaired Student's t-test . *n=6*

d, Phosphorylation of mTORC1 targets S6 and 4EBP1 in primary 4T1 breast tumors. m.f. refers to mammary fat pad injection. Quantification of phospho-S6 is shown in the graph. Data are normalized on Actin and are shown as fold change compared to the CTR group. Two-tailed unpaired Student's t-test. 4T1 CTR *n=5.* 4T1 shPHGDH *n=4.*

e, 4T1 primary breast tumor volume in NMRI nu/nu mice treated with Rapamycin (1mg per kg, every two days, i.p., starting 5 days after tumor initiation). sh*PHGDH* refers to *PHGDH* silencing. m.f. refers to mammary fat pad injection. Two-way ANOVA with Sidak's multiple comparison test on the tumor volumes measured on the last day (d21). *n=10*.

f, 4T1 primary breast tumor weight in NMRI nu/nu mice treated with Rapamycin (1mg per kg, every two days, i.p., starting 5 days after tumor initiation). sh*PHGDH* refers to *PHGDH* silencing. m.f. refers to mammary fat pad injection. Two-way ANOVA with Sidak's multiple comparison test. *n=9* for group sh*PHGDH* treated with vehicle, *n=10* for the other groups.

Error bars represent s.d. (panels c,d and f) and s.e.m (panels a, b and e) from mean of biologically independent samples.

Chapter 4. Conclusion and discussion

CONCLUSION AND DISCUSSION

In this PhD thesis, we focused on understanding the metabolic needs of metastatic breast cancer cells that have successfully colonized the lungs. In particular, we targeted our attention on the impact of nutrient availability on intracellular metabolism and its implications in sustaining metastatic outgrowth. Interestingly, we found that the extracellular pyruvate availability in the lung microenvironment induces serine biosynthesis-derived α-ketoglutarate production that activates mTORC1 signaling in lung metastases. Conversely, serine biosynthesis was not required for mTORC1 signaling in breast cancer cells growing in the mammary fat pad. Thus, this thesis provides evidence that mTORC1 growth signaling is differently regulated between metastases and primary tumors (Figure 4.1).

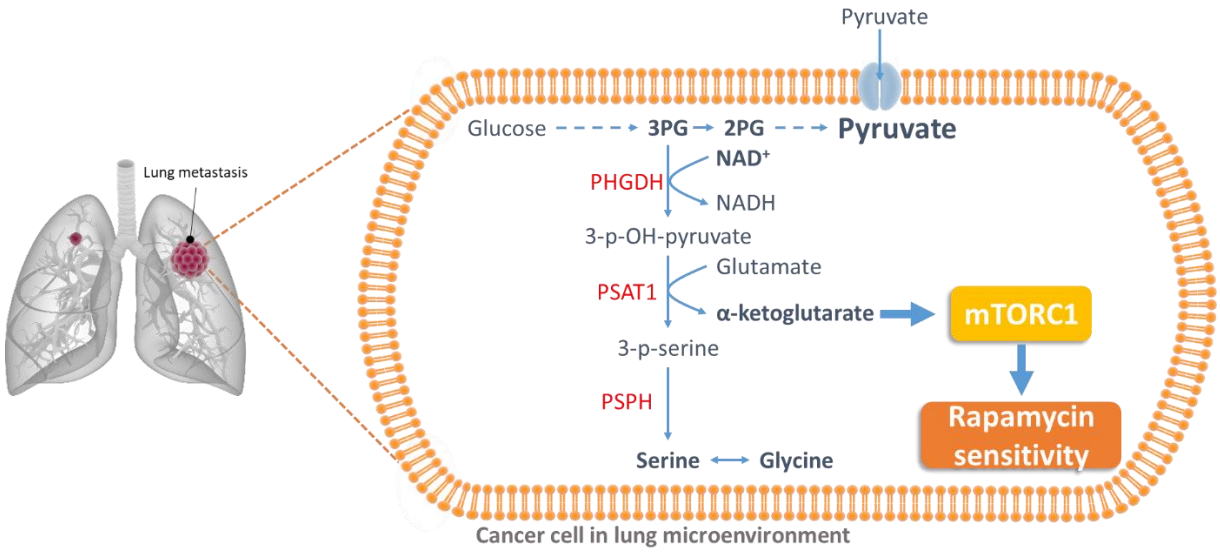

Fig 4.1 Schematic representation of the findings presented in this thesis. The pyruvate availability, that defines the nutritional microenvironment of the lung, induces activation of serine synthesis through increased 3PG, 2PG and NAD+/NADH ratio. As a consequence, more a-ketoglutarate is produced in the cytosol. Increased levels of a-ketoglutarate support mTORC1 activation and defines the sensitivity of cancer cells towards rapamycin treatment. Blue text represents metabolites. Blue text in bold represents metabolites upregulated in presence of pyruvate. Blue connections represent metabolic reactions. Dashed blue lines represent a series of metabolic reactions that are not listed in the scheme. Thick blue lines represent increased activation in presence of pyruvate.

In proliferating cancer cells, activation of serine synthesis is important because it sustains the antioxidant response and nucleotides production[138]. Thus, the activation of serine synthesis has often been found to be a metabolic feature and a predictor of poor prognosis in many types of tumor, including breast, melanoma, lung and Ewing sarcoma[72,73,139,140]. In particular, primary breast tumors frequently overexpress PHGDH, the first enzyme of serine synthesis, and a serine-enriched diet has been found to support their growth[141]. Thus, many groups have started investigating the potential of inhibiting this metabolic pathway as a targeted therapy in preclinical models. Consequently, recent studies suggest that activation of *de novo* serine biosynthesis may be critical also for the proliferation of distant metastasis. Accordingly, high PHGDH expression is found in breast cancer-derived lung, brain and bone metastasis[90,98,142]. Interestingly, the limited serine and glycine availability in the brain microenvironment induces a metabolic dependency on serine synthesis activation in brain metastasis that need to fulfill their biosynthetic needs for nucleotides [98]. Our work integrates and expands the understanding of the role of serine biosynthesis activation during metastasis formation. First, we identified a lung-specific dependency on serine biosynthesis, induced by the pyruvate-rich microenvironment. Second, we found that activation of serine synthesis has a critical non-metabolic role of sustaining cell growth and proliferation through mTORC1 signaling in lung metastasis. Therefore, these findings reinforce the general idea that breast cancer metastasis often rely on serine synthesis activation and that the site-specific nutrient availability is an important determinant of cellular metabolism of metastatic cells. Additionally, the data presented in this thesis suggest that serine synthesis activation supports proliferation not only by fulfilling metabolic needs such as antioxidant response and nucleotides production, but it also induces signaling transduction through activation of mTORC1. Interestingly, the link between mTORC1 activation and serine biosynthesis in cancer has been already investigated[143,144]. mTORC1 signaling has been found to positively regulate the expression of the serine biosynthesis enzymes PHGDH and PSAT[143]. Therefore, our findings suggest that the balance of serine

synthesis and mTORC1 activation represents a critical node of coordination between the cellular metabolism and signaling during metastatic cancer cell proliferation. Mechanistically, we found that serine biosynthesis activates the mTORC1 pathway via production of αKG. Thus, together with the already described αKG production linked to glutamine metabolism[116], we found an additional αKG -producing pathway that contributes to mTORC1 signaling. Interestingly, a recent study has shown, in the context of epidermal stem cells, that *de novo* serine synthesis induces significant increases of αKG that consequently promotes epigenetic modifications leading to differentiation[97]. Therefore, our findings, combined with the recent literature, suggest that activation of serine biosynthesis is a key modulator of αKG levels, a metabolite that functions as a signaling molecule able to regulate mTORC1 and epigenetic modifications.

The role of the nutrient microenvironment in determining the cellular metabolism of cancer cells is an emerging and rapidly growing field. Recent work from our group has shown in mice that the lung interstitial fluid is characterized by an increased pyruvate availability that is critical in supporting the extracellular matrix remodeling and biosynthetic needs of breast cancer-derived lung metastasis. In line with these results, the data presented in this thesis indicate that extracellular pyruvate is also increasing the proliferation potential of lung metastases through activation of serine biosynthesis-mediated mTORC1 signaling. Thus, these findings highlight that the lung nutritional microenvironment determines the metabolic adaptations of metastatic breast cancer cells during multiple steps of the metastatic cascade. Accordingly, we have shown in this thesis that a pyruvate-rich microenvironment can induce mTORC1 activation also in cancer cell lines other than breast cancer, suggesting that this regulatory link might be important also for other cancer types. Importantly, we observed a very similar pyruvate availability in the lung interstitial fluid of mice and humans, further expanding the potential clinical relevance of these findings.

Thus, our findings not only are coherent with what is known already in literature, but they also open up to new future scientific perspectives in the field of tumor metabolism and signaling. We found that, in breast

cancer-derived lung metastasis, *de novo* serine synthesis is induced by the characteristics of the extracellular environment. However, in other contexts, tumor cells have been found to induce serine biosynthesis through genetic aberrations. For instance, a somatic ribosomal protein mutation in T-cell acute lymphoblastic leukemia cells and the oncogenic transcription factor EWS-FLI1 in Ewing sarcoma, have been recently found to stimulate activation of serine biosynthesis[140,145]. Thus, the fact that increased serine biosynthesis has been identified to be a feature of multiple types of primary and secondary tumors indicates that it might be a general mechanism highjacked by cancer cells to meet their metabolic requirements and simultaneously activate cell signaling through mTORC1. Our findings raise the question whether serine biosynthesis-induced mTORC1 activation is a functional link supporting proliferation in different types of tumor. In addition, the data presented in this thesis show that increased *de novo* serine synthesis generates enough cytosolic α-ketoglutarate levels to activate mTORC1 in lung metastasis, raising the question whether, in other contexts, alternative a-ketoglutarate-generating pathways can play a role in sustaining mTORC1 signaling.

Interestingly, the mechanism that we found is highly dependent on the nutritional microenvironment in which the cells are growing. Thus, another immediate outcome of our work is the highlight that it poses on the relevance of nutrient availability and how much this impacts the findings of *in vitro* and *in vivo* models. In fact, even the data presented in this thesis show some discrepancies in the magnitude of the effect seen *in vitro* in non-physiological conditions compared to *in vivo.* While the inhibition of pyruvate uptake has a clear effect on mTORC1 activation in lung metastasis, the dynamics of mTORC1 *in vitro* in presence or absence of pyruvate are less clear and reproducible. Similarly, modulation of PHGDH expression *in vivo* significantly modifies the activation of mTORC1 and determines the sensitivity of lung tumors towards rapamycin treatment, while it only has a minimal impact on the phosphorylation status of the mTORC1 targets in cell culture conditions. We could speculate that a possible explanation for these discrepancies is the lack of physiological nutrient availability in our cell culture experiments. Main carbon sources such as

glucose and glutamine are generally highly abundant in the standard culture media, but the concentrations found *in vivo* are much lower. In particular, we describe a fine regulation that is part of a set of stimuli activating the mTORC1 pathway. For this reason, it is possible that the subtle regulation of mTORC1 activation by the serine biosynthesis pathway, becomes more relevant in a physiological context compared to an *in vitro* system where high abundance of nutrients and growth factors induce a constant strong activation of mTORC1 that might be less sensitive to changes in the availability of one nutrient. Thus, our work reinforces the idea that nutrient availability is a determinant of cellular metabolism and can have an impact on cell signaling activation.

Besides extending our understanding of the fundamental biological processes underlying breast cancer metastasis growing in the lung, our work provides new evidences that might have implications in clinical applications.

First, the data presented in this thesis suggest that, in line with the established literature, inhibition of serine biosynthesis could be effective not only in suppressing primary tumor growth, but also lung metastasis. Our findings support the hypothesis that serine biosynthesis activation is often a metabolic requirement for breast cancer cells that need to proliferate, either as primary tumors or established metastases. However, still little is known about *de novo* serine synthesis during the early events that lead to cancer cells dissemination. Recently, it has been shown that serine synthesis inhibition can promote tumor initiation in a pre-malignant model of squamous cell carcinoma[97], suggesting that serine biosynthesis has different roles during cancer progression and additional studies are necessary to design effective therapeutic strategies.

Second, the increased sensitivity of lung metastasis with high PHGDH expression toward the mTORC1 inhibitor Rapamycin, indicates that activation of the serine biosynthesis pathway may be further studied as a tool to predict therapeutic response and stratification of patients especially taking into consideration that mTORC1 inhibitors are already used and approved in the clinic. Inhibitors of mTOR pathway have been

found to improve the response of hormone therapies in hormone-receptor positive advanced breast cancer patients[9,146,147]. However, due to the heterogeneity of this disease, the effectiveness of these therapies can differ between patients, indicating that additional stratification strategies are needed to better predict therapeutic response[148]. Thus, the findings presented in this thesis suggest that a stratification strategy based on the activation of serine biosynthesis in the tumors of patients, may be successful in better predicting therapeutic response upon treatment with mTOR inhibitors. Therefore, our findings represent an initial step that, if further developed, may open new perspectives in utilizing a metabolic pathway as a biomarker for therapeutic response.

Third, we provided additional evidences that environmental pyruvate is critical for the outgrowth of lung metastasis and it is tempting to speculate that inhibiting pyruvate metabolism can be exploited to prevent and treat breast cancer-derived lung metastases and maybe other cancers growing in this environment. In a previous work from our group, inhibition of the pyruvate transporter MCT2 has been found to limit lung metastasis formation in murine models[99]. Here, we provide additional evidences that pyruvate uptake during metastasis formation not only promotes collagen deposition and biomass production like previously shown[86,99], but also mTORC1 activation. An inhibitor of both MCT1 and 2, namely AZD3965 (ClinicalTrials.gov Identifier: NCT01791595), is already in clinical trial for the treatment of diffuse large B cell lymphoma and Burkitt's lymphoma without showing concerning side effects. Thus, inhibition of pyruvate uptake may be a safe therapeutic strategy and our data suggest that further development of new inhibitors could be exploited for treatment of breast cancer-derived lung metastases.

In conclusion, we discovered that the nutrient environment defines which metabolic pathways cancer cells exploit to drive mTORC1 signaling. Consequently, lung metastases evolve to depend on different metabolic pathways than primary breast tumors to activate the same growth signaling pathway.

ACKNOWLEDGMENTS, PERSONAL CONTRIUBUTION AND CONFLICT OF INTEREST STATEMENTS

Authors List:

Gianmarco Rinaldi[1,2], Erica Pranzini[1,2,3], Joke Van Elsen[1,2], Dorien Broekaert[1,2], Cornelius M. Funk[4,5,6], Mélanie Planque[1,2], Ginevra Doglioni[1,2], Patricia Altea-Manzano[1,2], Matteo Rossi[1,2], Vincent Geldhof[7,8], Shao Thing Teoh[9], Christina Ross[10], Kent W. Hunter[10], Sophia Y. Lunt[9,11], Thomas G. P. Grünewald[4,5,6,12], and Sarah-Maria Fendt[1,2#]

[1]Laboratory of Cellular Metabolism and Metabolic Regulation, VIB-KU Leuven Center for Cancer Biology, VIB, Herestraat 49, 3000 Leuven, Belgium

[2]Laboratory of Cellular Metabolism and Metabolic Regulation, Department of Oncology, KU Leuven and Leuven Cancer Institute (LKI), Herestraat 49, 3000 Leuven, Belgium

[3]Department of Experimental and Clinical Biomedical Sciences, University of Florence, Viale Morgagni 50, 50134 Florence, Italy

[4]Max-Eder Research Group for Pediatric Sarcoma Biology, Institute of Pathology, Faculty of Medicine, LMU Munich, Thalkirchner Strasse 36, 80337 Munich, Germany

[5]Hopp Children's Cancer Center (KiTZ), Heidelberg, Germany

[6]Division of Translational Pediatric Sarcoma Research, German Cancer Research Center (DKFZ), German Cancer Consortium (DKTK), Heidelberg, Germany

[7]Laboratory of Angiogenesis and Vascular Metabolism, Department of Oncology, KU Leuven, Leuven, Belgium

[8]Laboratory of Angiogenesis and Vascular Metabolism, Center for Cancer Biology, VIB, Leuven, Belgium

[9]Department of Biochemistry and Molecular Biology, Michigan State University, East Lansing, MI, USA

[10]Laboratory of Cancer Biology and Genetics, Center for Cancer Research, National Cancer Institute, National Institutes of Health, Bethesda, MD, United States

[11]Department of Chemical Engineering and Materials Science, Michigan State University, East Lansing, MI, USA

[12]Institute of Pathology, Heidelberg University Hospital, Heidelberg, Germany

Author Contributions

Conception and design: GR and S-MF

Development of methodology: GR, EP, DB and MP

Acquisition of data (provided animals, acquired and managed patients, provided facilities, etc.): GR, EP, DB, GD, TGPG, JVE, MP, CF, STT, VG, CR, KW and SL

Analysis and interpretation of data (e.g., statistical analysis, biostatistics, computational analysis): GR, EP, MR, TGPG, and S-MF

Writing, review, and/or revision of the manuscript: GR and S-MF

Administrative, technical, or material support (i.e., reporting or organizing data, constructing databases): GR, EP, DB, JVE, and MP

Study supervision: S-MF

Conflict of interest

The authors do not declare any conflict of interest. S-MF has received funding from Bayer AG, Merck and Black Belt Therapeutic and has consulted for Fund +.

Scientific Acknowledgments

We would like to thank Peter Carmeliet (VIB-KU Leuven) for providing the shRNA against PHGDH, David Nittner (VIB histology core facility) for performing H&E staining, and John Blenis (Cornell Medical) as well as Roberto Zoncu (Berkley) for their advice on analyzing mTORC1 activity. We would also like to thank the Leuven Viral Vector Core for the luciferase virus, Stefan Soenen (KU Leuven MOSAIC) for help and assistance with the bioluminescence imaging, Matt Vander Heiden (MIT) for providing the PHGDH overexpression plasmid, Juan Fernandez Garcia and Martin Orth for advices on statistical analysis, Roberta Schmieder for

the setup of the *in vivo* glucose infusion methodology in the lab. We would like to thank Raze Therapeutics for providing us with the PHGDH inhibitor PH-755. We would like to acknowledge http://www.somersault1824.com for image elements used in the figures and in the cover of this thesis (Creative Commons license CC BY-NC-SA 4.0).

REFERENCES

1. Bray, F. *et al.* Global cancer statistics 2018: GLOBOCAN estimates of incidence and mortality worldwide for 36 cancers in 185 countries. *CA. Cancer J. Clin.* **68**, 394–424 (2018).
2. Harbeck, N. *et al.* Breast cancer. *Nat. Rev. Dis. Prim.* **5**, 1–31 (2019).
3. Koboldt, D. C. *et al.* Comprehensive molecular portraits of human breast tumours. *Nature* **490**, 61–70 (2012).
4. Golse, N. & Adam, R. Liver Metastases From Breast Cancer: What Role for Surgery? Indications and Results. *Clinical Breast Cancer* vol. 17 256–265 (2017).
5. Xie, Y. *et al.* Surgery of the primary tumor improves survival in women with stage IV breast cancer in Southwest China. *Med. (United States)* **96**, (2017).
6. Badwe, R. *et al.* Locoregional treatment versus no treatment of the primary tumour in metastatic breast cancer: An open-label randomised controlled trial. *Lancet Oncol.* **16**, 1380–1388 (2015).
7. Fitzal, F. *et al.* Impact of Breast Surgery in Primary Metastasized Breast Cancer: Outcomes of the Prospective Randomized Phase III ABCSG-28 POSYTIVE Trial. *Ann. Surg.* **269**, 1163–1169 (2019).
8. Bernier, J. Immuno-oncology: Allying forces of radio- and immuno-therapy to enhance cancer cell killing. *Critical Reviews in Oncology/Hematology* vol. 108 97–108 (2016).
9. Rugo, H. S. *et al.* Endocrine therapy for hormone receptor-positive metastatic breast cancer: American society of clinical oncology guideline. *J. Clin. Oncol.* **34**, 3069–3103 (2016).
10. Turner, N. C. *et al.* Overall survival with palbociclib and fulvestrant in advanced breast cancer. *N. Engl. J. Med.* **379**, 1926–1936 (2018).
11. Giordano, S. H. *et al.* Systemic therapy for patients with advanced human epidermal growth factor receptor 2–positive breast cancer: ASCO Clinical Practice Guideline Update. *J. Clin. Oncol.* **36**, 2736–2740 (2018).
12. Partridge, A. H. *et al.* Chemotherapy and targeted therapy for women with human epidermal growth factor receptor 2-negative (or unknown) advanced breast cancer: American society of clinical oncology clinical practice guideline. *J. Clin. Oncol.* **32**, 3307–3329 (2014).
13. Hanahan, D. & Weinberg, R. A. The hallmarks of cancer. *Cell* vol. 100 57–70 (2000).
14. Hanahan, D. & Weinberg, R. A. Hallmarks of cancer: The next generation. *Cell* vol. 144 646–674 (2011).
15. Lambert, A. W., Pattabiraman, D. R. & Weinberg, R. A. Emerging Biological Principles of Metastasis. *Cell* vol. 168 670–691 (2017).
16. Brabletz, T., Lyden, D., Steeg, P. S. & Werb, Z. Roadblocks to translational advances on metastasis research. *Nature Medicine* vol. 19 1104–1109 (2013).
17. Welch, D. R. & Hurst, D. R. Defining the Hallmarks of Metastasis. *Cancer Research* vol. 79 3011–3027 (2019).
18. Gupta, G. P. & Massagué, J. Cancer Metastasis: Building a Framework. *Cell* vol. 127 679–695 (2006).
19. Chiang, A. C. & Massagué, J. Molecular basis of metastasis. *New England Journal of Medicine* vol. 359 2814 (2008).
20. Fares, J., Fares, M. Y., Khachfe, H. H., Salhab, H. A. & Fares, Y. Molecular principles of metastasis: a hallmark of cancer revisited. *Signal Transduction and Targeted Therapy* vol. 5 (2020).
21. Nieto, M. A., Huang, R. Y. Y. J., Jackson, R. A. A. & Thiery, J. P. P. EMT: 2016. *Cell* vol. 166 21–45 (2016).
22. Kalluri, R. & Weinberg, R. A. The basics of epithelial-mesenchymal transition. *Journal of Clinical Investigation* vol. 119 1420–1428 (2009).
23. Lamouille, S., Xu, J. & Derynck, R. Molecular mechanisms of epithelial-mesenchymal transition. *Nature Reviews Molecular Cell Biology* vol. 15 178–196 (2014).

24. Mani, S. a *et al.* Epithelial-Mesenchymal Transition Generates Cells Which Have Stem Cell Properties. *Cell* **133**, 704–715 (2009).
25. Long, H. *et al.* CD133+ ovarian cancer stem-like cells promote non-stem cancer cell metastasis via CCL5 induced epithelial-mesenchymal transition. *Oncotarget* **6**, 5846–5859 (2015).
26. Zhou, D. *et al.* RBP2 induces stem-like cancer cells by promoting EMT and is a prognostic marker for renal cell carcinoma. *Exp. Mol. Med.* **48**, e238 (2016).
27. Friedl, P., Locker, J., Sahai, E. & Segall, J. E. Classifying collective cancer cell invasion. *Nature Cell Biology* vol. 14 777–783 (2012).
28. Chung, Y. C. *et al.* Rab11 collaborates E-cadherin to promote collective cell migration and indicates a poor prognosis in colorectal carcinoma. *Eur. J. Clin. Invest.* **46**, 1002–1011 (2016).
29. Veracini, L. *et al.* Elevated Src family kinase activity stabilizes E-cadherin-based junctions and collective movement of head and neck squamous cell carcinomas. *Oncotarget* **6**, 7570–7583 (2015).
30. Cheung, K. J. *et al.* Polyclonal breast cancer metastases arise from collective dissemination of keratin 14-expressing tumor cell clusters. *Proc. Natl. Acad. Sci. U. S. A.* **113**, E854–E863 (2016).
31. Cheung, K. J. & Ewald, A. J. A collective route to metastasis: Seeding by tumor cell clusters. *Science* vol. 352 167–169 (2016).
32. Konen, J. *et al.* Image-guided genomics of phenotypically heterogeneous populations reveals vascular signalling during symbiotic collective cancer invasion. *Nat. Commun.* **8**, 15078 (2017).
33. Massagué, J. & Obenauf, A. C. Metastatic colonization by circulating tumour cells. *Nature* vol. 529 298–306 (2016).
34. Nagrath, S. *et al.* Isolation of rare circulating tumour cells in cancer patients by microchip technology. *Nature* **450**, 1235–1239 (2007).
35. Luzzi, K. J. *et al.* Multistep nature of metastatic inefficiency: Dormancy of solitary cells after successful extravasation and limited survival of early micrometastases. *Am. J. Pathol.* **153**, 865–873 (1998).
36. Cameron, M. D. *et al.* Temporal progression of metastasis in lung: Cell survival, dormancy, and location dependence of metastatic inefficiency. *Cancer Res.* **60**, 2541–2546 (2000).
37. Labelle, M. & Hynes, R. O. The initial hours of metastasis: The importance of cooperative host-tumor cell interactions during hematogenous dissemination. *Cancer Discovery* vol. 2 1091–1099 (2012).
38. Paoli, P., Giannoni, E. & Chiarugi, P. Anoikis molecular pathways and its role in cancer progression. *Biochimica et Biophysica Acta - Molecular Cell Research* vol. 1833 3481–3498 (2013).
39. Ubellacker, J. M. *et al.* Lymph protects metastasizing melanoma cells from ferroptosis. *Nature* 1–6 (2020) doi:10.1038/s41586-020-2623-z.
40. Labuschagne, C. F., Cheung, E. C., Blagih, J., Domart, M. C. & Vousden, K. H. Cell Clustering Promotes a Metabolic Switch that Supports Metastatic Colonization. *Cell Metab.* **30**, 720-734.e5 (2019).
41. Eyles, J. *et al.* Tumor cells disseminate early, but immunosurveillance limits metastatic outgrowth, in a mouse model of melanoma. *J. Clin. Invest.* **120**, 2030–2039 (2010).
42. Bidwell, B. N. *et al.* Silencing of Irf7 pathways in breast cancer cells promotes bone metastasis through immune escape. *Nat. Med.* **18**, 1224–1231 (2012).
43. Paolino, M. *et al.* The E3 ligase Cbl-b and TAM receptors regulate cancer metastasis via natural killer cells. *Nature* **507**, 508–512 (2014).
44. Valiente, M. *et al.* Serpins promote cancer cell survival and vascular Co-option in brain metastasis. *Cell* **156**, 1002–1016 (2014).
45. Morrison, S. J. & Spradling, A. C. Stem Cells and Niches: Mechanisms That Promote Stem Cell Maintenance throughout Life. *Cell* vol. 132 598–611 (2008).
46. Hsu, Y. C., Li, L. & Fuchs, E. Emerging interactions between skin stem cells and their niches. *Nature Medicine* vol. 20 847–856 (2014).
47. Müller, A. *et al.* Involvement of chemokine receptors in breast cancer metastasis. *Nature* **410**, 50–

56 (2001).
48. Oskarsson, T. *et al.* Breast cancer cells produce tenascin C as a metastatic niche component to colonize the lungs. *Nat. Med.* **17**, 867–874 (2011).
49. Malanchi, I. *et al.* Interactions between cancer stem cells and their niche govern metastatic colonization. *Nature* **481**, 85–91 (2012).
50. Hoshino, A. *et al.* Tumour exosome integrins determine organotropic metastasis. *Nature* **527**, 329–335 (2015).
51. Wculek, S. K. & Malanchi, I. Neutrophils support lung colonization of metastasis-initiating breast cancer cells. *Nature* **528**, 413–417 (2015).
52. Costa-Silva, B. *et al.* Pancreatic cancer exosomes initiate pre-metastatic niche formation in the liver. *Nat. Cell Biol.* **17**, 816–826 (2015).
53. Peinado, H. *et al.* Melanoma exosomes educate bone marrow progenitor cells toward a pro-metastatic phenotype through MET. *Nat. Med.* **18**, 883–891 (2012).
54. Aguirre-Ghiso, J. A. Models, mechanisms and clinical evidence for cancer dormancy. *Nature Reviews Cancer* vol. 7 834–846 (2007).
55. Acharyya, S. *et al.* A CXCL1 paracrine network links cancer chemoresistance and metastasis. *Cell* **150**, 165–178 (2012).
56. Zhang, X. H. F. *et al.* Latent Bone Metastasis in Breast Cancer Tied to Src-Dependent Survival Signals. *Cancer Cell* **16**, 67–78 (2009).
57. Nowak, D. G. *et al.* MYC drives Pten/Trp53-deficient proliferation and metastasis due to IL6 secretion and AKT suppression via PHLPP2. *Cancer Discov.* **5**, 637–651 (2015).
58. Rinaldi, G., Rossi, M. & Fendt, S. M. Metabolic interactions in cancer: cellular metabolism at the interface between the microenvironment, the cancer cell phenotype and the epigenetic landscape. *Wiley Interdisciplinary Reviews: Systems Biology and Medicine* vol. 10 (2018).
59. Hsu, P. P. & Sabatini, D. M. Cancer cell metabolism: Warburg and beyond. *Cell* **134**, 703–707 (2008).
60. Warburg, O. On the origin of cancer cells. *Science (80-.).* **123**, 309–314 (1956).
61. Lunt, S. Y. & Vander Heiden, M. G. Aerobic glycolysis: Meeting the metabolic requirements of cell proliferation. *Annu. Rev. Cell Dev. Biol.* **27**, 441–464 (2011).
62. Elia, I., Schmieder, R., Christen, S. & Fendt, S. M. Organ-specific cancer metabolism and its potential for therapy. in *Handbook of Experimental Pharmacology* vol. 233 321–353 (Springer New York LLC, 2016).
63. Müller, H. J. & Boos, J. Use of L-asparaginase in childhood ALL. *Critical Reviews in Oncology/Hematology* vol. 28 97–113 (1998).
64. Sciacovelli, M. & Frezza, C. Oncometabolites: Unconventional triggers of oncogenic signalling cascades. *Free Radical Biology and Medicine* vol. 100 175–181 (2016).
65. Golub, D. *et al.* Mutant isocitrate dehydrogenase inhibitors as targeted cancer therapeutics. *Front. Oncol.* **9**, 417 (2019).
66. Martinez-Outschoorn, U. E. *et al.* Autophagy in cancer associated fibroblasts promotes tumor cell survival: Role of hypoxia, HIF1 induction and NFκB activation in the tumor stromal microenvironment. *Cell Cycle* **9**, 3515–3533 (2010).
67. Sotgia, F. *et al.* Understanding the Warburg effect and the prognostic value of stromal caveolin-1 as a marker of a lethal tumor microenvironment. *Breast Cancer Research* vol. 13 (2011).
68. Tchou, J. *et al.* Degree of Tumor FDG Uptake Correlates with Proliferation Index in Triple Negative Breast Cancer. *Mol. Imaging Biol.* **12**, 657–662 (2010).
69. Koo, H. R. *et al.* 18F-FDG uptake in breast cancer correlates with immunohistochemically defined subtypes. *Eur. Radiol.* **24**, 610–618 (2014).
70. Doyen, J. *et al.* Expression of the hypoxia-inducible monocarboxylate transporter MCT4 is increased in triple negative breast cancer and correlates independently with clinical outcome. *Biochem.*

Biophys. Res. Commun. **451**, 54–61 (2014).
71. Choi, J., Kim, D. H., Jung, W. H. & Koo, J. S. Metabolic interaction between cancer cells and stromal cells according to breast cancer molecular subtype. *Breast Cancer Res.* **15**, (2013).
72. Possemato, R. *et al.* Functional genomics reveal that the serine synthesis pathway is essential in breast cancer. *Nature* **476**, 346–350 (2011).
73. Locasale, J. W. *et al.* Phosphoglycerate dehydrogenase diverts glycolytic flux and contributes to oncogenesis. *Nat. Genet.* **43**, 869–874 (2011).
74. Pacold, M. E. *et al.* A PHGDH inhibitor reveals coordination of serine synthesis and one-carbon unit fate. *Nat. Chem. Biol.* **12**, 452–458 (2016).
75. Rodriguez, A. E. *et al.* Serine Metabolism Supports Macrophage IL-1β Production. *Cell Metab.* **29**, 1003-1011.e4 (2019).
76. Bonuccelli, G. *et al.* Ketones and lactate 'fuel' tumor growth and metastasis: Evidence that epithelial cancer cells use oxidative mitochondrial metabolism. *Cell Cycle* **9**, 3506–3514 (2010).
77. Elia, I., Doglioni, G. & Fendt, S. M. Metabolic Hallmarks of Metastasis Formation. *Trends Cell Biol.* **28**, 673–684 (2018).
78. Lebleu, V. S. *et al.* PGC-1α mediates mitochondrial biogenesis and oxidative phosphorylation in cancer cells to promote metastasis. *Nat. Cell Biol.* **16**, 992–1003 (2014).
79. Knott, S. R. V. *et al.* Asparagine bioavailability governs metastasis in a model of breast cancer. *Nature* **554**, 378–381 (2018).
80. Keckesova, Z. *et al.* LACTB is a tumour suppressor that modulates lipid metabolism and cell state. *Nature* **543**, 681–686 (2017).
81. Fong, M. Y. *et al.* Breast-cancer-secreted miR-122 reprograms glucose metabolism in premetastatic niche to promote metastasis. *Nat. Cell Biol.* **17**, 183–194 (2015).
82. Lunt, S. Y. & Fendt, S. M. Metabolism – A cornerstone of cancer initiation, progression, immune evasion and treatment response. *Curr. Opin. Syst. Biol.* **8**, 67–72 (2018).
83. Elia, I. *et al.* Proline metabolism supports metastasis formation and could be inhibited to selectively target metastasizing cancer cells. *Nat. Commun.* **8**, (2017).
84. AR, G., CM, M., JL, C., G, S. & JS, B. Erk regulation of pyruvate dehydrogenase flux through PDK4 modulates cell proliferation. *Genes Dev.* **25**, (2011).
85. Andrzejewski, S. *et al.* PGC-1α Promotes Breast Cancer Metastasis and Confers Bioenergetic Flexibility against Metabolic Drugs. *Cell Metab.* **26**, 778-787.e5 (2017).
86. Christen, S. *et al.* Breast Cancer-Derived Lung Metastases Show Increased Pyruvate Carboxylase-Dependent Anaplerosis. *Cell Rep.* **17**, 837–848 (2016).
87. Tseng, C. W. *et al.* Transketolase Regulates the Metabolic Switch to Control Breast Cancer Cell Metastasis via the a-Ketoglutarate Signaling Pathway. *Cancer Res.* **78**, 2799–2812 (2018).
88. Chen, J. *et al.* Gain of glucose-independent growth upon metastasis of breast cancer cells to the brain. *Cancer Res.* **75**, 554–565 (2015).
89. Mashimo, T. *et al.* Acetate is a bioenergetic substrate for human glioblastoma and brain metastases. *Cell* **159**, 1603–1614 (2014).
90. Pollari, S. *et al.* Enhanced serine production by bone metastatic breast cancer cells stimulates osteoclastogenesis. *Breast Cancer Res. Treat.* **125**, 421–430 (2011).
91. Lemma, S. *et al.* MDA-MB-231 breast cancer cells fuel osteoclast metabolism and activity: A new rationale for the pathogenesis of osteolytic bone metastases. *Biochim. Biophys. Acta - Mol. Basis Dis.* **1863**, 3254–3264 (2017).
92. Schild, T., Low, V., Blenis, J. & Gomes, A. P. Unique Metabolic Adaptations Dictate Distal Organ-Specific Metastatic Colonization. *Cancer Cell* vol. 33 347–354 (2018).
93. Muir, A., Danai, L. V. & Vander Heiden, M. G. Microenvironmental regulation of cancer cell metabolism: Implications for experimental design and translational studies. *DMM Disease Models*

and Mechanisms vol. 11 (2018).
94. Condon, K. J. & Sabatini, D. M. Nutrient regulation of mTORC1 at a glance. *J. Cell Sci.* **132**, (2019).
95. Voorde, J. Vande *et al.* Improving the metabolic fidelity of cancer models with a physiological cell culture medium. *Sci. Adv.* **5**, (2019).
96. Davidson, S. M. *et al.* Environment impacts the metabolic dependencies of ras-driven non-small cell lung cancer. *Cell Metab.* **23**, 517–528 (2016).
97. Baksh, S. C. *et al.* Extracellular serine controls epidermal stem cell fate and tumour initiation. *Nat. Cell Biol.* **22**, 779–790 (2020).
98. Ngo, B. *et al. Limited Environmental Serine and Glycine Confer Brain Metastasis Sensitivity to PHGDH Inhibition*. *Cancer Discovery* (2020). doi:10.1158/2159-8290.cd-19-1228.
99. Elia, I. *et al.* Breast cancer cells rely on environmental pyruvate to shape the metastatic niche. *Nature* vol. 568 117–121 (2019).
100. Kuo, M. H. *et al.* Glucose Transporter 3 is Essential for the Survival of Breast Cancer Cells in the Brain. *Cells* **8**, (2019).
101. Sato, R. *et al.* RNA Sequencing Analysis Reveals Interactions between Breast Cancer or Melanoma Cells and the Tissue Microenvironment during Brain Metastasis. *Biomed Res. Int.* **2017**, (2017).
102. Lanzardo, S. *et al.* Immunotargeting of antigen xCT attenuates stem-like cell behavior and metastatic progression in breast cancer. *Cancer Res.* **76**, 62–72 (2016).
103. Sever, R. & Brugge, J. S. Signal transduction in cancer. *Cold Spring Harb. Perspect. Med.* **5**, (2015).
104. Cargnello, M., Tcherkezian, J. & Roux, P. P. The expanding role of mTOR in cancer cell growth and proliferation. *Mutagenesis* **30**, 169–176 (2015).
105. Hare, S. H. & Harvey, A. J. mTOR function and therapeutic targeting in breast cancer. *Am. J. Cancer Res.* **7**, 383–404 (2017).
106. Ueng, S. H. *et al.* Phosphorylated mTOR expression correlates with poor outcome in early-stage triple negative breast carcinomas. *Int. J. Clin. Exp. Pathol.* **5**, 806–813 (2012).
107. Walsh, S. *et al.* MTOR in breast cancer: Differential expression in triple-negative and non-triple-negative tumors. *Breast* **21**, 178–182 (2012).
108. Wang, M. H. *et al.* Epithelial cell adhesion molecule overexpression regulates epithelial-mesenchymal transition, stemness and metastasis of nasopharyngeal carcinoma cells via the PTEN/AKT/mTOR pathway. *Cell Death Dis.* **9**, 1234567890 (2018).
109. Yu, T. *et al.* MicroRNA-193a-3p and -5p suppress the metastasis of human non-small-cell lung cancer by downregulating the ERBB4/PIK3R3/mTOR/S6K2 signaling pathway. *Oncogene* **34**, 413–423 (2015).
110. Yu, T. *et al.* Meta Lnc9 facilitates lung cancer metastasis via a PGK1-activated AKT/mTOR pathway. *Cancer Res.* **77**, 5782–5794 (2017).
111. Yang, H. *et al.* Mechanosensitive caveolin-1 activation-induced PI3K/Akt/mTOR signaling pathway promotes breast cancer motility, invadopodia formation and metastasis in vivo. *Oncotarget* **7**, 16227–16247 (2016).
112. Condon, K. J. & Sabatini, D. M. Nutrient regulation of mTORC1 at a glance. *J. Cell Sci.* **132**, 0–2 (2019).
113. Mossmann, D., Park, S. & Hall, M. N. mTOR signalling and cellular metabolism are mutual determinants in cancer. doi:10.1038/s41568-018-0074-8.
114. Lorendeau, D., Christen, S., Rinaldi, G. & Fendt, S. M. Metabolic control of signalling pathways and metabolic auto-regulation. *Biology of the Cell* vol. 107 251–272 (2015).
115. Roberts, D. J., Tan-Sah, V. P., Ding, E. Y., Smith, J. M. & Miyamoto, S. Hexokinase-II Positively Regulates Glucose Starvation-Induced Autophagy through TORC1 Inhibition. *Mol. Cell* **53**, 521–533 (2014).
116. Durá, R. V *et al.* Molecular Cell Glutaminolysis Activates Rag-mTORC1 Signaling. (2012) doi:10.1016/j.molcel.2012.05.043.

117. Durán, R. V. *et al.* HIF-independent role of prolyl hydroxylases in the cellular response to amino acids. *Oncogene* **32**, 4549–4556 (2013).
118. Cai, X. *et al.* Alpha-ketoglutarate promotes skeletal muscle hypertrophy and protein synthesis through Akt/mTOR signaling pathways. *Sci. Rep.* **6**, 1–11 (2016).
119. Bernfeld, E. *et al.* Phospholipase D-dependent mTOR complex 1 (mTORC1) activation by glutamine. *J. Biol. Chem.* **293**, 16390–16401 (2018).
120. Schmidt, E. K., Clavarino, G., Ceppi, M. & Pierre, P. SUnSET, a nonradioactive method to monitor protein synthesis. *Nat. Methods* **6**, 275–277 (2009).
121. Buescher, J. M. *et al.* A roadmap for interpreting 13C metabolite labeling patterns from cells. *Current Opinion in Biotechnology* vol. 34 189–201 (2015).
122. Fernández-García, J., Altea-Manzano, P., Pranzini, E. & Fendt, S. M. Stable Isotopes for Tracing Mammalian-Cell Metabolism In Vivo. *Trends in Biochemical Sciences* vol. 45 185–201 (2020).
123. Broekaert, D. & Fendt, S. M. Measuring in vivo tissue metabolism using 13C glucose infusions in mice. in *Methods in Molecular Biology* vol. 1862 67–82 (Humana Press Inc., 2019).
124. Lorendeau, D. *et al.* Dual loss of succinate dehydrogenase (SDH) and complex I activity is necessary to recapitulate the metabolic phenotype of SDH mutant tumors. *Metab. Eng.* **43**, (2017).
125. Young, J. D., Walther, J. L., Antoniewicz, M. R., Yoo, H. & Stephanopoulos, G. An elementary metabolite unit (EMU) based method of isotopically nonstationary flux analysis. *Biotechnol. Bioeng.* **99**, 686–699 (2008).
126. Fernandez, C. A., Des Rosiers, C., Previs, S. F., David, F. & Brunengraber, H. Correction of 13C mass isotopomer distributions for natural stable isotope abundance. *J. Mass Spectrom.* **31**, 255–262 (1996).
127. Clasquin, M. F., Melamud, E. & Rabinowitz, J. D. LC-MS data processing with MAVEN: A metabolomic analysis and visualization engine. *Curr. Protoc. Bioinforma.* **Chapter 14**, (2012).
128. Nonnenmacher, Y., Palorini, R. & Hiller, K. Determining compartment-specific metabolic fluxes. in *Methods in Molecular Biology* vol. 1862 137–149 (Humana Press Inc., 2019).
129. Nonnenmacher, Y. *et al.* Analysis of mitochondrial metabolism in situ: Combining stable isotope labeling with selective permeabilization. *Metab. Eng.* **43**, 147–155 (2017).
130. Zhang, Y. *et al.* A Pan-Cancer Proteogenomic Atlas of PI3K/AKT/mTOR Pathway Alterations. *Cancer Cell* **31**, 820-832.e3 (2017).
131. Vivian, J. *et al.* Toil enables reproducible, open source, big biomedical data analyses. *Nature Biotechnology* vol. 35 314–316 (2017).
132. Mossmann, D., Park, S. & Hall, M. N. mTOR signalling and cellular metabolism are mutual determinants in cancer. *Nature Reviews Cancer* vol. 18 744–757 (2018).
133. Schmidt, E. K., Clavarino, G., Ceppi, M. & Pierre, P. SUnSET, a nonradioactive method to monitor protein synthesis. *Nat. Methods* **6**, 275–277 (2009).
134. Orozco, J. M. *et al.* Dihydroxyacetone phosphate signals glucose availability to mTORC1. *Nat. Metab.* 1–9 (2020) doi:10.1038/s42255-020-0250-5.
135. Oslund, R. C. *et al.* Bisphosphoglycerate mutase controls serine pathway flux via 3-phosphoglycerate. *Nat. Chem. Biol.* **13**, 1081–1087 (2017).
136. Diehl, F. F., Lewis, C. A., Fiske, B. P. & Vander Heiden, M. G. Cellular redox state constrains serine synthesis and nucleotide production to impact cell proliferation. *Nat. Metab.* **1**, 861–867 (2019).
137. Ye, J. *et al.* Pyruvate kinase M2 promotes de novo serine synthesis to sustain mTORC1 activity and cell proliferation. *Proc. Natl. Acad. Sci. U. S. A.* **109**, 6904–6909 (2012).
138. Mattaini, K. R., Sullivan, M. R. & Vander Heiden, M. G. The importance of serine metabolism in cancer. *Journal of Cell Biology* vol. 214 249–257 (2016).
139. Zhu, J. *et al.* High expression of PHGDH predicts poor prognosis in non-small cell lung cancer. *Transl. Oncol.* **9**, 592–599 (2016).

140. Issaq, S. H. *et al.* EWS-FLI1-regulated Serine Synthesis and Exogenous Serine are Necessary for Ewing Sarcoma Cellular Proliferation and Tumor Growth. *Mol. Cancer Ther.* **19**, 1520–1529 (2020).
141. Sullivan, M. R. *et al.* Increased Serine Synthesis Provides an Advantage for Tumors Arising in Tissues Where Serine Levels Are Limiting. *Cell Metab.* **29**, 1410-1421.e4 (2019).
142. Samanta, D. *et al.* PHGDH expression is required for mitochondrial redox homeostasis, breast cancer stem cell maintenance, and lung metastasis. *Cancer Res.* **76**, 4430–4442 (2016).
143. Ben-Sahra, I., Hoxhaj, G., Ricoult, S. J. H., Asara, J. M. & Manning, B. D. mTORC1 induces purine synthesis through control of the mitochondrial tetrahydrofolate cycle. *Science (80-.).* **351**, 728–733 (2016).
144. Chaneton, B. *et al.* Serine is a natural ligand and allosteric activator of pyruvate kinase M2. *Nature* **491**, 458–462 (2012).
145. Kampen, K. R. *et al.* Translatome analysis reveals altered serine and glycine metabolism in T-cell acute lymphoblastic leukemia cells. *Nat. Commun.* **10**, (2019).
146. Piccart, M. *et al.* Everolimus plus exemestane for hormonereceptor- positive, human epidermal growth factor receptor-2-negative advanced breast cancer: Overall survival results from BOLERO-2. *Ann. Oncol.* **25**, 2357–2362 (2014).
147. Bachelot, T. *et al.* Randomized Phase II Trial of Everolimus in Combination With Tamoxifen in Patients With Hormone Receptor-Positive, Human Epidermal Growth Factor Receptor 2-Negative Metastatic Breast Cancer With Prior Exposure to Aromatase Inhibitors: A GINECO Study. (2012) doi:10.1200/JCO.2011.39.0708.
148. Martelotto, L. G., Ng, C. K. Y., Piscuoglio, S., Weigelt, B. & Reis-Filho, J. S. Breast cancer intra-tumor heterogeneity. *Breast Cancer Research* vol. 16 1–11 (2014).

ADDENDUM

This addendum shortly describes my research experience and the list of the studies to which I have contributed that are already published or in the course of publication. I have contributed to these studies by performing, analyzing and interpreting metabolomic or labeling experiments.

Research experience

KU Leuven (Leuven, Belgium)

2014-present

As PhD student in the laboratory of Prof. Sarah-Maria Fendt (VIB, KU Leuven), I currently

- investigate the metabolic vulnerabilities of metastatic breast cancer cells
- define the role of nutritional microenvironment during metastasis formation
- apply ^{13}C tracer analysis and metabolomics to define cancer cell metabolism
- combine molecular and cell biology techniques to study the interplay between metabolism and cellular signaling

Sapienza University (Rome, Italy)

2011-2014

As MS student in the laboratory of Prof. Giovanna Serino, I studied the functions and the interactions of the subunit 6 of the COP9 signalosome, a protein complex involved in the regulation of the ubiquitin-proteasome system in *Arabidopsis thaliana.*

2011

As BS student in the laboratory of Prof. Giovanna Serino, I characterized the genotype and the phenotype of a transgenic line of *Arabidopsis thaliana.*

Peking university (Beijing, China)

2012

As visiting MS student, I spent two months in the laboratory of Prof. Li-Jia Qu where I have learned the basics of confocal microscopy and studied the co-localization of two proteins in *Arabidopsis thaliana.*

Fellowships

2016-2020 FWO (Research foundation Flanders) PhD fellowship

2015 Emmanuel van der Schueren fellowship for starting PhD Students

2010 Student collaboration scholarship from Sapienza University

International meetings

2019

Keystone Symposia "Cancer Metastasis: The Role of Metabolism, Immunity and the Microenvironment (M2)", Florence, Italy, 15th-19th March 2019

Pyruvate availability drives mTORC1 activation during metastatic outgrowth
Gianmarco Rinaldi, Matteo Rossi, Dorien Broekaert and Sarah-Maria Fendt. Poster presentation.

2018 VIB conference "Metabolism in Cancer and Stromal Cells" Leuven, Belgium, 26th-27th November 2018
Pyruvate availability drives mTORC1 activation during metastatic outgrowth
Gianmarco Rinaldi, Matteo Rossi, Dorien Broekaert and Sarah-Maria Fendt. Poster presentation.

EACR conference "Mechanism to Therapies: Innovations in Cancer Metabolism" Bilbao, Spain, 9th-11th October 2018
Pyruvate availability drives mTORC1 activation during metastatic outgrowth
Gianmarco Rinaldi, Matteo Rossi, Dorien Broekaert and Sarah-Maria Fendt. Poster presentation.

2017 Beatson International Cancer Conference, Glasgow, UK, 2nd-5th July 2017
De novo serine biosynthesis drives mTORC1 activation and proliferation in breast cancer cells that have metastasized to the lungs.
Gianmarco Rinaldi, Matteo Rossi, Dorien Broekaert and Sarah-Maria Fendt. Poster presentation.

Publications

[Research articles on cancer metabolism]

Rinaldi G, Pranzini E, Van Elsen J,Broekaert D, Funk C, Planque M, Doglioni G, Altea-Manzano P, Rossi M, Geldhof V, Teoh ST, Ross C, Hunter K, Lunt S, Grünewald TGP, Fendt SM. "Serine biosynthesis is required for mTORC1 signaling in lung metastasis but not in primary breast tumors", *accepted for publication in Molecular Cell.*

Triki M, **Rinaldi G**, Planque M, Broekaert D, Winkelkotte AM, Maier CR, Janaki Raman S, Vandekeere A, Van Elsen J, Orth MF, Grünewald TGP, Schulze A, Fendt SM. "mTOR Signaling and SREBP Activity Increase FADS2 Expression and Can Activate Sapienate Biosynthesis" *PMID: 32579932, Cell reports 2020.*

Stegen S, **Rinaldi G**, Loopmans S, Stockmans I, Moermans K, Thienpont B, Fendt SM, Carmeliet P, Carmeliet G. "Glutamine Metabolism Controls Chondrocyte Identity and Function" *PMID: 32470321, Developmental cell 2020.*

Kampen KR, Fancello L, Girardi T, **Rinaldi G**, Planque M, Sulima SO, Loayza-Puch F, Verbelen B, Vereecke S, Verbeeck J, Op de Beeck J, Royaert J, Vermeersch P, Cassiman D, Cools J, Agami R, Fiers M, Fendt SM, De Keersmaecker K. "Translatome analysis reveals altered serine and glycine metabolism in T-cell acute lymphoblastic leukemia cells." *PMID 31186416, Nature Communications 2019.*

Meléndez-Rodríguez F, Urrutia AA, Lorendeau D, **Rinaldi G**, Roche O, Böğürcü-Seidel N, Ortega Muelas M, Mesa-Ciller C, Turiel G, Bouthelier A, Hernansanz-Agustín P, Elorza A, Escasany E, Li QOY, Torres-Capelli M, Tello D, Fuertes E, Fraga E, Martínez-Ruiz A, Pérez B, Giménez-Bachs JM, Salinas-Sánchez AS, Acker T, Sánchez Prieto R, Fendt SM, De Bock K, Aragonés J. "HIF1α Suppresses Tumor Cell Proliferation through Inhibition of Aspartate Biosynthesis." *PMID: 30811976, Cell Reports 2019.*

Vriens K, Christen S, Parik S, Broekaert D, Yoshinaga K, Talebi A, Dehairs J, Escalona-Noguero C, Schmieder R, Cornfield T, Charlton C, Romero-Pérez L, Rossi M, **Rinaldi G**, Orth MF, Boon R, Kerstens A, Kwan SY, Faubert B, Méndez-Lucas A, Kopitz CC, Chen T, Fernandez-Garcia J, Duarte JAG, Schmitz AA, Steigemann P, Najimi M, Hägebarth A, Van Ginderachter JA, Sokal E, Gotoh N, Wong KK, Verfaillie C, Derua R, Munck S, Yuneva M, Beretta L, DeBerardinis RJ, Swinnen JV, Hodson L, Cassiman D, Verslype C, Christian S, Grünewald S, Grünewald TGP, Fendt SM. "Evidence for an alternative fatty acid desaturation pathway increasing cancer plasticity." *PMID: 30728499, Nature 2019.*

Stegen S, Laperre K, Eelen G, **Rinaldi G**, Fraisl P, Torrekens S, Van Looveren R, Loopmans S, Bultynck G, Vinckier S, Meersman F, Maxwell PH, Rai J, Weis M, Eyre DR, Ghesquière B, Fendt SM, Carmeliet P, Carmeliet G. "HIF-1α metabolically controls collagen synthesis and modification in chondrocytes." *PMID: 30651640, Nature 2019.*

Kampen KR, Sulima SO, Verbelen B, Girardi T, Vereecke S, **Rinaldi G**, Verbeeck J, Op de Beeck J, Uyttebroeck A, Meijerink JPP, Moorman AV, Harrison CJ, Spincemaille P, Cools J, Cassiman D, Fendt SM, Vermeersch P, De Keersmaecker K. "The ribosomal RPL10 R98S mutation drives IRES-dependent BCL-2 translation in T-ALL." *PMID: 29930300, Leukemia 2019.*

Lorendeau D, **Rinaldi G**, Boon R, Spincemaille P, Metzger K, Jäger C, Christen S, Dong X, Kuenen S, Voordeckers K, Verstreken P, Cassiman D, Vermeersch P, Verfaillie C, Hiller K, Fendt SM. "Dual loss of succinate dehydrogenase (SDH) and complex I activity is necessary to recapitulate the metabolic phenotype of SDH mutant tumors." *PMID: 27847310, Metabolic Engineering 2016.*

[Reviews on cancer metabolism]

Rinaldi G, Rossi M, Fendt SM. "Metabolic interactions in cancer: cellular metabolism at the interface between the microenvironment, the cancer cell phenotype and the epigenetic landscape." *PMID: 28857478, Wiley Interdiscip Rev Syst Biol Med. 2017.*

Lorendeau D, Christen S, **Rinaldi G**, Fendt SM. " Metabolic control of signalling pathways and metabolic auto-regulation." *PMID: 25913226, Biol Cell. 2015.*

[Research articles on plant molecular biology]

Ghelli R, Brunetti P, Napoli N, De Paolis A, Cecchetti V, Tsuge T, Serino G, Matsui M, Mele G, **Rinaldi G**, Palumbo GA, Barozzi F, Costantino P, Cardarelli M. "A Newly Identified Flower-Specific Splice Variant of AUXIN RESPONSE FACTOR8 Regulates Stamen Elongation and Endothecium Lignification in Arabidopsis." *PMID: 29514943, Plant Cell 2018.*

Franciosini A, Lombardi B, Iafrate S, Pecce V, Mele G, Lupacchini L, **Rinaldi G**, Kondou Y, Gusmaroli G, Aki S, Tsuge T, Deng XW, Matsui M, Vittorioso P, Costantino P, Serino G. "The Arabidopsis COP9 SIGNALOSOME INTERACTING F-BOX KELCH 1 protein forms an SCF ubiquitin ligase and regulates hypocotyl elongation." *PMID: 23475998, Molecular Plant 2013.*